

# **Development of Aptamer-Actuated Two-Dimensional Photonic Crystal Hydrogel Sensors**

by

**James Henry Westbay**

B.S. Chemistry, University of Pittsburgh, 2018

B.A. Japanese, University of Pittsburgh, 2018

Submitted to the Graduate Faculty of the  
Dietrich School of Arts and Sciences in partial fulfillment  
of the requirements for the degree of  
Doctor of Philosophy

University of Pittsburgh

2023

UNIVERSITY OF PITTSBURGH

DIETRICH SCHOOL OF ARTS AND SCIENCES

This dissertation was presented

by

**James Henry Westbay**

It was defended on

April 27, 2023

and approved by

Dr. Jennifer Laaser, Assistant Professor, Department of Chemistry, University of Pittsburgh

Dr. Jill Millstone, Professor, Department of Chemistry, University of Pittsburgh

Dr. Sachin Velankar, Professor, Department of Bioengineering, University of Pittsburgh

Dissertation Director: Dr. Sanford A. Asher, Distinguished Professor of Chemistry, Department  
of Chemistry, University of Pittsburgh

Copyright © by James Henry Westbay

2023

# Development of Aptamer-Actuated Two-Dimensional Photonic Crystal Hydrogel Sensors

James H. Westbay, PhD

University of Pittsburgh, 2023

We developed a novel DNA-functionalized 2D photonic crystal hydrogel sensing motif utilizing aptamer molecular recognition groups. Photonic crystal hydrogels consist of a photonic crystal array embedded in a stimuli-responsive hydrogel. Stimuli-responsive hydrogels undergo chemoselective volume changes. In our DNA-functionalized hydrogels, hybridized DNA forms reversible hydrogel crosslinks. One of the DNA strands contains an aptamer sequence. Aptamers are short oligonucleotides that are selected to sensitively and specifically bind a chemical target. On addition of the aptamer's binding target, competitive aptamer-target binding breaks hydrogel crosslinks, causing the hydrogel to swell. This, in turn, increases the particle spacing of the embedded photonic crystal array, shifting photonic crystal diffraction. Thus, the concentration of the chemical target can be monitored through shifts in photonic crystal diffraction.

In this work, we utilized this novel sensing motif to fabricate a sensor that detects a small molecule, adenosine. Our sensor detects adenosine in buffer and serum solutions with  $< 30 \mu\text{M}$  limits of detection in under 30 min. We demonstrated the generalizability of this sensing motif by fabricating another sensor that detects a protein, human thrombin. Our thrombin sensor detects thrombin in buffer and serum solutions with  $< 500 \text{ nM}$  limits of detection in under 2 h . We further examined the tunability of our DNA-functionalized photonic crystal hydrogels, and optimized steps in their fabrication and operation for sensing applications.

The novel sensors reported here are robust, require minimal training to operate, and have readouts that are easy to interpret, ideally positioning them for use in resource-limited settings.

The tunable properties of our photonic crystal hydrogels enable their use beyond sensing applications, for example, as drug delivery vesicles. Importantly, we have demonstrated the generalizability of this sensing platform, suggesting that sensors for other chemical targets can be readily fabricated using the described procedures.

## Table of Contents

Preface.....	xxii
<b>1.0 Introduction.....</b>	<b>1</b>
<b>1.1 Scope of Introduction.....</b>	<b>1</b>
<b>1.2 Motivations.....</b>	<b>1</b>
<b>1.3 Two-Dimensional Photonic Crystals.....</b>	<b>3</b>
<b>1.3.1 Two-Dimensional Photonic Crystal Fabrication.....</b>	<b>3</b>
<b>1.3.2 Two-Dimensional Photonic Crystal Diffraction.....</b>	<b>5</b>
<b>1.4 Stimuli-Responsive Hydrogels and Volume Phase Transitions.....</b>	<b>10</b>
<b>1.4.1 Free Energy of Mixing.....</b>	<b>11</b>
<b>1.4.2 Elastic Free Energy.....</b>	<b>12</b>
<b>1.4.3 Ionic Free Energy.....</b>	<b>13</b>
<b>1.5 Two-Dimensional Photonic Crystal Hydrogel Sensors.....</b>	<b>14</b>
<b>1.6 Overview of Research Program.....</b>	<b>17</b>
<b>2.0 DNA-Functionalized Hydrogel Sensors.....</b>	<b>18</b>
<b>2.1 DNA Aptamers as a Molecular Recognition Agent.....</b>	<b>18</b>
<b>2.2 DNA-Crosslinked Hydrogels.....</b>	<b>19</b>
<b>2.3 DNA-Functionalized Photonic Crystal Hydrogels.....</b>	<b>25</b>
<b>2.4 Aptamer-Actuated Photonic Crystal Hydrogel Sensing Motif.....</b>	<b>26</b>
<b>3.0 DNA- Crosslinked 2D Photonic Crystal Hydrogel Sensor for Detection of Adenosine Actuated by an Adenosine-Binding Aptamer.....</b>	<b>29</b>
<b>3.1 Introduction.....</b>	<b>30</b>

<b>3.2 Experimental.....</b>	<b>32</b>
<b>3.2.1 Materials .....</b>	<b>32</b>
<b>3.2.2 Annealing DNA Strands .....</b>	<b>33</b>
<b>3.2.3 PicoGreen Fluorescence Assay.....</b>	<b>34</b>
<b>3.2.4 2DPC Hydrogel Fabrication .....</b>	<b>35</b>
<b>3.2.5 Scanning Electron Microscopy Characterization .....</b>	<b>36</b>
<b>3.2.6 2DPC Particle Spacing Measurements.....</b>	<b>37</b>
<b>3.2.7 Adenosine Sensing in Buffer Solutions.....</b>	<b>39</b>
<b>3.2.8 Adenosine Sensing in Fetal Bovine Serum.....</b>	<b>39</b>
<b>3.3 Results and Discussion .....</b>	<b>40</b>
<b>3.3.1 Adenosine Sensing Motif Using DNA-Crosslinked 2DPC Hydrogels That Contain the Adenosine-Binding Aptamer.....</b>	<b>40</b>
<b>3.3.2 Optimizing Adenosine-Binding Buffer Conditions via Fluorometric Quantitation of dsDNA Using PicoGreen .....</b>	<b>42</b>
<b>3.3.3 Adenosine Sensing in Buffer Solutions.....</b>	<b>44</b>
<b>3.3.4 Selectivity of Adenosine-Sensing 2DPC Hydrogels.....</b>	<b>47</b>
<b>3.3.5 Adenosine Sensing in FBS .....</b>	<b>49</b>
<b>3.4 Conclusion .....</b>	<b>50</b>
<b>3.4.1 Acknowledgements.....</b>	<b>52</b>
<b>4.0 DNA-Crosslinked Photonic Crystal Hydrogel Sensors: Optimization of Fabrication and Function .....</b>	<b>53</b>
<b>4.1 Introduction .....</b>	<b>54</b>
<b>4.2 Experimental Section .....</b>	<b>57</b>

4.2.1 Materials .....	57
4.2.2 2DPC Hydrogel Fabrication .....	58
4.2.3 2DPC Particle Spacing Measurements.....	59
4.2.4 Adenosine Sensing.....	61
4.2.5 PicoGreen Fluorescence Assay.....	62
4.2.6 DNA Annealing .....	62
4.2.7 DNA Concentration .....	63
4.2.8 Hydrogel Size and Sample Volume .....	64
4.2.9 DNA Sequence .....	64
4.2.10 Adenosine Sensing in Bovine Serum using Optimized PC Hydrogels .....	65
4.3 Results and Discussion .....	65
4.3.1 DNA Annealing .....	65
4.3.2 DNA Concentration .....	69
4.3.3 Hydrogel Size and Sample Volume .....	72
4.3.4 DNA Sequence .....	76
4.3.5 Adenosine Sensing in Bovine Serum using Optimized PC Hydrogels .....	80
4.4 Conclusion .....	82
4.4.1 Acknowledgements.....	83
<b>5.0 Aptamer-Actuated Two-Dimensional Photonic Crystal Hydrogel Sensor for</b>	
<b>Detection of Human Thrombin.....</b>	<b>84</b>
5.1 Introduction .....	85
5.2 Experimental Section .....	87
5.2.1 Materials .....	87

5.2.2 2DPC Hydrogel Fabrication .....	88
5.2.3 2DPC Particle Spacing Measurements.....	90
5.2.4 Thrombin Sensing in Buffer Solution .....	92
5.2.5 Changing the Buffer System .....	92
5.2.6 DNA Concentration Optimization.....	93
5.2.7 Thrombin Sensing in Fetal Bovine Serum .....	93
5.2.8 Selectivity Measurements .....	94
5.2.9 Free Energy of Mixing Measurements.....	94
<b>5.3 Results and Discussion .....</b>	<b>95</b>
5.3.1 Aptamer-Actuated 2DPC Hydrogel Sensing Motif for Detection of Thrombin .....	95
5.3.2 Thrombin Detection in Buffer Solution .....	97
5.3.3 Changing the Buffer System .....	100
5.3.4 Optimization of DNA Concentration .....	104
5.3.5 Thrombin Detection in Fetal Bovine Serum.....	107
5.3.6 Selectivity of Thrombin-Sensing 2DPC Hydrogels .....	109
5.3.7 Investigation of Free Energy of Mixing Phenomena .....	110
<b>5.4 Conclusion .....</b>	<b>116</b>
5.4.1 Acknowledgements.....	117
<b>6.0 Summary of Conclusions and Future Works.....</b>	<b>118</b>
6.1 Conclusions .....	118
6.2 Future Works.....	120

6.2.1 Alternative Aptamer-Actuated, DNA-Crosslinked 2DPC Hydrogel Sensing Motifs for Protein Detection.....	120
6.2.2 Further Investigation of Tunable Properties of Aptamer-Actuated PC Hydrogels .....	122
6.2.3 Reversibility of Aptamer-Actuated 2DPC Hydrogels.....	124
6.2.4 Aptamer-Actuated 2DPC Hydrogel Sensors for Novel Targets .....	124
Appendix A Supporting Information for Chapter 3 .....	126
Appendix A.1 Calculating dissociation constant of adenosine-binding aptamer .....	126
Appendix A.2 Optimizing acrylamide (AAM) monomer and MBAAM crosslinker concentrations in 2DPC hydrogel fabrication .....	128
Appendix B Supporting Information for Chapter 4.....	130
Appendix B.1 PicoGreen Assay.....	130
Appendix B.2 Statistical analysis and linear fit data for annealing protocols .....	131
Appendix B.3 Particle spacing change of PC hydrogels fabricated with 0.08 mM DNA .....	132
Appendix B.4 Impact of increasing [DNA] on PC hydrogel response and variability.....	133
Appendix B.5 Linear fit data for changing [DNA] .....	134
Appendix B.6 Statistical analysis for particle spacing measurements investigating hydrogel size and sample volume .....	135
Appendix C Supporting Information for Chapter 5 .....	137
Appendix C.1 Determination of thrombin concentration.....	137
Appendix C.2 Calculating the dissociation constant ( $K_D$ ) of the thrombin-binding aptamer.....	137

<b>Appendix C.3 Linear fit data for calibration curve in thrombin-binding buffer.....</b>	<b>138</b>
<b>Appendix C.4 Linear fit data for calibration curve in Alternate Buffer.....</b>	<b>138</b>
<b>Appendix C.5 Linear fit data for calibration curve in diluted serum .....</b>	<b>139</b>
<b>Bibliography .....</b>	<b>140</b>

## List of Tables

<b>Table 3.1: Composition of monomer solutions used in preparation of hydrogel samples ...</b>	<b>36</b>
<b>Table 4.1: DNA Annealing Protocols .....</b>	<b>66</b>
<b>Table 4.2: Concentrations of DNA .....</b>	<b>69</b>
<b>Table 4.3: PC Hydrogel Size and Sample Volume.....</b>	<b>73</b>
<b>Appendix Table 1: Concentrations of AAm and MBAAm used in preparation of 2DPC hydrogels.....</b>	<b>129</b>
<b>Appendix Table 2: t statistics for PG fluorescence measurements investigating annealing protocols.....</b>	<b>131</b>
<b>Appendix Table 3: Linear fit data for annealing protocols .....</b>	<b>132</b>
<b>Appendix Table 4: Particle spacing change data for PC hydrogels fabricated with 0.08 mM DNA.....</b>	<b>132</b>
<b>Appendix Table 5: Impact of increasing [DNA] on particle spacing change and standard deviation.....</b>	<b>133</b>
<b>Appendix Table 6: Impact of increasing [DNA] on particle spacing change and standard deviation.....</b>	<b>134</b>
<b>Appendix Table 7: t statistics for particle spacing measurements investigating hydrogel size and sample volume in 200 <math>\mu</math>M adenosine solutions .....</b>	<b>135</b>
<b>Appendix Table 8: t statistics for particle spacing measurements investigating hydrogel size and sample volume in 2 mM adenosine solutions .....</b>	<b>136</b>
<b>Appendix Table 9: Linear fit data for calibration curve in thrombin-binding buffer .....</b>	<b>138</b>
<b>Appendix Table 10: Linear fit data for calibration curve in alternate buffer .....</b>	<b>138</b>

**Appendix Table 11: Linear fit data for calibration curve in diluted serum..... 139**

## List of Figures

Figure 1.1: Needle tip flow method for 2DPC self-assembly .....	4
Figure 1.2: Bragg condition .....	6
Figure 1.3: (A) 2D hexagonal lattice and (B) 2D Bragg diffraction on a hexagonal lattice. The particle spacing ( $a$ ), angle of incidence ( $\alpha$ ), and angle of diffraction ( $\beta$ ) are labelled accordingly.....	7
Figure 1.4: Vector representation of 2D hexagonal lattice diffraction. ....	8
Figure 1.5: Relationship between lattice spacing ( $d$ ) and particle spacing ( $a$ ) for a 2D hexagonal lattice.....	10
Figure 1.6: 2DPC hydrogel volume changes actuate changes in 2DPC diffraction wavelength. ....	15
Figure 1.7: Debye ring measurement setup.....	16
Figure 2.1: Hydrogel with DNA crosslinks that undergoes reversible sol-to-gel transitions. ....	21
Figure 2.2: DNA-crosslinked hydrogel with aptamer molecular recognition group.....	23
Figure 2.3: Simplified DNA-crosslinked hydrogel for detection of chemical targets. ....	24
Figure 2.4: Aptamer-actuated, DNA-crosslinked 2DPC hydrogel sensing motif. ....	27
Figure 3.1: Method for fabricating 2DPC hydrogels. (a-e) A polymerizable monomer solution was layered on top of a pre-formed 2DPC array on a glass slide. A cover glass sealed the solution, after which polymerization proceeded for 30 min at room temperature. (f) The resulting cross-linked polymer embedded the ordered 2DPC array monolayer within the hydrogel network (2DPC hydrogel). ....	36

**Figure 3.2: SEM images of (a) the close-packed 2DPC monolayer and (b) the non-close-packed 2DPC monolayer embedded in a hydrogel. .... 37**

**Figure 3.3: 2DPC hydrogel particle spacing measurement. A 2DPC hydrogel piece was placed on a stand above a white screen. (a) Experimental setup and (b) schematic diagram showing the Debye ring illuminated by a 532 nm laser. .... 38**

**Figure 3.4: (a) Sequences of DNA strands that form adenosine-responsive crosslinks in the hydrogel. (b) Schematic diagram of the adenosine-sensing mechanism using a DNA-crosslinked 2DPC hydrogel. .... 41**

**Figure 3.5: Quantification of aptamer-adenosine binding using the PicoGreen assay in different buffer solutions. TNM buffer contains Tris, NaCl, and MgCl<sub>2</sub>. PicoGreen fluorescence is enhanced more on binding to dsDNA (hybridized DNA) than ssDNA. Aptamer-adenosine binding actuates the DNA conformational change from dsDNA to ssDNA. Thus, a decrease in the fluorescence emission on addition of adenosine indicates that more aptamer-adenosine binding has occurred. Error bars indicate standard deviations (n = 3). .... 43**

**Figure 3.6: Time dependence of 2DPC hydrogel particle spacing on the concentration of adenosine. Error bars indicate standard deviations (n = 3). .... 45**

**Figure 3.7: Particle spacing changes' dependence on adenosine concentration in buffer solutions (detection time = 30 min). The X-axis is in a logarithmic scale. The red line shows a linear fit (adjusted R-Squared = 0.9874). Error bars indicate standard deviations (n = 3). .... 47**

**Figure 3.8: Selectivity of adenosine-sensing 2DPC hydrogels. 2DPC hydrogel particle spacing was measured in a blank sample containing no nucleosides, and in samples containing**

1 mM concentration of adenosine, cytidine, guanosine, or uridine. Each 2DPC hydrogel contained the adenosine-binding aptamer, except for a control containing no DNA (“hydrogel w/ no DNA”) and a control containing a mutated aptamer that did not bind adenosine (“hydrogel w/ mutated aptamer”). The particle spacing change of each sample was measured after immersion in each solution for 30 min. Error bars indicate standard deviations (n = 3)..... 48

**Figure 3.9: Particle spacing changes’ dependence on adenosine concentration in 50% protein-removed FBS (detection time = 30 min). The X-axis is in a logarithmic scale. The red line shows a linear fit (adjusted R-Squared = 0.9936). Error bars indicate standard deviations (n = 3)..... 50**

**Figure 4.1: Debye ring measurement setup..... 60**

**Figure 4.2: Relative PicoGreen fluorescence for DNA annealing protocols. Each annealing protocol is described in Table 4.1. For each protocol, PicoGreen fluorescence of at least three different DNA samples were measured and averaged. Each average was divided by the largest average fluorescence signal, and the results reported as relative fluorescence. Larger relative fluorescence is indicative of greater hybridization, and thus more successful annealing. Error bars indicate standard deviations (n ≥ 3).... 67**

**Figure 4.3: Responsivity of PC hydrogel sensors utilizing DNA annealed by heating followed by different cooling times. Responsivity was evaluated by measuring PC hydrogel particle spacing changes in different concentrations of adenosine after 60 min. The average response of a blank sample measured in solution without adenosine was subtracted from each data point. Lines show linear fits for each protocol (see Appendix B.2). Error bars indicate standard deviations (n = 3)..... 68**

**Figure 4.4: Responsivity of PC hydrogel sensors with varying concentrations of DNA.**  
 Responsivity was evaluated by measuring PC hydrogel particle spacing changes in different concentrations of adenosine after 60 min. The average response of a blank sample measured in solution without adenosine was subtracted from each data point. Lines show linear fits for each concentration of DNA (see Appendix B.5). Error bars indicate standard deviations ( $n = 3$ ). ..... 70

**Figure 4.5: Responsivity of PC hydrogels with varying size and sample volume in (A) 200  $\mu$ M and (B) 2 mM adenosine solution.** Responsivity was evaluated by measuring PC hydrogel particle spacing changes after 60 min. PC hydrogels of two different sizes were analyzed in two different volumes of adenosine solution (Table 4.3). The average response of a blank sample measured in solution without adenosine was subtracted from each data point. Error bars indicate standard deviations ( $n \geq 3$ ). ..... 74

**Figure 4.6: DNA sequences used to fabricate PC hydrogels.** Bases that make up the aptamer sequence are shaded. Complementary sequences are aligned and italicized. .... 77

**Figure 4.7: PicoGreen fluorescence of DNA 1+2 (partially complementary) and DNA 1+3 (fully complementary).** For each pair of DNA strands, PicoGreen fluorescence was measured at least three times and averaged. Each average was divided by the average fluorescence of DNA 1+2, and results were reported as relative fluorescence. Error bars indicate standard deviations ( $n \geq 3$ ). ..... 78

**Figure 4.8: Particle spacing changes for PC hydrogels fabricated using DNA 1+3 (fully complementary).** PC hydrogel particle spacing changes were measured after 60 min in solutions containing 0 (blank), 2, and 4 mM adenosine ( $n=3$ ), and after heat treatment ( $n=2$ ). Error bars represent standard deviations. .... 79

**Figure 4.9: Dependence of particle spacing change on adenosine concentration for optimized PC hydrogels. Particle spacing measurements were made after 60 mins in solutions of diluted fetal bovine serum spiked with adenosine. The average response of a blank sample measured in solution without adenosine was subtracted from each data point. The red line shows a linear fit (adjusted  $R$ -squared = 0.9898). Error bars indicate standard deviations (n=3)..... 81**

**Figure 5.1: 2DPC hydrogel fabrication procedure. A 2DPC array is fabricated through a self-assembly process by injecting polystyrene particles onto the surface of water. The array is picked up on a glass substrate and dried. A monomer solution containing acrylamide, methylenebisacrylamide, DNA, and initiator is deposited onto the dried 2DPC array. A glass cover is placed over the monomer solution. After polymerization, the 2DPC hydrogel is peeled from the glass substrate, washed in buffer, and cut into pieces. .... 90**

**Figure 5.2: 2DPC hydrogel particle spacing measurement setup. .... 91**

**Figure 5.3: (A) Structure of acrdyite. (B) DNA sequences used to fabricate PC hydrogels. Bases that make up the aptamer sequence are shaded. Complementary sequences are aligned and italicized. (C) The thrombin-sensing mechanism using a DNA-crosslinked 2DPC hydrogel. DNA 1 (blue) and 2 (red) are attached to the polyacrylamide hydrogel network, and competitive aptamer-thrombin binding actuates the sensing response..... 96**

**Figure 5.4: 2DPC hydrogel particle spacing changes over time in different concentrations of thrombin solution. Error bars indicate standard deviations (n=3)..... 98**

**Figure 5.5: Dependence of particle spacing changes on thrombin concentration in buffer solutions at t=120 min. The average particle spacing change in blank solution without thrombin was subtracted from each data point. The red line shows a linear fit (see Appendix C.3). Error bars indicate standard deviations (n=3)..... 100**

**Figure 5.6: 2DPC hydrogel particle spacing changes over time in an alternate buffer system with varying concentrations of thrombin. Error bars indicate standard deviations (n=3). ..... 102**

**Figure 5.7: Dependence of particle spacing changes on thrombin concentration in an alternate buffer system at t=120 min. The average particle spacing change in blank solution without thrombin was subtracted from each data point. The red line shows a linear fit (see Appendix C.4). Error bars indicate standard deviations (n=3). .... 103**

**Figure 5.8: Particle spacing changes of 2DPC hydrogels fabricated with different amounts of DNA in buffer solutions with 1000 nM thrombin after 120 min. The average particle spacing change in blank solution without thrombin was subtracted from each data point. Error bars indicate standard deviations (n=3). ..... 105**

**Figure 5.9: Dependence of particle spacing changes on thrombin concentration in protein-removed FBS solutions at t=120 min. The average particle spacing change in blank solution without thrombin was subtracted from each data point. The red line shows a linear fit (see Appendix C.5). Error bars indicate standard deviations (n=3). .... 108**

**Figure 5.10: Selectivity measurements for thrombin-binding 2DPC hydrogels. Particle spacing change was measured after 120 min in buffer solutions spiked with 0 (blank) or 1000 nM protein. The response of a 2DPC hydrogel without DNA (labeled “hydrogel w/ no DNA”) in 1000 nM thrombin was also measured. The average**

response in a blank solution without protein was subtracted from each data point. Error bars indicate standard deviations (n=3)..... 110

**Figure 5.11: Thrombin-sensing mechanism using a 2DPC hydrogel with melted DNA crosslinks to investigate the effect of free energy of mixing phenomena. The PC hydrogels are first heated to break DNA crosslinks, and then immersed in solutions containing thrombin. If aptamer-thrombin binding causes a change in the free energy of mixing of the system, the PC hydrogel will swell or shrink, shifting PC diffraction. .... 112**

**Figure 5.12: Thrombin-sensing mechanism using a 2DPC hydrogel to investigate the effect of free energy of mixing phenomena. The PC hydrogels contain a dangling, single-stranded aptamer instead of hybridized DNA crosslinks. If aptamer-thrombin binding causes a change in the free energy of mixing of the system, the PC hydrogel will swell or shrink, shifting PC diffraction. .... 113**

**Figure 5.13: Particle spacing changes of 2DPC hydrogels to investigate free energy of mixing phenomena. Particle spacing changes were measured after 120 min incubation in buffer solutions with 1000 nM thrombin. 2DPC hydrogels with DNA crosslinks (“DNA Crosslinks”), crosslinks broken by heating (“Melted DNA Crosslinks”), and dangling, single-stranded aptamer sequences (“Dangling DNA Strands”) were analyzed. The average particle spacing change in blank solution without thrombin was subtracted from each data point. Error bars indicate standard deviations (n=3). .... 114**

**Figure 6.1: Alternative thrombin sensing motif. 2DPC hydrogels are fabricated with two different aptamers that bind different sites on thrombin. On addition of thrombin,**

each aptamer binds to a unique binding site, creating effective hydrogel crosslinks.

This causes the hydrogel to shrink, shifting 2DPC diffraction..... 122

**Figure 6.2: Adenosine-binding aptamer (DNA A) and two complementary DNA strands (DNA B and C) that share the same number of complementary bases, but bind to different parts of the aptamer..... 123**

**Appendix Figure 1: Log ([adenosine]) vs. particle spacing change. A weighted-least square method in OriginLab was used to generate a linear fit of  $y = 30.65366x - 8.49099$  (adjusted R-Squared = 0.9746). ..... 128**

**Appendix Figure 2: Log ([adenosine]) vs. particle spacing change. A weighted-least square method in OriginLab was used to generate a linear fit of  $y = 30.65366x - 8.49099$  (adjusted R-Squared = 0.9746). ..... 131**

## Preface

I would like to acknowledge my colleagues for navigating these unprecedented times and aiding me in completing this dissertation. My research advisor, Dr. Sanford Asher, fostered a collaborative environment and challenged me to become an independent thinker and scientist. I am grateful for his mentorship, support, and the stellar research group he has built. I would like to thank the entire Asher Group, and particularly those who were here when I was—Sharon Mansfield, Ryan Roppel, Sergei Bykov, Andrew Coukouma, Ivan Pallares, Daniel Maienshein, Tom Deering, Dipak Rout, Stephen White, and Ryan Jakubek—for their friendship, advice, and discussions about chemistry and beyond. I am especially thankful to Dr. Kyeongwoo Jang and Dr. Natasha Smith for their mentorship and collaboration throughout this project, and Sarah Goda for assisting me with this work and keeping me sane as graduation approached.

I appreciate and will miss all the friendly faces in the chemistry department. Having spent nearly a decade in the department, I owe many favors that I hope to repay in the future. I would also like to acknowledge my friends in other research groups, especially Sydney Giles, who kept me recharged with frequent coffee, lunch, and dinner breaks.

Outside of the department, many friends in Pittsburgh and beyond offered me refuge from the stresses of research. Through many conversations, game and movie nights, shared meals and drinks—both in-person and virtual—you provided an escape from the lab and kept me motivated so that I could continue to do my best work.

Finally, I would like to acknowledge and thank my family. My parents, Theresa and Joe, inspired my love for science and have supported me throughout my education. My sister, Katie, has been an outlet for me to vent and has ensured I've maintained a sense of humor. And weekly

calls with my grandparents have brightened even my worst weeks. I could not have done it without you.

## **1.0 Introduction**

### **1.1 Scope of Introduction**

Chapter 1 provides an overview of the research goals of this work, motivations behind them, and fundamental background for attaining them. This section will highlight the fabrication of two-dimensional (2D) photonic crystals (PCs) and discuss how these materials Bragg diffract light. It will next introduce stimuli-responsive hydrogels, and how these hydrogels undergo volume phase transitions (VPTs) by swelling or shrinking with changes in the chemical environment. Finally, this section will explain how these two materials can be combined to make user-friendly sensors. The chapter concludes with an overview of what follows in the rest of this work.

### **1.2 Motivations**

There is a need to develop novel sensing technologies that are accessible to end users.<sup>1</sup> The recent, global pandemic has highlighted this need. In the initial phases of the pandemic, early detection and isolation of infected individuals was the only strategy for mitigating transmission of SARS-CoV-2.<sup>2</sup> As such, US Congress allotted over \$1 billion to develop new sensors in the form of diagnostics.<sup>3</sup> Sensing platforms that are generalizable can be easily tailored to detect new targets, and may help prevent the next pandemic.

Developing accessible, generalizable sensors has benefits beyond assisting pandemic response. Such sensors would improve patient care and reduce health care costs.<sup>4</sup> For example, easy-to-use glucose monitoring devices have significantly improved outcomes for patients with insulin-dependent diabetes mellitus.<sup>5</sup> Sensors that enable self-testing would drive biomarker research, and enhance our understanding of the prognostic and diagnostic value of chemical markers.<sup>6-8</sup> Sensors that can be used in resource-limited settings would improve health care in underdeveloped nations<sup>1</sup>, and have military utility, for example, to detect chemical warfare agents<sup>9</sup>.

To assist in the development of sensing technologies, the World Health Organization specified ASSURED criteria (**A**ffordable, **S**ensitive, **S**pecific, **U**ser-friendly, **R**apid/Robust, **E**quipment-free, **D**eliverable to end users) to identify ideal properties for accessible sensors.<sup>1</sup> The Asher research group has spent decades developing novel sensing motifs meeting many of the ASSURED criteria using smart materials called photonic crystal (PC) hydrogels.

Considering this, the motivations of this work are to (1) develop a novel PC hydrogel sensing motif that can be used to fabricate accessible sensors, and (2) develop a highly generalizable sensing platform, such that sensors can be easily and rapidly tailored for novel targets. Completion of these goals will include extensive characterization of the sensing response and investigation into the tunable properties of the materials for different sensing applications.

## 1.3 Two-Dimensional Photonic Crystals

Photonic crystals (PCs) are material arrays with periodic dielectric constants that can uniquely alter the propagation of light.<sup>10, 11</sup> Of academic interest since the late 1980's, these materials have been applied to a variety of research areas, including laser optics<sup>12, 13</sup>, information science<sup>14, 15</sup>, ecology<sup>16</sup>, and wearable materials<sup>17</sup>. Due to their unique optical properties, PCs have received much attention as components of sensors.<sup>18-22</sup>

PCs can be categorized by the dimensions of their periodicity.<sup>23, 24</sup> Unlike three-dimensional (3D) PCs, which consist of several layers of ordered dielectric material, two-dimensional (2D) PCs, are a single plane or monolayer of crystal. As components of sensors, 2DPCs are advantageous because it is less expensive and labor intensive to fabricate large areas of 2D crystals.<sup>25</sup> Recently, 2DPCs have been incorporated into numerous sensing technologies.<sup>22, 26-28</sup>

### 1.3.1 Two-Dimensional Photonic Crystal Fabrication

Early attempts to fabricate PCs focused on 3DPC fabrication. Techniques to fabricate 3DPCs include lithography<sup>29, 30</sup> and laser-directed writing<sup>31, 32</sup>. While these techniques can fabricate highly ordered structures, they are costly and labor intensive, inhibiting their widespread use. In the early 2000s, self-assembly methods arose as a convenient alternative.<sup>33-35</sup> While offering less control over the fabrication process, self-assembly techniques are less tedious, less expensive, and enable the fabrication of PCs with large areas.<sup>36</sup> Despite the advantages of self-assembly, 3DPC fabrication is highly sensitive to ionic impurities.<sup>18, 25</sup> Thus, regardless of the

technique, even small amounts of ionic impurities can cause 3DPC disordering, inhibiting fabrication.

In contrast, 2DPCs are not as sensitive to ionic impurities.<sup>25, 37</sup> Thus, 2DPC self-assembly is less expensive and labor-intensive than its 3D counterpart. Techniques for 2DPC assembly include spin-coating<sup>38</sup>, solvent evaporation<sup>39</sup>, self-assembly using microgels<sup>40</sup>, and self-assembly using magnets<sup>41</sup>. However, the simplest 2DPC fabrication techniques involve self-assembly on an air-liquid interface. During these processes, the liquid acts as a flexible substrate on which the PC array can easily order relative to solid substrates. Strategies to initiate self-assembly in these cases include addition of surfactants<sup>42</sup> or alcohol<sup>43</sup> to the substrate medium.

The Asher group pioneered the needle tip flow method for 2DPC self-assembly.<sup>19, 25, 44</sup> Briefly, a mixture of highly charged colloidal nanospheres, water, and alcohol is injected onto a liquid surface. Initially, mercury was used as a liquid substrate<sup>19, 44</sup>, but water was later adopted as a safer alternative<sup>25</sup>. The PC self-assembles on the liquid interface due to the difference in surface tension between the suspension and the liquid substrate, in addition to electrostatic interactions and other attractive and repulsive intermolecular forces.<sup>45, 46</sup> The PC can then be simply transferred to a solid substrate. Conveniently, the needle tip flow method can be automated using an electronic syringe pump. Figure 1.1 summarizes the needle tip flow process.

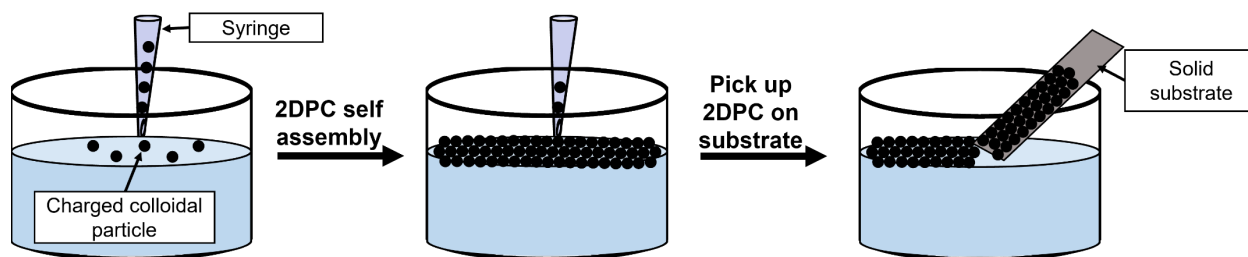


Figure 1.1: Needle tip flow method for 2DPC self-assembly

The needle tip flow method requires highly charged, colloidal particles. Nanospheres derived from polymers, such as polystyrene, poly(methyl methacrylate), and poly(N-isopropylacrylamide), are commonly used to fabricate PCs.<sup>47-50</sup> This work uses polystyrene nanospheres due to their low cost and straightforward synthesis via dispersion polymerization.<sup>48</sup> Briefly, styrene monomer is dissolved in a methanol-water mixture with sodium styrene sulfonate stabilizer. Polymerization proceeds after addition of initiator and heat. The water-methanol mixture is a good solvent for styrene monomer, but not for polystyrene. Thus, as polymerization continues, the polystyrene begins to aggregate. Stabilizer covalently attaches to the growing polymer, enabling the formation of nanospheres that ultimately precipitate out of the water-methanol mixture. The resulting polystyrene nanospheres are monodisperse with diameters on the order of ~1000 nm.<sup>48</sup>

### 1.3.2 Two-Dimensional Photonic Crystal Diffraction

PC arrays diffract light according to the Bragg condition (Equation 1.1), where  $m$  is an integer representing the diffraction order,  $\lambda$  is the wavelength of light,  $n$  is the effective refractive index of the crystal,  $d$  is the PC array lattice spacing, and  $\theta$  is the Bragg diffraction angle.<sup>44, 51-53</sup>

$$m\lambda = 2nd \sin \theta \qquad \text{Equation 1.1}$$

Figure 1.2 summarizes why this phenomenon occurs. Light that reflects off parallel diffracting planes in the PC lattice align and constructively interfere when the Bragg condition is met. Thus, as the PC lattice spacing,  $d$ , changes, so change the diffracted wavelengths and angles of light.

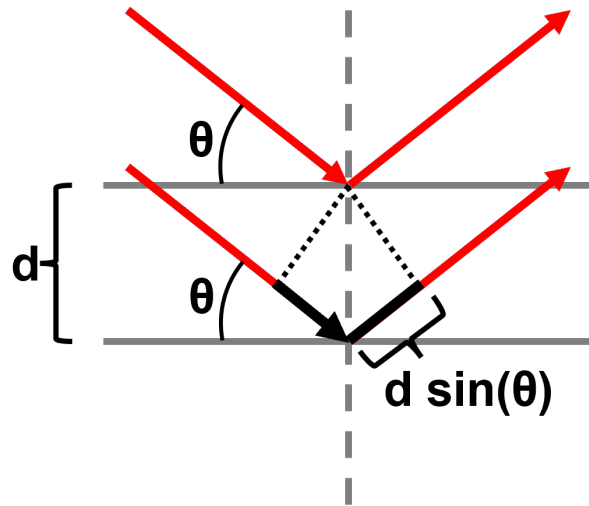


Figure 1.2: Bragg condition

When the PC array is a two-dimensional (2D) hexagonal lattice, the Bragg condition becomes Equation 1.2, where  $a$  is the 2DPC array particle spacing, and  $\alpha$  and  $\beta$  are the angle of incidence and diffraction, respectively.

$$m\lambda = \frac{\sqrt{3}}{2} a(\sin \alpha + \sin \beta) \quad \text{Equation 1.2}$$

Figure 1.3 depicts a 2D hexagonal lattice and shows how light diffracts off of the lattice according to the Bragg condition.

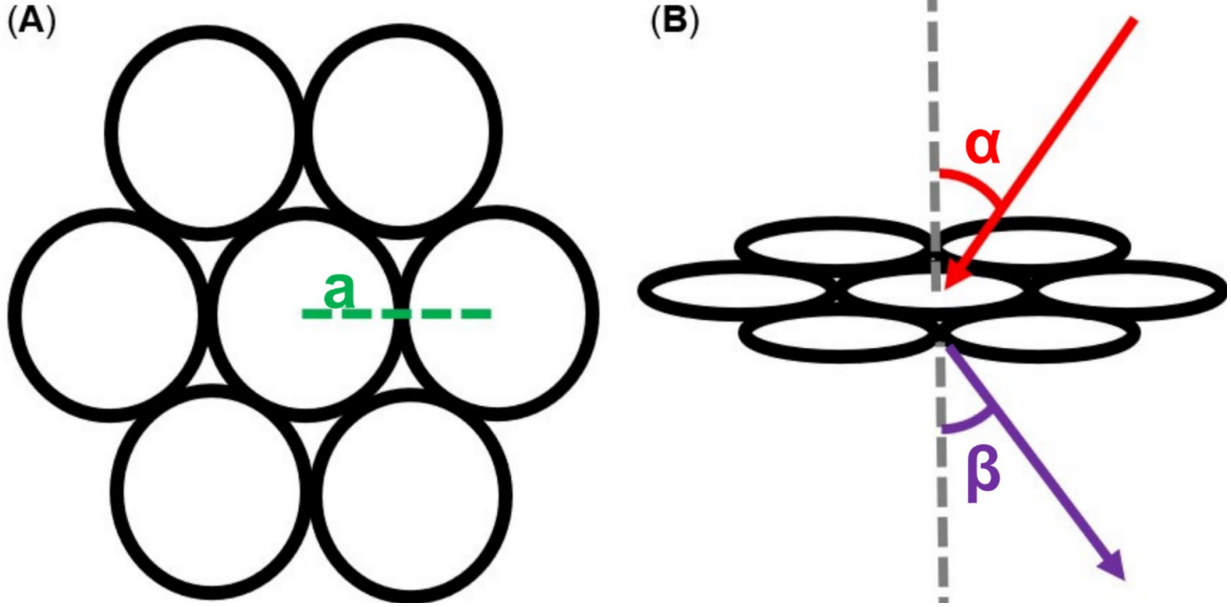


Figure 1.3: (A) 2D hexagonal lattice and (B) 2D Bragg diffraction on a hexagonal lattice. The particle spacing ( $a$ ), angle of incidence ( $\alpha$ ), and angle of diffraction ( $\beta$ ) are labelled accordingly.

The derivation of Equation 1.2 for a 2DPC hexagonal lattice can be understood through crystal lattice theory.<sup>54</sup> First, we define  $\mathbf{k}$  as a wavevector that describes the incident light. The magnitude of  $\mathbf{k}$  is described by Equation 1.3, where  $\lambda$  is the wavelength of light.

$$\|\mathbf{k}\| = \frac{2\pi}{\lambda} \quad \text{Equation 1.3}$$

We define  $\mathbf{k}'$  in a similar manner as a wavevector that describes the diffracted light. Since diffraction is an elastic phenomenon, the magnitudes of these wave vectors must be the same. Thus, Equation 1.4 holds.

$$\|\mathbf{k}\| = \|\mathbf{k}'\| \quad \text{Equation 1.4}$$

We can define a third vector,  $\mathbf{G}$ , as the sum of the projections of  $\mathbf{k}$  and  $\mathbf{k}'$  onto the PC lattice. A projection for an arbitrary vector,  $\mathbf{a}$ , onto another vector,  $\mathbf{b}$ , can be described by Equation 1.5, where  $\theta$  is the angle between  $\mathbf{a}$  and  $\mathbf{b}$ .

$$\text{Projection } \mathbf{a} \text{ on } \mathbf{b} = \|\mathbf{a}\| \cos \theta \quad \text{Equation 1.5}$$

Figure 1.4 shows a visual representation of the relationship between  $\mathbf{G}$ ,  $\mathbf{k}$ , and  $\mathbf{k}'$ .

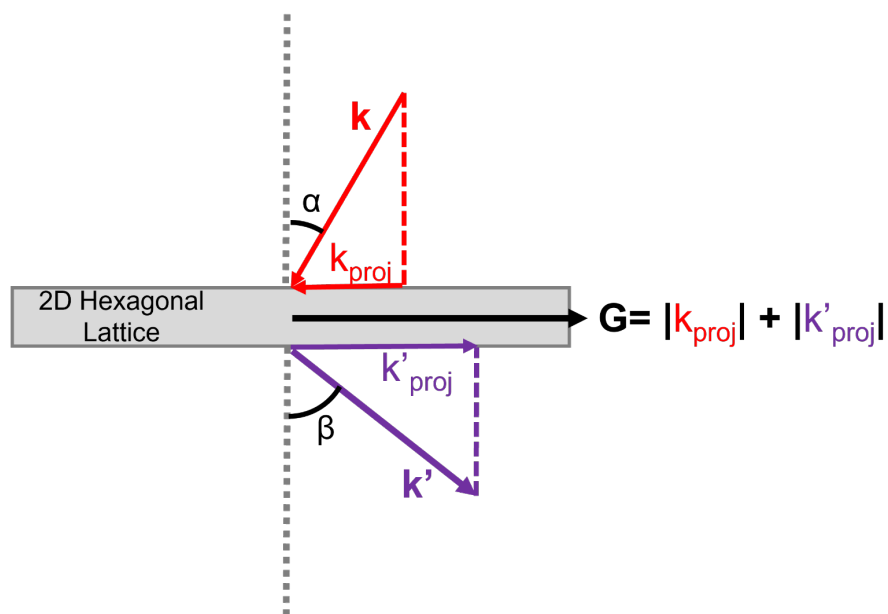


Figure 1.4: Vector representation of 2D hexagonal lattice diffraction.

Since the projections of  $\mathbf{k}$  and  $\mathbf{k}'$  are parallel to  $\mathbf{G}$ , the magnitude of  $\mathbf{G}$  can be defined by Equation 1.6.

$$\|\mathbf{G}\| = |k_{proj}| + |k'_{proj}| \quad \text{Equation 1.6}$$

From the above definitions and the geometry of the interaction between the light and the lattice as shown in Figure 1.4, Equation 1.7 can be derived.

$$\begin{aligned} \|\mathbf{G}\| &= \|\mathbf{k}\| \cos(90 - \alpha) \\ &+ \|\mathbf{k}'\| \cos(90 - \beta) = \|\mathbf{k}\| \sin \alpha + \|\mathbf{k}'\| \sin \beta \end{aligned} \quad \text{Equation 1.7}$$

The relationship between the 2D hexagonal lattice spacing,  $d$ , and the magnitude of  $\mathbf{G}$  is well understood for a hexagonal lattice as Equation 1.8.

$$d = \frac{2\pi}{\|\mathbf{G}\|} \quad \text{Equation 1.8}$$

Finally, Figure 1.5 shows the geometric relationship between the lattice spacing,  $d$ , and the 2DPC hexagonal particle spacing,  $a$ , as described by Equation 1.9.

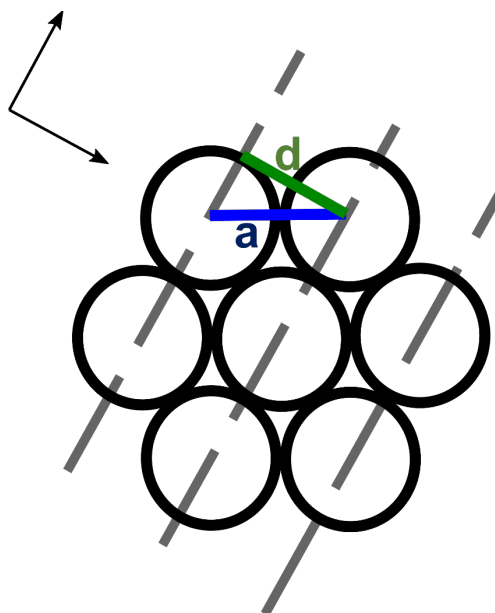


**Figure 1.5: Relationship between lattice spacing ( $d$ ) and particle spacing ( $a$ ) for a 2D hexagonal lattice.**

$$d = \frac{\sqrt{3}a}{2} \quad \text{Equation 1.9}$$

Combining Equations 1.3-1.9 gives Equation 1.2, the Bragg condition for a 2D hexagonal lattice. Importantly, the Bragg condition enables changes in the PC particle spacing,  $a$ , to be monitored through changes in the diffraction wavelength,  $\lambda$ , or diffraction angle,  $\beta$ .

#### **1.4 Stimuli-Responsive Hydrogels and Volume Phase Transitions**

Hydrogels are crosslinked polymer networks immersed in an aqueous mobile phase. Stimuli-responsive hydrogels can take in mobile phase and swell or expel mobile phase and shrink in response to changes in their chemical environment. These volume phase transitions (VPTs) can be described using Flory polymer theory as relieving hydrogel osmotic pressure.<sup>55</sup> Equation 1.10

defines osmotic pressure as the volume derivative of the change in Gibbs free energy of the hydrogel.

$$\Pi = -\frac{\partial \Delta G_{tot}}{\partial V} \quad \text{Equation 1.10}$$

The Gibbs free energy of the hydrogel can be further broken into three parts—a free energy of mixing, an elastic free energy, and an ionic free energy, as described by Equation 1.11.

$$\Pi = -\frac{\partial \Delta G_{mix}}{\partial V} - \frac{\partial \Delta G_{el}}{\partial V} - \frac{\partial \Delta G_{ion}}{\partial V} = \Pi_{mix} + \Pi_{el} + \Pi_{ion} \quad \text{Equation 1.11}$$

At equilibrium, these contributions to the hydrogel Gibbs free energy cancel, and the net osmotic pressure is zero. However, changes in the chemical environment that cause changes in the Gibbs free energy generate an osmotic pressure, and the hydrogel swells or shrinks until a new equilibrium is reached where the net osmotic pressure is again zero.<sup>55, 56</sup> Importantly, hydrogels designed with specific molecular recognition groups undergo chemoselective VPTs, enabling the development of highly specific sensors.

### 1.4.1 Free Energy of Mixing

The free energy of mixing arises from hydrogel polymer-mobile phase interactions, as described by Equation 1.12, where  $R$  is the universal gas constant,  $T$  is the temperature,  $V_s$  is the molar volume of the solvent,  $V_0$  is the dry hydrogel polymer volume,  $V$  is the volume of the swollen or shrunken hydrogel, and  $\chi$  is the Flory-Huggins Interaction Parameter.<sup>55, 57</sup>

$$-\frac{\partial \Delta G_{mix}}{\partial V} = -\frac{RT}{V_s} \left[ \ln \left[ 1 - \left( \frac{V_0}{V} \right) \right] + \left( \frac{V_0}{V} \right) + \chi \left( \frac{V_0}{V} \right)^2 \right] \quad \text{Equation 1.12}$$

The Flory-Huggins interaction parameter is a function of the solubility parameters of the hydrogel polymer and mobile phase solvent and evaluates the energy associated with polymer-solvent interactions.<sup>55</sup> Generally, if polymer-solvent interactions are energetically favorable, the hydrogel will take in mobile phase and swell, while if polymer-solvent interactions are energetically unfavorable, the hydrogel will expel mobile phase and shrink.

The Asher group has used free energy of mixing phenomena to fabricate sensors. For example, hydrogels were designed with carboxyl recognition groups. As pH increased from acidic to neutral conditions, the carboxyl groups ionized, resulting in more favorable polymer-solvent interactions that caused the hydrogel to swell.<sup>19</sup>

#### 1.4.2 Elastic Free Energy

Elastic free energy arises from the hydrogel crosslink density, as described by Equation 1.13, where  $R$  is the universal gas constant,  $T$  is the temperature,  $n_{cr}$  is the effective number of moles of crosslinked polymer chains in the hydrogel network,  $V_m$  is the volume of the initially prepared hydrogel, and  $V$  is the volume of the swollen or shrunken hydrogel.<sup>55, 57</sup>

$$-\frac{\partial \Delta G_{el}}{\partial V} = -\frac{RTn_{cr}}{V_m} \left[ \left( \frac{V_m}{V} \right)^{\frac{1}{3}} - \frac{1}{2} \left( \frac{V_m}{V} \right) \right] \quad \text{Equation 1.13}$$

The elastic free energy acts as a restoring force that counteracts contributions from the free energy of mixing and ionic free energy.<sup>55</sup> Hydrogels with a larger number of crosslinks swell less than hydrogels with fewer crosslinks. Similarly, removing crosslinks from a hydrogel at equilibrium causes the hydrogel to swell, while adding crosslinks causes the hydrogel to shrink.

The Asher group designed hydrogels with the protein Concanavalin A, a recognition group that binds mannan groups on the microbe *Candida albicans*.<sup>58</sup> The multivalent binding of the microbe to the hydrogel proteins created effective hydrogel crosslinks, causing the hydrogel to shrink.

### 1.4.3 Ionic Free Energy

The ionic free energy arises from the presence of charges on the hydrogel polymer network, as described by Equation 1.14, where  $R$  is the universal gas constant,  $T$  is the temperature,  $c_x$  is the concentration of mobile ions inside the hydrogel, and  $c_x^*$  is the concentration of mobile ions outside the hydrogel.<sup>55, 57</sup>

$$-\frac{\partial \Delta G_{ion}}{\partial V} = RT \sum_x (c_x - c_x^*) \quad \text{Equation 1.14}$$

Ions on the hydrogel polymer network attract mobile counter ions, generating a potential based on the difference between ions inside and outside of the hydrogel.<sup>59</sup> Mobile phase enters the hydrogel to alleviate this potential, causing the hydrogel to swell. Since this potential is dependent on the difference between mobile ions inside and outside the hydrogel, ionic free energy phenomena are screened in high ionic strength solutions.

The Asher group designed hydrogels with acetylcholinesterase molecular recognition groups that bind organophosphorus compounds.<sup>9</sup> Incorporation of the charged organophosphorus compounds into the hydrogel network generated an ionic osmotic pressure, causing the hydrogel to swell.

### **1.5 Two-Dimensional Photonic Crystal Hydrogel Sensors**

To fabricate 2DPC hydrogel sensors, a 2DPC array is embedded into a stimuli-responsive hydrogel.<sup>19</sup> This couples the 2DPC particle spacing to the hydrogel volume. Thus, changes in the chemical environment that actuate hydrogel VPTs can be readout through shifts in 2DPC diffraction. In this way, the chemical environment can be monitored through 2DPC diffraction shifts.

As shown in Figures 1.6 and 1.7, 2DPC diffraction shifts can be monitored as changes in wavelength or diffraction angle.<sup>19, 60</sup> Changes in wavelength correspond with changes in 2DPC color, and can be monitored using an absorption spectrometer, or by visual inspection.<sup>19</sup> Alternatively, changes in diffraction angle can be monitored using a reflectance spectrometer, or by measuring the Debye ring diameter.<sup>60, 61</sup>

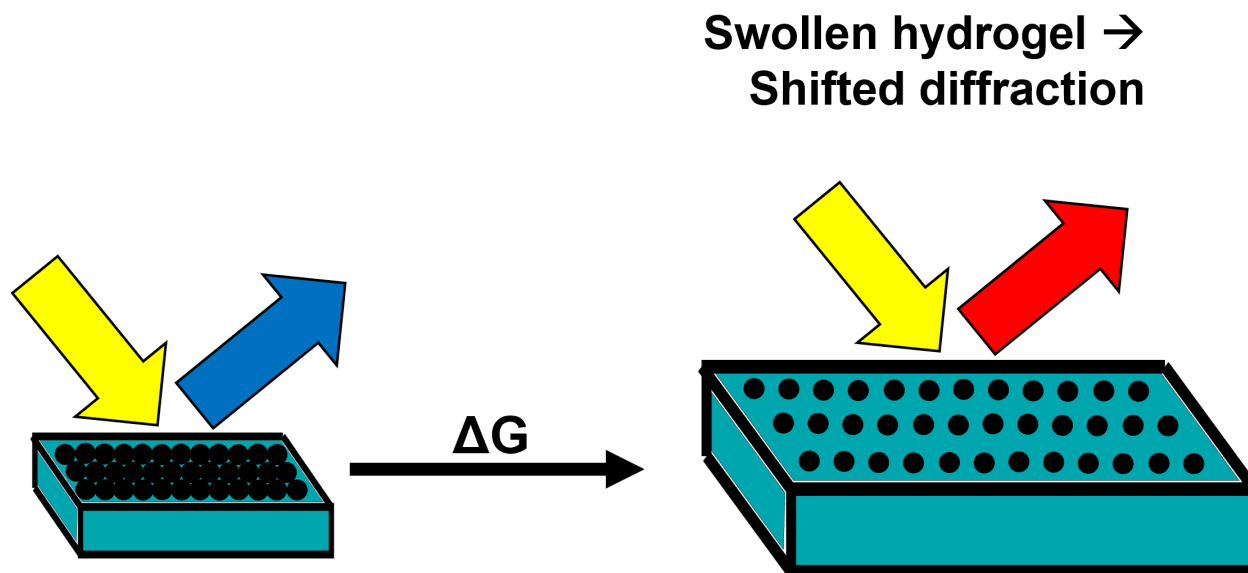


**Figure 1.6: 2DPC hydrogel volume changes actuate changes in 2DPC diffraction wavelength.**

Figure 1.7 shows a setup for measuring Debye ring diameter. Briefly, a 2DPC hydrogel is placed on an elevated stand. A laser pointer with wavelength  $\lambda$  penetrates the 2DPC hydrogel along its normal ( $\alpha = 0$ ), illuminating a Debye ring. The Debye ring consists of rays of light that have been diffracted at angle  $\beta$  according to the Bragg condition (see Equation 1.2).

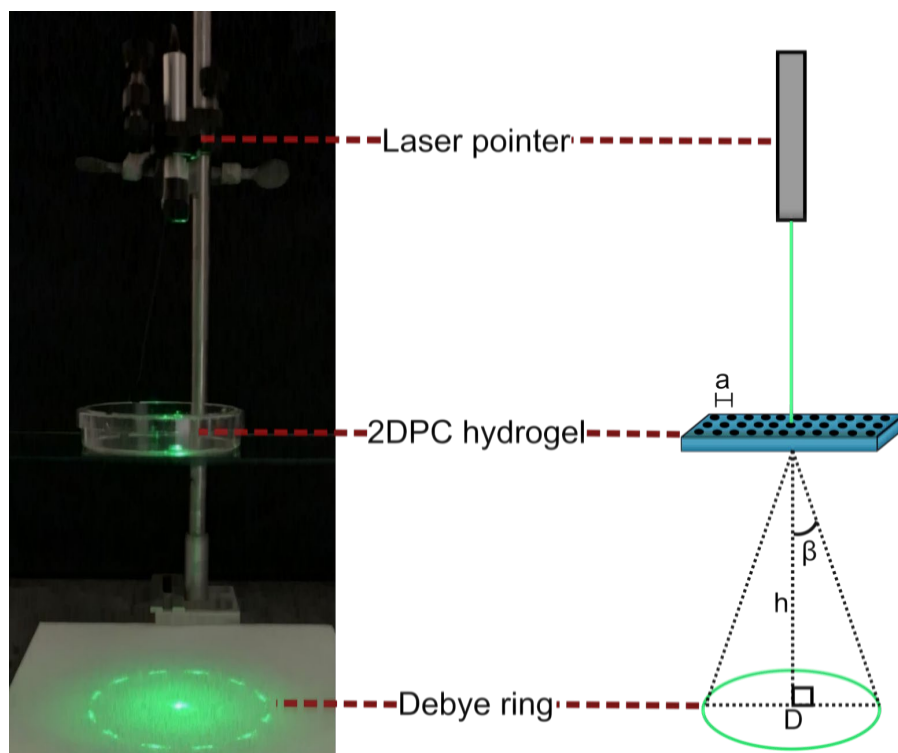


**Figure 1.7: Debye ring measurement setup.**

If the height,  $h$ , between the 2DPC hydrogel and Debye ring, and the Debye ring diameter,  $D$ , are known, then  $\beta$  can be calculated using Equation 1.15.

$$\beta = \tan^{-1}\left(\frac{D}{2h}\right) \quad \text{Equation 1.14}$$

Thus, the diffraction angle,  $\beta$  (Equation 1.15), and the 2DPC hydrogel particle spacing,  $a$  (Equation 1.2), can be simply monitored using a laser pointer and ruler.

These simple, colorimetric readouts are user-friendly and enable PC hydrogel operation with minimal to no equipment. These properties make PC hydrogel sensors accessible, even in

resource-limited settings. Sensitive and specific PC hydrogel sensors have been developed for a variety of targets, including ions<sup>57</sup>, small molecules<sup>28, 62</sup>, proteins<sup>63, 64</sup>, and whole cells<sup>58</sup>.

## **1.6 Overview of Research Program**

Herein, a novel 2DPC hydrogel sensing motif is presented using DNA-crosslinked hydrogels actuated by aptamer molecular recognition groups. Chapter 2 introduces DNA aptamers and provides pertinent background on DNA-crosslinked hydrogels. This chapter concludes with a theoretical description of our novel 2DPC hydrogel sensing motif. Chapter 3 features our proof-of-concept work applying our novel sensing motif to the detection of a small molecule, adenosine. This is the first reported aptamer-actuated 2DPC hydrogel sensor. In Chapter 4, we investigate the tunability of our sensing materials and discuss efforts to optimize their response for sensing applications. In Chapter 5, we demonstrate the generalizability of our sensing motif through detection of a protein, thrombin. This is the first report of an aptamer-actuated 2DPC hydrogel sensing motif being used to fabricate sensors for chemically diverse targets—a small molecule, adenosine, and a protein, thrombin. Finally, in Chapter 6, we summarize the important results of this dissertation and highlight future directions for this work.

## 2.0 DNA-Functionalized Hydrogel Sensors

Deoxyribonucleic acid (DNA) is a naturally occurring polymer that carries genetic information. In the last several decades, researchers have incorporated DNA into hydrogel polymer networks. More recently, DNA aptamers have emerged as molecular recognition agents that can bind to specific chemical targets and actuate selective hydrogel responses. This chapter introduces aptamers and DNA-functionalized hydrogels, and highlights preceding developments in these fields that inform this work. This chapter concludes with the theoretical basis for our novel sensing motif utilizing aptamer-actuated, DNA-crosslinked PC hydrogels.

### 2.1 DNA Aptamers as a Molecular Recognition Agent

Aptamers are short DNA or ribonucleic acid (RNA) strands that sensitively and specifically bind a chemical target.<sup>65, 66</sup> Discovered independently by Ellington<sup>65</sup> and Tuerk<sup>66</sup>, aptamers are selected through the in-vitro SELEX (Systematic Evolution of Ligands by Exponential Enrichment) process. Briefly, a library of  $\sim 10^{15}$  random oligonucleotide sequences are incubated with the intended chemical target. After incubation, unbound strands are removed, while strands that did bind are replicated and amplified. This cycle is repeated until only the sequences with the highest binding affinities remain.<sup>65, 66</sup>

Aptamers have binding affinities and specificities analogous to antibodies.<sup>65-68</sup> However, because they are nucleic acids and not proteins, and because they are selected in-vitro, they tend to be more stable and less expensive to produce than antibodies.<sup>67</sup> Aptamers for a variety of targets

have been reported, including ions,<sup>69</sup> small molecules,<sup>70-72</sup> proteins,<sup>73-76</sup> and whole cells<sup>77, 78</sup>. Aptamer dissociation constants can range from the  $\mu\text{M}$  to sub-nM.<sup>73, 79</sup> Since they are not degraded by ubiquitous ribonucleases, DNA aptamers tend to be more stable and easier to work with than their RNA counterparts.<sup>80</sup>

Given these advantages, aptamers are a compelling candidate for incorporation into sensing technologies as molecular recognition groups. Sensors containing aptamers are generally categorized as aptasensors.<sup>81</sup> Aptasensors have great variety, and their applications include colorimetric<sup>28, 69, 82</sup>, fluorometric<sup>83-85</sup>, and electrochemical<sup>86, 87</sup> assays. Furthermore, aptamers are increasingly replacing antibodies in immunoassays.<sup>88-91</sup> In response to the COVID-19 pandemic, several groups reported using aptamers to bind and detect SARS-CoV-2.<sup>76, 92-95</sup>

## 2.2 DNA-Crosslinked Hydrogels

In the early 1980's, Seeman pioneered the use of DNA as a building block for complex nanostructures and molecular machines.<sup>96-98</sup> Since then, there has been intense interest in the construction of hydrogel polymer networks that contain DNA.

One family of DNA-functionalized hydrogels involve “dangling” strands. In these hydrogels, one end of the DNA is attached to the hydrogel polymer network. The unattached end of the DNA dangles from the polymer network and more freely interacts with the surrounding chemical environment. This dangling sequence can be designed to interact with a chemical target, including a complementary DNA sequence<sup>99</sup>, nanoparticles<sup>100, 101</sup>, fluorescent dyes<sup>102</sup>, or, if the dangling end contains an aptamer sequence, an aptamer's binding target<sup>103</sup>.

In other hydrogels, DNA acts as a crosslinker, joining strands of the hydrogel polymer network. This family of DNA-functionalized hydrogels is most pertinent to the present work, and so will be the focus of the rest of this subchapter.

DNA can function as either a covalent or non-covalent crosslinker. As a covalent crosslinker, each end of the DNA is covalently attached to a different polymer strand in the hydrogel network, often via amine chemistry.<sup>28, 69</sup> These crosslinks are relatively inert, and thus their utility in triggering hydrogel sensing responses is limited compared to that of non-covalent crosslinks.<sup>28, 69</sup>

Examples of DNA as a non-covalent crosslinker are more diverse. The Luo group developed a procedure by which DNA strands are enzymatically elongated and entangle with each other.<sup>104</sup> The entanglements function as non-covalent crosslinks, enabling the formation of a hydrogel on introduction of an aqueous mobile phase. Depending on their environment, these DNA hydrogels can have either liquid-like or solid-like properties, in addition to other unique qualities, such as shape memory.<sup>104</sup> However, the formation of these hydrogels is non-specific, and they fail to take advantage of the unique tunability of DNA afforded by the hybridization of base pairs.

Nagahara and Matsuda were the first to use short DNA strands to form specific, non-covalent hydrogel crosslinks.<sup>105</sup> They synthesized complementary DNA strands capped with amino groups that were polymerized into polymer chains and hybridized to form physical crosslinks. On heating, the DNA melted, breaking crosslinks, causing the hydrogel to dissolve.<sup>105</sup> The Langrana group built upon these concepts and designed DNA-crosslinked hydrogels with tunable mechanical properties.<sup>106, 107</sup>

Figure 2.1 describes the working principle behind these hydrogels. Briefly, DNA strands capped with a phosphoramidite group are polymerized into polyacrylamide chains. The DNA

strands are complementary to a third strand, the Linker Strand. On addition of the Linker Strand, DNA hybridization induces the formation of crosslinks. Once a critical number of crosslinks are formed, a sol-to-gel transition occurs. The Linker Strand contains a single-stranded tail, dubbed the “toehold”, that is complementary to neither DNA sequence, and thus not involved in the hydrogel crosslinking. If a free DNA strand fully complementary to the Linker Strand is introduced, competitive hybridization, initiated at the toehold, induces the breaking of hydrogel crosslinks, actuating a gel-to-sol transition. After dissolution, reintroduction of the Linker Strand again actuates a sol-to-gel transition. In this way, hydrogels with tunable mechanical properties that undergo reversible phase transitions can be fabricated.<sup>106, 107</sup>

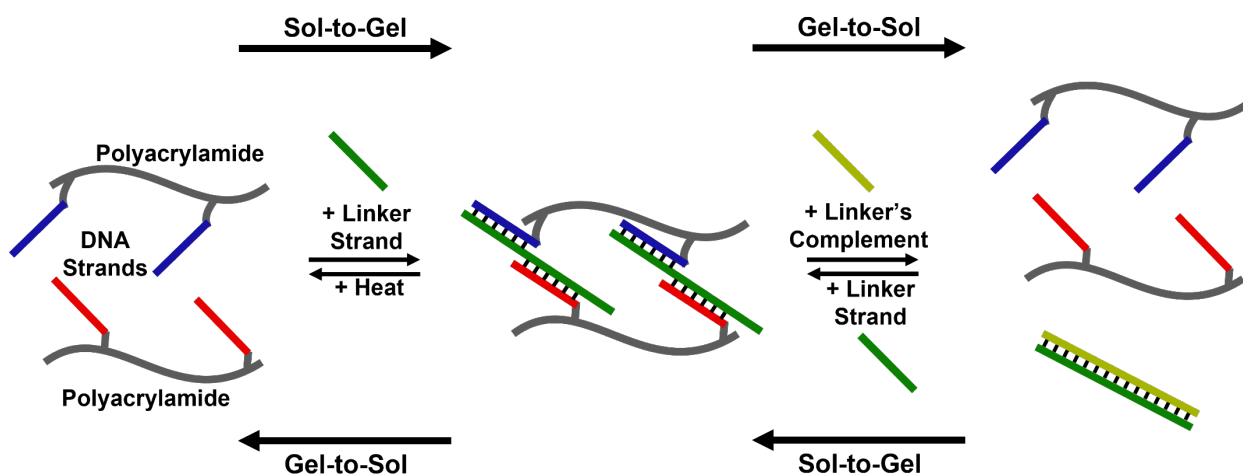


Figure 2.1: Hydrogel with DNA crosslinks that undergoes reversible sol-to-gel transitions.

These hydrogels can be designed to detect specific DNA sequences.<sup>108</sup> For example, a hydrogel designed such that the Linker Strand is complementary to a target DNA sequence will undergo a gel-to-sol transition in the presence of that target sequence. Thus, that target sequence can be detected through observation of a gel-to-sol transition. By utilizing branched DNA

networks, this sensing response can be used as a logic gate such that different stimuli actuate different responses.<sup>82</sup>

Nutiu and Li revolutionized the use of DNA as a sensing recognition group by developing a structure-switching assay utilizing DNA aptamers.<sup>83</sup> Their assay requires three DNA strands—FDNA, consisting of a DNA sequence modified with a fluorophore; QDNA, consisting of DNA modified with a quencher; and a reporter strand, a DNA sequence containing a portion complementary to FDNA, a portion complementary to QDNA, and an aptamer sequence that binds the target of the assay. Initially, the reporter strand hybridizes with the complementary sequences on the FDNA and QDNA. As a result of this hybridization, the fluorophore and quencher are in close proximity, resulting in maximum fluorescence quenching. On addition of the aptamer's binding target, aptamer-target binding causes the QDNA to dissociate from the reporter strand. This removes the quencher, causing an increase in fluorescence. Thus, the target concentration can be monitored through fluorescence measurements.<sup>83</sup>

The Tan group combined the reversible DNA-crosslinked hydrogel motif and aptamer structure-switching motif to develop a novel hydrogel sensor.<sup>109,110</sup> In their hydrogels, summarized in Figure 2.2, phosphoramidite-capped DNA is polymerized into polyacrylamide chains. The DNA is complementary to a third strand, the Linker Strand, such that on addition of the Linker Strand, the DNA hybridizes. This initiates a sol-to-gel transition, with the hybridized DNA acting as non-covalent hydrogel crosslinks. The Linker Strand contains an aptamer sequence. On addition of the aptamer's binding target, competitive aptamer-target binding causes the DNA to dissociate. This actuates a gel-to-sol transition. Thus, the aptamer's binding target can be detected through observation of the dissolution of the hydrogel.<sup>109</sup>

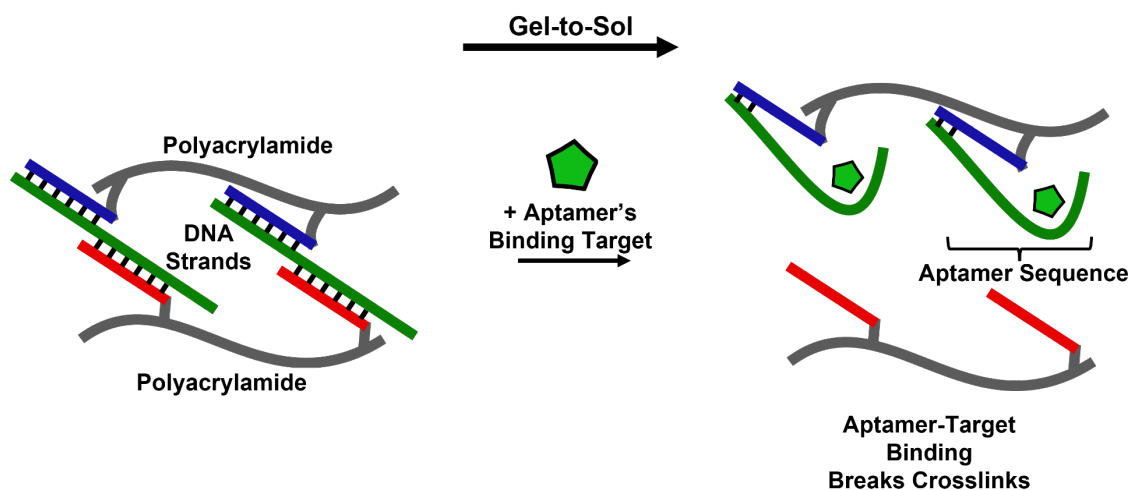


**Figure 2.2: DNA-crosslinked hydrogel with aptamer molecular recognition group.**

To improve the sensing response of their hydrogels, the Tan group trapped gold nanoparticles within the hydrogel network.<sup>109</sup> In this case, on addition of the aptamer's binding target, the dissociation of crosslinks causes the hydrogel to swell. This enables diffusion of the gold nanoparticles from within the hydrogel to the external, bulk solution. Thus, the aptamer's binding target can be monitored by measuring the absorption of the gold nanoparticles in the bulk solution.<sup>109</sup> Later, they coupled the hydrogel swelling with an enzymatic reaction that actuates an obvious color change in the presence of the aptamer's binding target.<sup>110</sup> Using these hydrogel-based sensing motifs, the Tan group developed sensors for small molecules<sup>109, 110</sup> and proteins<sup>109</sup>.

The Tan group further simplified this DNA-crosslinked sensing mechanism by reducing the number of DNA strands in the hydrogel from three to two, as summarized in Figure 2.3.<sup>109</sup> In these simplified hydrogels, polyacrylamide chains are prepared with grafted DNA sequences that are directly complementary. This eliminates the need for a third Linker Strand. On mixing of the polymer solutions, hybridization of the complementary strands induces the formation of crosslinks, actuating gelation. One of the DNA strands contains an aptamer sequence. As was the case in the

three-stranded system, on addition of the aptamer's binding target, competitive aptamer-target binding causes crosslinks to break, actuating hydrogel swelling, and ultimately dissolution. In this way, the sensing mechanism is maintained, while reducing the cost and complexity of fabrication.

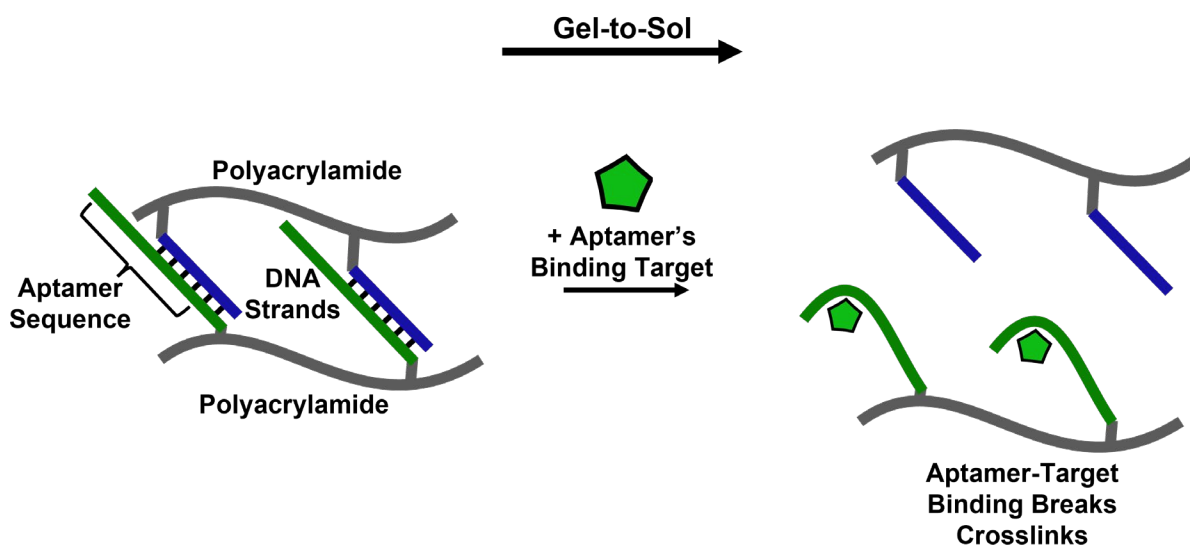


**Figure 2.3: Simplified DNA-crosslinked hydrogel for detection of chemical targets.**

While promising, these hydrogel sensors are qualitative. Quantitative determination of the concentration of the target would require further characterization of the hydrogel sensing response, in addition to external instrumentation. Furthermore, since the hydrogel crosslinks are non-covalent and reversible, these hydrogels lack the mechanical robustness of other sensing materials and can spontaneously dissolve over time.

The addition of stabilizing covalent crosslinks can improve the mechanical strength of DNA-crosslinked hydrogels. Recently, the Hill group has begun characterizing hydrogels with both non-covalent crosslinks formed by hybridized DNA and crosslinks that are covalently attached to the hydrogel polymer network.<sup>111-113</sup> These dual-crosslinked hydrogels are a promising

new avenue for designing highly responsive sensors that are also robust and long-lasting. However, more characterization is needed to better understand how these hydrogels behave in different chemical environments.

### **2.3 DNA-Functionalized Photonic Crystal Hydrogels**

With promising developments in DNA-functionalized hydrogel technology, there has been recent interest in incorporating these hydrogels into PC hydrogel sensors.

The Gu group developed 3DPC hydrogels that utilize covalent DNA crosslinks.<sup>69</sup> In these hydrogels, amine-capped DNA are covalently attached at either end to the hydrogel polymer network. The DNA crosslinks contain aptamer sequences that bind heavy metal ions—either mercury ions or lead ions. On addition of the aptamer's binding target, aptamer-target binding causes a DNA conformational change, effectively shrinking the length of the DNA crosslinks. This actuates shrinking of the hydrogel, which in turn decreases the PC lattice spacing, shifting PC diffraction. Thus, metal ion concentration can be monitored through PC diffraction shifts.<sup>69</sup>

This sensing motif involving shrinking DNA crosslinks was later applied to a 2DPC hydrogel to detect a small molecule, adenosine.<sup>28</sup> While promising, this sensing motif has two major shortcomings—(1) It relies on an aptamer-target-binding conformational change that is not universal to all aptamers, and thus is limited with respect to generalizability; and, (2) The change in diffraction is actuated by shrinking of the hydrogel, and thus the sensor response is limited by the diameter of the particles that make up the PC.

Later on, a more complex 2DPC hydrogel utilizing DNA double networks was designed for detection of pH and silver ions.<sup>114</sup> These sensors similarly rely on target-induced DNA

conformational changes that shrink the hydrogel. In addition to the above shortcomings, the added complexity of a DNA double network complicates fabrication and increases cost.

More recently, 2DPC hydrogels containing dangling DNA aptamers were fabricated to detect Human Immuno-Deficiency Virus-1 and SARS-CoV-2.<sup>115, 116</sup> According to these studies, introduction of the viral target actuates hydrogel swelling that can be monitored through 2DPC diffraction shifts. A mechanistic explanation for this phenomenon is not proposed, and so it is unclear if this sensing motif is generalizable to non-viral targets.<sup>115, 116</sup>

## **2.4 Aptamer-Actuated Photonic Crystal Hydrogel Sensing Motif**

In this work, we present a novel 2DPC hydrogel sensing motif that utilizes DNA-crosslinked hydrogels with aptamer molecular recognition groups. As summarized in Figure 2.4, a 2DPC array is embedded into a DNA-crosslinked hydrogel. The hydrogel contains both stabilizing covalent crosslinks and reversible, non-covalent DNA crosslinks. The DNA crosslinks are formed by hybridization of complementary DNA strands. One of the DNA strands contains an aptamer sequence. On addition of the aptamer's binding target, competitive aptamer-target binding breaks hydrogel crosslinks. This alters the elastic free energy of the system, causing the hydrogel to swell. Hydrogel swelling causes the 2DPC particle spacing to increase, shifting 2DPC diffraction. Thus, concentration of the aptamer's binding target can be monitored through shifts in 2DPC diffraction.

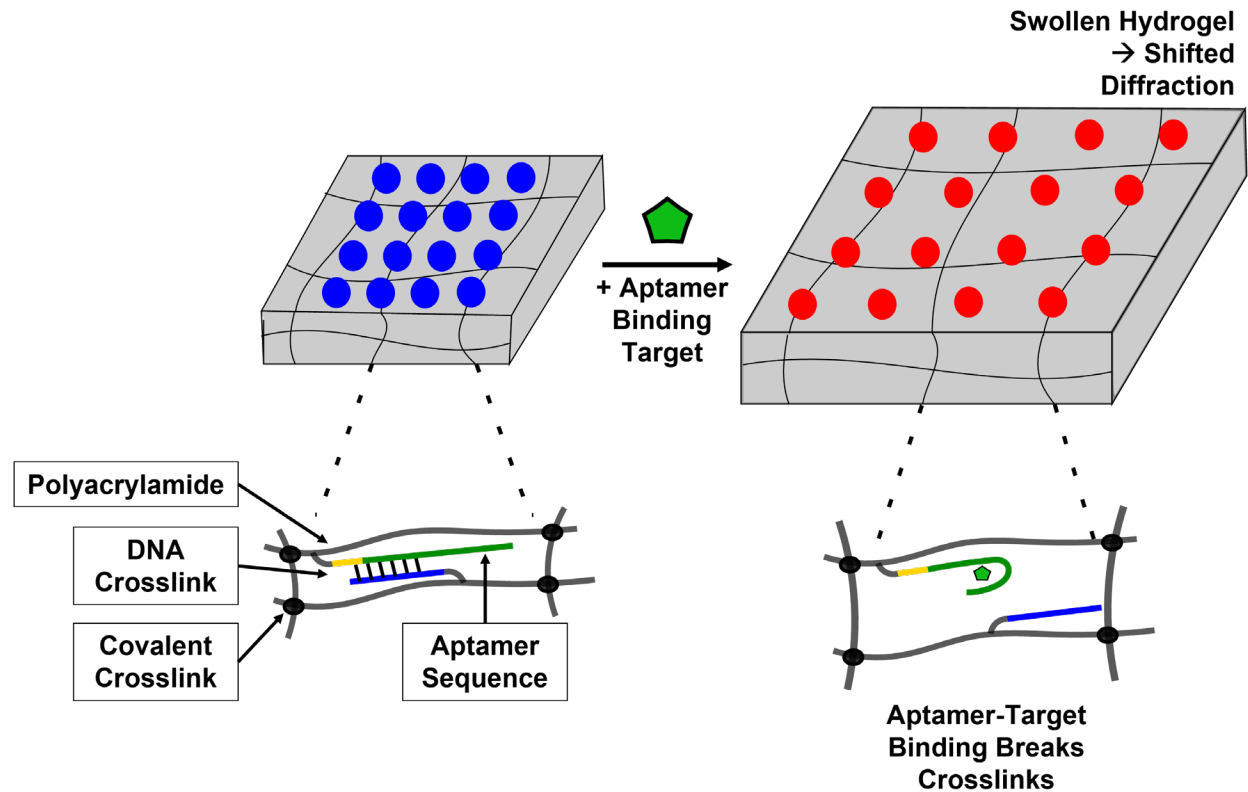


Figure 2.4: Aptamer-actuated, DNA-crosslinked 2DPC hydrogel sensing motif.

This sensing motif is simple, user-friendly, and requires minimal equipment to operate. 2DPC diffraction changes can be readout using a spectrometer, through visual inspection of PC hydrogel color, or via Debye ring measurements.

Unlike other DNA-functionalized PC hydrogel sensors, this sensing motif does not rely on a unique conformational change on aptamer-target binding. Thus, it is highly generalizable, and sensors for different targets can be fabricated by exchanging the aptamer recognition groups in the hydrogel. Furthermore, the sensing response relies on hydrogel swelling, and thus is not limited by 2DPC particle diameter.

In the rest of this work, we utilize this sensing motif to design and fabricate 2DPC hydrogel sensors that detect a small molecule, adenosine, and a protein, human thrombin. We further investigate the tunability of these materials to better optimize their sensing responses.

### 3.0 DNA- Crosslinked 2D Photonic Crystal Hydrogel Sensor for Detection of Adenosine Actuated by an Adenosine-Binding Aptamer

This chapter was previously published in the journal *ACS Sensors* as Jang, K.\*; Westbay, J. H.\*; Asher, S. A., DNA-Crosslinked 2D Photonic Crystal Hydrogels for Detection of Adenosine Actuated by an Adenosine-Binding Aptamer. *ACS sensors* **2022**, \* denotes co-first authors, and is reprinted with permission. J. H. W. and K. J., conceived experiments, and collected and analyzed data. The manuscript was prepared by J. H. W. and K. J. with assistance from S. A. A.

There is a need to develop versatile sensing motifs that can be used to detect a variety of chemical targets in resource-limited settings, for example, at the Point-of-Care. While numerous sensing technologies have been developed towards this effort, these technologies can be overly complex and require a skilled technician, extensive sample preparation, or sophisticated instrumentation to use, limiting their generalizability and application in resource-limited settings. Here we report a novel sensing motif that utilizes DNA-crosslinked two-dimensional photonic crystal (2DPC) hydrogels. These hydrogel sensors contain a DNA aptamer recognition group that binds a target analyte. As proof-of-concept, we fabricated 2DPC hydrogels using a well-studied adenosine-binding aptamer. This adenosine aptamer is duplexed with a partially complementary strand and forms responsive crosslinks in the hydrogel polymer network. When adenosine is introduced, aptamer-adenosine binding occurs, breaking the DNA crosslinks and causing the hydrogel to swell. This in turn increases the particle spacing of an embedded 2DPC array, shifting the 2DPC Bragg diffraction. Thus, adenosine concentration can be monitored through 2DPC Bragg diffraction measurements. A linear range of 20  $\mu\text{M}$  – 2 mM was observed. The detection limits were calculated to be 13.9  $\mu\text{M}$  in adenosine-binding buffer and 26.7  $\mu\text{M}$  in fetal bovine serum.

This reported sensing motif has a readout that is simple, rapid, and requires minimal equipment. We hypothesize that this sensing motif is generalizable and that other sensors can be easily fabricated by simply exchanging the aptamer that serves as a molecular recognition group.

### 3.1 Introduction

There is a need to develop sensing motifs that are generalizable and can be used in resource-limited settings, especially at the Point-of-Care.<sup>1</sup> Developing accessible Point-of-Care sensors that operate outside of a laboratory without the need for skilled technicians would save time, improve patient compliance, and reduce health care costs.<sup>4, 117</sup> For example, easy-to-use glucose monitoring devices have significantly improved outcomes for patients with insulin-dependent diabetes mellitus.<sup>5</sup>

Recently, various sensing methods have been reported utilizing aptamers. Aptamers are short, single-stranded RNA or DNA that are selected using the systemic evolution of ligands by exponential enrichment (SELEX) process to specifically bind chemical targets.<sup>65, 66</sup> Aptamers have specificities and binding affinities analogous to antibodies but are generally more stable, easier to engineer, and less expensive to produce, thus they have been widely used in recent sensor development.<sup>67, 118</sup> For example, aptasensors have been developed utilizing technologies such as FRET,<sup>119, 120</sup> fluorescence,<sup>121, 122</sup> SPR spectroscopy,<sup>123, 124</sup> and electrochemistry.<sup>125, 126</sup> While these sensing methods offer high specificity and sensitivity, they can require a skilled technician, extensive sample preparation, and/or sophisticated instrumentation, limiting their application in resource-limited environments.

Low-cost photonic crystal (PC) hydrogel sensors are a simple sensing platform that have been fabricated for a variety of chemical targets including pH,<sup>127, 128</sup> ions,<sup>69, 129</sup> small molecules,<sup>62, 127, 130-134</sup> and proteins.<sup>63, 64</sup> PC hydrogels consist of a periodic PC array embedded in a stimuli-responsive hydrogel. The stimuli-responsive hydrogel contains molecular recognition groups that actuate specific volume phase transitions (VPT) in the presence of target analytes. The target-induced VPT are monitored by shifts in the PC Bragg diffraction and used to quantify analyte concentrations.<sup>60, 135</sup> These PC sensors require minimal or no sample preparation and have simple, colorimetric readouts, ideally positioning the PC hydrogels for use in resource-limited settings.

Recently, the Gu group utilized PC hydrogels with aptamers to develop sensors for metal ions.<sup>69, 136</sup> They covalently attached  $\text{Pb}^{2+}$ ,  $\text{Hg}^{2+}$ , and  $\text{Ag}^+$ -binding aptamers to PC hydrogels. Upon binding the target metal ion, each aptamer underwent a specific hairpin-like conformational change that shrank the hydrogel, blue-shifting PC array diffraction. This specific sensing motif is limited in versatility because not all aptamers undergo these hairpin-like conformational changes that trigger hydrogel VPT and PC diffraction shifts on binding target molecules.

Here, we report the development of novel DNA-crosslinked two-dimensional (2D) PC hydrogels. This sensing motif utilizes duplexed DNA crosslinks that do not rely on a specific conformational change, and thus are generalizable to any aptamer-target interaction.<sup>109, 110</sup> As proof-of-concept, we fabricated hydrogel sensors using a well-studied adenosine-binding aptamer.<sup>79, 137</sup> Adenosine is an endogenous, regulatory molecule that frequently serves as a model small molecule in aptamer studies.<sup>109, 138-141</sup> We fabricated an adenosine-binding PC hydrogel by attaching a 2DPC array to a DNA-crosslinked hydrogel containing the adenosine-binding aptamer. In the presence of adenosine, competitive aptamer-adenosine binding occurs and breaks the DNA crosslinks. This generates an osmotic pressure in the system that actuates hydrogel swelling. The

hydrogel swelling in turn increases the particle spacing of the embedded 2DPC array and shifts the 2DPC Bragg diffraction. These adenosine-induced particle spacing changes were monitored through 2DPC diffraction measurements and used to quantify the concentration of adenosine. The limit of detections (LoDs) are calculated to be 13.9  $\mu\text{M}$  in adenosine-binding buffer and 26.7  $\mu\text{M}$  in 50% protein-removed fetal bovine serum (FBS) (detection time = 30 min).

The reported DNA-crosslinked 2DPC hydrogels require minimal equipment and sample preparation to use, ideally positioning them for application in resource-limited settings. We hypothesize that this sensing motif is generalizable, and sensors for other targets can be fabricated by simply exchanging the aptamer molecular recognition group. Aptamers for a wide variety of targets including ions,<sup>69, 136</sup> small molecules,<sup>70-72</sup> proteins,<sup>73-76</sup> and whole cells<sup>77, 78</sup> with sub- $\mu\text{M}$  dissociation constants have been reported, enabling the development of versatile sensors with ultralow limits of detection.

## 3.2 Experimental

### 3.2.1 Materials

Acrydite-modified DNA strands (DNA 1: 5'-acrydite-AGA GAA CCT GGG GGA GTA TTG CGG AGG AAG GT-3', DNA 2: 5'-acrydite-CCC AGG TTC TCT-3', DNA 3: 5'-acrydite-AGA GAA CCT GGG GGA GTA ATG CGG AGC AAG GT-3', purified with high performance liquid chromatography) were purchased from Integrated DNA Technologies. Stock solutions of DNA 1, 2, and 3 were prepared separately at 2 mM concentration in TE buffer (10 mM Tris, pH 8.0; 0.1 mM EDTA) and stored at -20 °C. Tris base ( $\geq 99.9\%$ ), magnesium chloride, HEPES (99%),

sodium hydroxide pellets ( $\geq 97\%$ ), sodium styrene sulfonate (NaSS) ( $\geq 90\%$ ), 2,2'-Azobisisobutyronitrile (AIBN) (98%), styrene (99%), acrylamide ( $\geq 99\%$ ), N,N'-methylenebisacrylamide (MBAAm) (99%), ammonium persulfate (98%), tetramethylethylenediamine (TEMED) (99%), adenosine ( $\geq 99\%$ ), cytidine (99%), uridine ( $\geq 99\%$ ), and guanosine (98%) were purchased from Sigma-Aldrich. Ethylenediaminetetraacetic acid (EDTA) (99.5%) was purchased from JT Baker. Sodium chloride was purchased from EMD Millipore. Hydrochloric acid (36.5-38% w/w), potassium acetate (99%), methanol (99.8%), and 2-propanol ( $\geq 99.5\%$ ) were purchased from Thermo Fisher Scientific. Ethanol (200 proof) was purchased from Decon Labs, Inc. Quant-iT PicoGreen dsDNA Assay Kit was purchased from Invitrogen. Cover glass (thickness 1,  $24 \times 60 \text{ mm}^2$ ) and FBS were purchased from Corning. To remove serum proteins, FBS was filtered using 10 kDa centrifugal filters. Microscope premium frosted glass slides ( $25 \times 75 \times 1 \text{ mm}^3$ ) were purchased from Fisher Scientific. All chemicals were used as received unless otherwise specified. Ultrapure water ( $18.2 \text{ m}\Omega \cdot \text{cm}$ ) obtained from a Milli-Q Reference A+ was used for all experiments.

### **3.2.2 Annealing DNA Strands**

DNA annealing solution was prepared by adding 20  $\mu\text{L}$  each of stock DNA 1 and DNA 2 solutions (2 mM concentration prepared in TE buffer) to a 160  $\mu\text{L}$  solution of 1.25X duplex buffer. The DNA annealing solution contained the following components: 200  $\mu\text{M}$  of DNA 1 and DNA 2; 1X duplex buffer (30 mM HEPES, pH 7.5; 100 mM potassium acetate); and 0.2X TE buffer. To ensure thorough mixing, the solution was pipetted up and down 20 times, then centrifuged at 1,000 RCF for 30 sec. The solution was then heated to 95  $^{\circ}\text{C}$  on a Corning LSE Digital Dry Bath Heater for 5 min and cooled at room temperature for 30 min. For the fluorescence assay, the

annealed DNA solution was used as is. For 2DPC hydrogel fabrication, the annealed DNA solution was dried on a Labconco Centrivap Concentrator (78100-00 A) for 6 h.

### 3.2.3 PicoGreen Fluorescence Assay

A PicoGreen fluorescence assay was used for optimization of aptamer-adenosine binding buffer. The assay procedure was modified from that of Lv et al.<sup>85</sup> A solution of annealed DNA was diluted with the following three different buffer solutions to a final concentration of 2  $\mu\text{M}$  DNA: (i) duplex buffer (30 mM HEPES, pH 7.5; 100 mM potassium acetate), (ii) TNM (5 mM  $\text{MgCl}_2$ ) (20 mM Tris, pH 7.5; 300 mM NaCl; 5 mM  $\text{MgCl}_2$ ), (iii) TNM (10 mM  $\text{MgCl}_2$ ) (20 mM Tris, pH 7.5; 300 mM NaCl; 10 mM  $\text{MgCl}_2$ ). For samples containing only DNA, a 300  $\mu\text{L}$  solution of 40 nM DNA was prepared in each of the three buffers by diluting an aliquot of the 2  $\mu\text{M}$  DNA solution. For samples containing DNA and adenosine, a 300  $\mu\text{L}$  solution of 40 nM DNA and 400  $\mu\text{M}$  adenosine was prepared in each of the three buffers. After mixing the DNA and adenosine solutions, the mixture was stored on a laboratory bench at room temperature under aluminum foil for 30 min to allow time for aptamer-adenosine binding. A 300  $\mu\text{L}$  solution of 200X diluted PicoGreen, prepared in the same buffer as each DNA sample, was added to 300  $\mu\text{L}$  of each DNA sample. This final solution was pipetted up and down 15 times, then transferred to a quartz cuvette after 3 min. Fluorescence spectra were measured in triplicate for each sample using a HORIBA Jobin Yvon Fluoromax-3 Spectrofluorometer with 480 nm excitation, 525 nm emission, and slit widths of 2 nm for excitation and emission. Blank PicoGreen fluorescence in the three different buffers was measured separately. The background signal in the corresponding buffer was subtracted from each DNA measurement.

### 3.2.4 2DPC Hydrogel Fabrication

Negatively charged polystyrene (PS) particles with diameter 1.21  $\mu\text{m}$  were synthesized by dispersion polymerization using methods described by Zhang et al.<sup>48</sup> These PS particles (12% (w/w) in water) were mixed in a 3:1 ratio with 2-propanol. Using our previously reported needle tip flow method,<sup>142, 143</sup> this dispersion was injected at the air-water interface of a crystallization dish (Figure 3.1a). Then, the PS particles were self-assembled into a hexagonally closed-packed 2DPC array monolayer (Figure 3.1b). A glass substrate (24  $\times$  60  $\text{mm}^2$ , cover glass, Corning) was used to pick up the 2DPC array (Figure 3.1c), and the 2DPC array was dried at room temperature for 24 h (Figure 3.1d). Tape was applied in two layers onto the 2DPC array glass substrate to section off a 2.4  $\times$  1  $\text{cm}^2$  strip of the 2DPC array (Figure 3.1e). Polymerizable monomer solutions were prepared using the compositions described in Table 3.1. The monomer solutions were degassed in a vacuum desiccator for 15 min. After adding initiators (0.7  $\mu\text{L}$  of 5% (v/v) TEMED in water and 0.7  $\mu\text{L}$  of 10% (w/v) ammonium persulfate in water), the mixtures were stirred for 5 sec using a micropipette tip and then were deposited onto the preformed 2DPC array glass substrate (2.4  $\times$  1  $\text{cm}^2$ ) (Figure 3.1e). A glass slide cover (25  $\times$  75  $\times$  1  $\text{mm}^3$ , microscope premium frosted glass slides, Fisher Scientific) was placed over the solution. Then, polymerization occurred under vacuum in a desiccator for 30 min. The resulting cross-linked polymer embedded the 2DPC array into the hydrogel network (Figure 3.1f). After polymerization, the sandwiched glass substrates containing the 2DPC hydrogel were placed in buffer (20 mM Tris, pH 7.5; 10 mM  $\text{MgCl}_2$ ; 300 mM NaCl) for 10 min. The glass substrates were separated using a razorblade, and the 2DPC hydrogel was peeled off the substrate. The 2DPC hydrogel was washed in buffer for 3 min and cut into 0.4  $\times$  0.5  $\text{cm}^2$  pieces. Each piece was stored in a refrigerated, sealed petri dish without buffer.

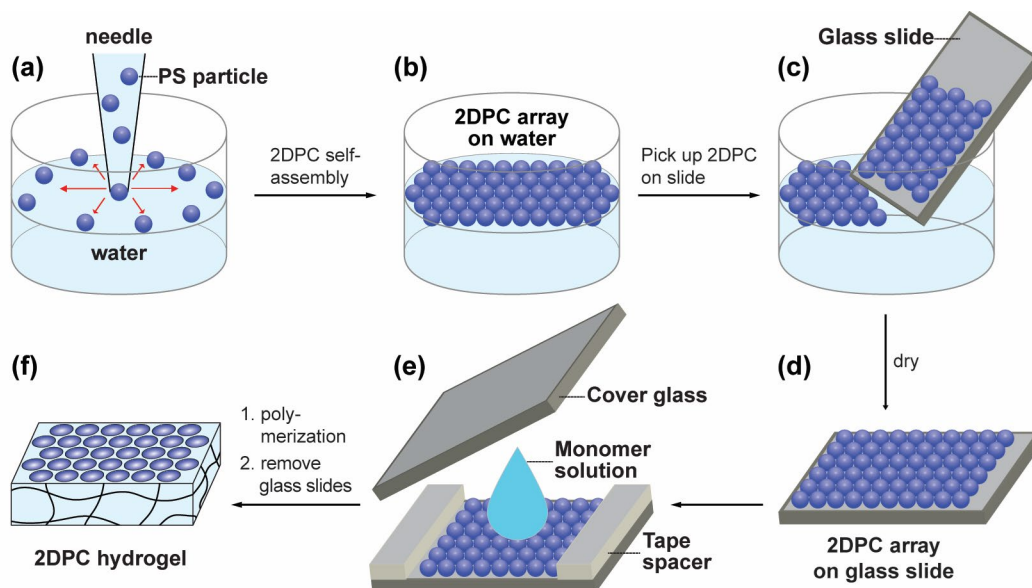


**Figure 3.1: Method for fabricating 2DPC hydrogels. (a-e)** A polymerizable monomer solution was layered on top of a pre-formed 2DPC array on a glass slide. A cover glass sealed the solution, after which polymerization proceeded for 30 min at room temperature. **(f)** The resulting cross-linked polymer embedded the ordered 2DPC array monolayer within the hydrogel network (2DPC hydrogel).

**Table 3.1: Composition of monomer solutions used in preparation of hydrogel samples**

Component	Concentration
Acrylamide	25% (w/v)
MBAAm	0.02% (w/v)
Hybridized (annealed) DNA strands	0.8 mM
Total volume	50 $\mu$ L

### 3.2.5 Scanning Electron Microscopy Characterization

Periodic orderings of the close-packed 2DPC monolayer (Figure 3.2a) and the non-close-packed 2DPC monolayer embedded in swollen hydrogels (Figure 3.2b) were monitored using a field emission SEM (Zeiss Sigma 500 VP) with an SE2 detector at an accelerating voltage of 3 kV

(2DPC) or 5 kV (2DPC hydrogel). For SEM characterization, swollen 2DPC hydrogels were sandwiched between glass slides and dried. Before taking SEM images, the samples were sputter-coated with gold for 75 sec at 30 mA using an auto sputter coater (PELCO SC-7).

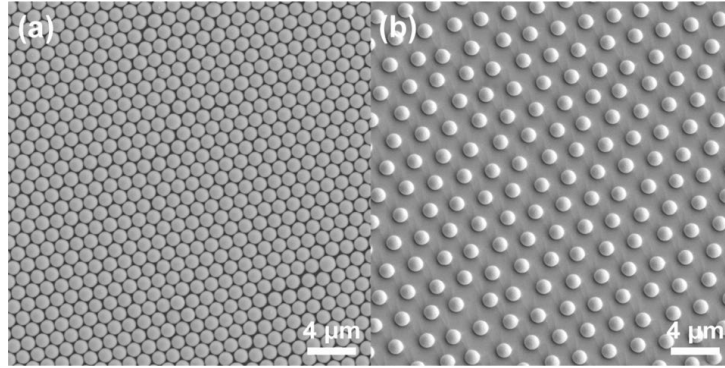


**Figure 3.2: SEM images of (a) the close-packed 2DPC monolayer and (b) the non-close-packed 2DPC monolayer embedded in a hydrogel.**

### 3.2.6 2DPC Particle Spacing Measurements

Adenosine-induced hydrogel swelling was monitored through 2DPC particle spacing measurements using described methods.<sup>61</sup> Briefly, Equation 3.1 gives the condition for Bragg diffraction of a hexagonally close-packed 2DPC array where  $m$  is the order of diffraction,  $\lambda$  is the wavelength of light,  $d$  is the 2DPC array nearest neighbor particle spacing, and  $\alpha$  and  $\beta$  are the angle of incidence and diffraction, respectively.

$$m\lambda = \frac{\sqrt{3}}{2}d(\sin \alpha + \sin \beta) \quad \text{Equation 3.1}$$

As shown in Figure 3.3, 2DPC hydrogels were excited along their normal with a 532 nm laser pointer, eliminating dependence on the angle of incidence ( $\alpha = 0$ ). A perfectly ordered 2DPC array shows six spots diffracted at angle  $\beta$ .<sup>144</sup> 2DPC arrays with small rotational disorder diffract a Debye ring pattern.<sup>61, 62</sup> Equation 3.2 relates Debye ring diameter to  $\beta$ , where  $D$  is the Debye ring diameter and  $h$  is the distance between the 2DPC array and the Debye ring plane.

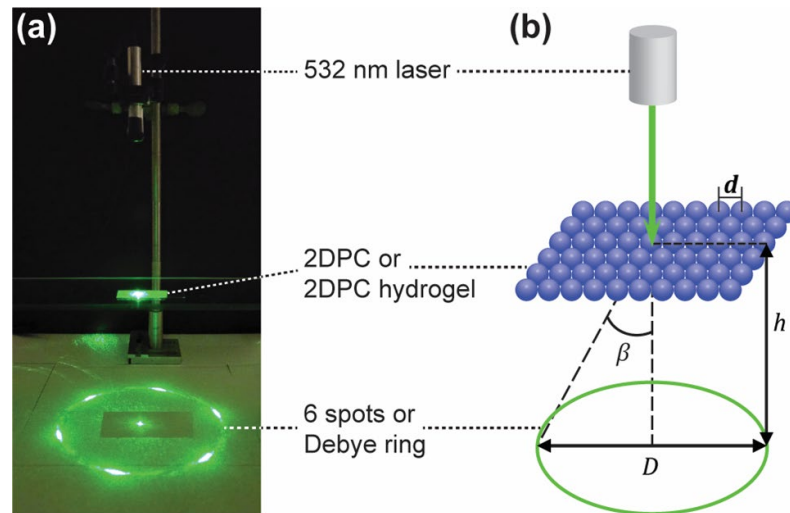


**Figure 3.3: 2DPC hydrogel particle spacing measurement. A 2DPC hydrogel piece was placed on a stand above a white screen. (a) Experimental setup and (b) schematic diagram showing the Debye ring illuminated by a 532 nm laser.**

$$\beta = \tan^{-1}\left(\frac{D}{2h}\right) \quad \text{Equation 3.2}$$

Equations 3.1 and 3.2 combine to give Equation 3.3.

$$d = \frac{2\lambda}{\sqrt{3} \sin\left(\tan^{-1}\left(\frac{D}{2h}\right)\right)}$$

**Equation 3.3**

$h$  was fixed at 15 cm and  $\lambda$  of the light source was known (532 nm). Thus, particle spacing was monitored by measuring  $D$ . To calculate  $d$ , we measured and averaged different  $D$  values from five different positions within each 2DPC hydrogel sample.

### **3.2.7 Adenosine Sensing in Buffer Solutions**

2DPC hydrogel pieces were brought to room temperature on a lab bench and each was incubated in 10 mL of adenosine-binding buffer solution (20 mM Tris, pH 7.5; 10 mM MgCl<sub>2</sub>; 300 mM NaCl). After 10 min, the initial particle spacing of the 2DPC hydrogels was measured. The hydrogel pieces were then each submerged in 20 mL of adenosine-binding buffer solution containing 0 (blank) to 2 mM adenosine. Particle spacing measurements were made at time intervals of 5, 15, 30, and 60 min. For control measurements, 2DPC hydrogel pieces were each submerged in 20 mL of adenosine-binding buffer solution containing 1 mM of either adenosine, cytidine, guanosine, or uridine. The particle spacing was measured after 30 min of incubation. Each measurement was repeated 3 times using a different gel piece.

### **3.2.8 Adenosine Sensing in Fetal Bovine Serum**

Protein-removed FBS was diluted to 50% with serum diluting buffer (40 mM Tris, pH 7.5; 19 mM MgCl<sub>2</sub>; 450 mM NaCl). The final salt concentration of the 50% protein-removed FBS was

the same as that of the pure adenosine-binding buffer (20 mM Tris, pH 7.5; 10 mM MgCl<sub>2</sub>; 300 mM NaCl).

2DPC hydrogel pieces were brought to room temperature on a lab bench and each was incubated in 10 mL of adenosine-binding buffer solution (20 mM Tris, pH 7.5; 10 mM MgCl<sub>2</sub>; 300 mM NaCl). After 10 min, the initial particle spacing of the 2DPC hydrogels was measured. The 2DPC hydrogel pieces were then each submerged in 10 mL of 50% protein-removed FBS containing 0 (blank) to 2 mM adenosine. The particle spacing was measured after 30 min of incubation. Each measurement was repeated 3 times using a different gel piece.

### **3.3 Results and Discussion**

#### **3.3.1 Adenosine Sensing Motif Using DNA-Crosslinked 2DPC Hydrogels That Contain the Adenosine-Binding Aptamer**

Figure 3.4 shows a simplified representation of our DNA-crosslinked 2DPC hydrogel and its adenosine-sensing mechanism. As described in Chapter 3.2.4, the hydrogels were copolymerized with acrylamide, MBAAm, and the DNA strands onto pre-formed 2DPCs. The polyacrylamide backbone chains and the additional covalent MBAAm crosslinks ensured that the hydrogels were mechanically robust enough to embed the 2DPC array. To find the optimal 2DPC hydrogel fabrication conditions, we systematically varied the concentrations of acrylamide and MBAAm (see Appendix A.2). The DNA strands were modified with acrydite, an acrylic phosphoramidite group with similar activity to that of the acrylamide monomer.<sup>145</sup> This modification enabled covalent incorporation of the DNA into the hydrogel polymer network.

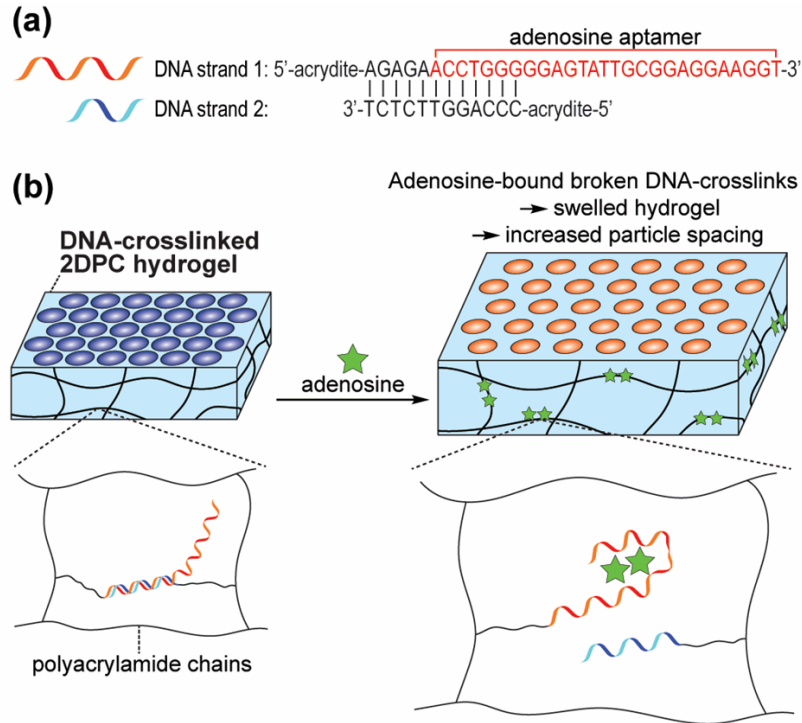


**Figure 3.4: (a) Sequences of DNA strands that form adenosine-responsive crosslinks in the hydrogel. (b) Schematic diagram of the adenosine-sensing mechanism using a DNA-crosslinked 2DPC hydrogel.**

For this proof-of-concept study, we utilized a 32-mer DNA strand 1 and a 12-mer DNA strand 2 (Figure 3.4a) based on Yang et al.'s work that demonstrated the fabrication of DNA-crosslinked hydrogels.<sup>109</sup> DNA strand 1 contains an adenosine-binding aptamer segment in its sequence. Without adenosine, DNA strand 1 hybridizes with DNA strand 2 and forms 12 base pairs that are stable enough to serve as DNA crosslinks in the hydrogels. Upon addition of adenosine, the adenosine aptamer segment in DNA strand 1 competitively binds adenosine with high affinity, resulting in an aptamer conformational change (Figure 4b). This conformational change breaks the pre-formed DNA base pairs (or DNA crosslinks), which in turn decreases the elasticity of the hydrogel network and generates an osmotic pressure.<sup>55, 146</sup> As a result, the hydrogel swells by absorbing water to relieve this pressure as the system reaches a new equilibrium where

the net osmotic pressure evolves to zero.<sup>55, 146</sup> This adenosine-induced hydrogel swelling homogeneously increases the particle spacing of the embedded 2DPC array, maintaining the hexagonal ordering. This shifts the Bragg diffraction angle in proportion to the amount of adenosine present. Based on preliminary data, the 2DPC hydrogels were fabricated with the chosen DNA concentration that showed large enough particle spacing changes in response to adenosine.

### **3.3.2 Optimizing Adenosine-Binding Buffer Conditions via Fluorometric Quantitation of dsDNA Using PicoGreen**

Buffer conditions can affect the binding affinity and stability of DNA aptamers.<sup>147, 148</sup> For the adenosine-binding aptamer used as a recognition agent, several different salt concentrations were previously examined.<sup>79, 85, 109, 141</sup> In particular, it has been reported that  $Mg^{2+}$  may play an important role in assisting the adenosine-binding aptamer because the salt stabilizes the structure of the aptamer-adenosine complex.<sup>149, 150</sup> However, different sources suggest different amounts of  $Mg^{2+}$  for optimal aptamer-adenosine binding.

Thus, to optimize buffer conditions in our 2DPC hydrogel system, we utilized a PicoGreen assay. PicoGreen is an intercalating dye that becomes more fluorescent on binding to dsDNA, compared to single-stranded DNA (ssDNA) or RNA.<sup>151, 152</sup> Since our adenosine-sensing motif involves a DNA conformational change from dsDNA to ssDNA upon adenosine-binding, PicoGreen can be used to monitor the extent of adenosine-binding by measuring fluorescence signal changes.

Figure 3.5 shows the PicoGreen assay data for optimization of aptamer-adenosine binding buffer. We compared PicoGreen fluorescence in samples of hybridized DNA before and after incubation with adenosine under different buffer conditions. When the hybridized DNA

aptamer binds adenosine, its competitive binding breaks DNA hybridization and converts dsDNA to ssDNA. As a result, the fluorescence emission decreases because PicoGreen fluorescence is more enhanced in the presence of dsDNA than ssDNA. Thus, the largest decrease in relative fluorescence indicates maximal aptamer-adenosine binding.<sup>85</sup>

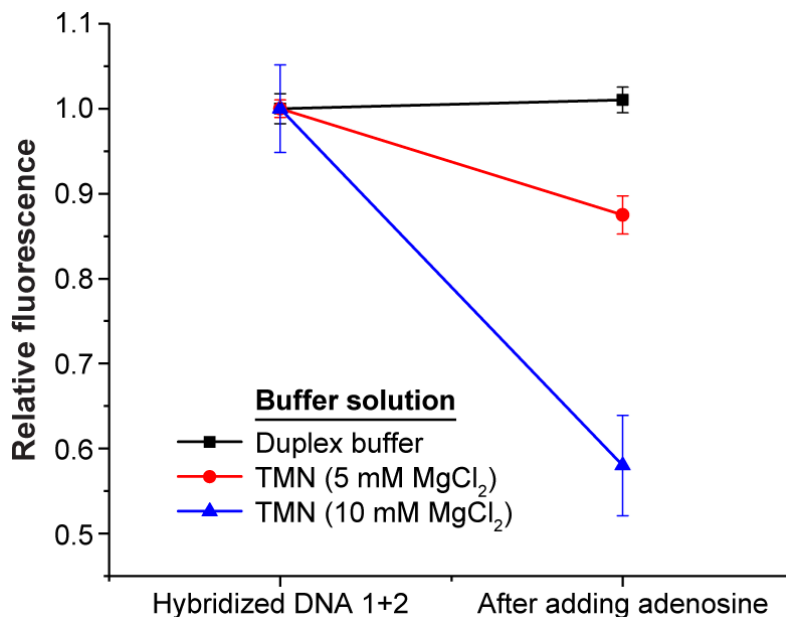


**Figure 3.5: Quantification of aptamer-adenosine binding using the PicoGreen assay in different buffer solutions. TNM buffer contains Tris, NaCl, and MgCl<sub>2</sub>. PicoGreen fluorescence is enhanced more on binding to dsDNA (hybridized DNA) than ssDNA. Aptamer-adenosine binding actuates the DNA conformational change from dsDNA to ssDNA. Thus, a decrease in the fluorescence emission on addition of adenosine indicates that more aptamer-adenosine binding has occurred. Error bars indicate standard deviations (n = 3).**

We first examined PicoGreen fluorescence in duplex buffer (30 mM HEPES, pH 7.5; 100 mM potassium acetate) that was used to anneal the DNA strands and notably did not contain Mg<sup>2+</sup>. We observed a negligible change in fluorescence when adenosine was added (Figure 3.5), indicating that the aptamer did not bind adenosine in this buffer. We then tested TNM (5 mM

MgCl<sub>2</sub>) and TNM (10 mM MgCl<sub>2</sub>) buffers, containing 20 mM Tris (pH 7.5) and 300 mM NaCl with different concentrations of Mg<sup>2+</sup>. In both TNM buffers, the fluorescence decreased after addition of adenosine (Figure 3.5). This signal decrease indicates that the aptamer bound adenosine and the structure of DNA strands changed from dsDNA to ssDNA. These results from various buffers support that Mg<sup>2+</sup> must be present for the aptamer to bind adenosine. We observed that further increases in Mg<sup>2+</sup> concentration did not induce larger fluorescence quenching (data not shown). Therefore, the TNM (10 mM MgCl<sub>2</sub>) buffer, which showed the largest decrease in fluorescence, was adopted as the adenosine-binding buffer for future 2DPC hydrogel measurements.

### 3.3.3 Adenosine Sensing in Buffer Solutions

The adenosine-sensing response of our DNA-crosslinked 2DPC hydrogels was monitored by measuring the 2DPC particle spacing. Each 0.4 × 0.5 cm<sup>2</sup> piece of the 2DPC hydrogel was first immersed in blank adenosine-binding buffer, TNM (10 mM MgCl<sub>2</sub>), that did not contain adenosine for 10 min. After measuring the particle spacing, each hydrogel sample was then immersed in buffer solution additionally containing adenosine ranging in concentration from 0 to 2 mM.

Figure 3.6 shows the changes in particle spacing of 2DPC hydrogels over time at different concentrations of adenosine. Particle spacing change was calculated by subtracting the initial particle spacing (at time = 0) from each sample. At larger concentrations of adenosine, the 2DPC hydrogel particle spacing increased more rapidly and to a greater extent than at smaller concentrations of adenosine. For example, at 2 mM adenosine, the particle spacing increased by more than 90 nm in 5 min, while at 20 μM adenosine, the particle spacing increased by only 30 nm after 60 min. Regardless of adenosine concentration, the adenosine-induced particle spacing

changes began to level off as the aptamer-adenosine binding reaction gradually reached equilibrium over time.

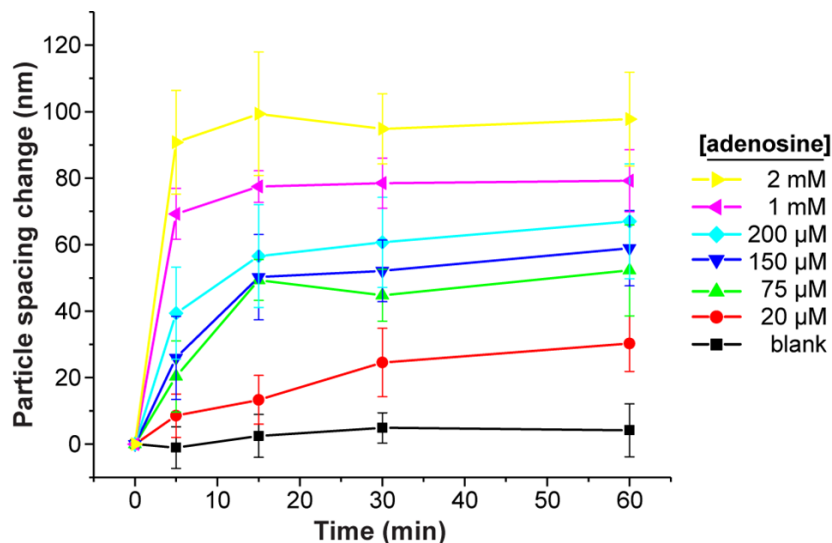


**Figure 3.6: Time dependence of 2DPC hydrogel particle spacing on the concentration of adenosine. Error bars indicate standard deviations (n = 3).**

The particle spacing change depends on the adenosine concentration because, as aforementioned in subchapter 3.3.1, aptamer-adenosine binding induces particle spacing increases. As the concentration of adenosine increases, the amount of aptamer-adenosine binding increases. The increased amount of aptamer-adenosine binding breaks a greater amount of hydrogel DNA-crosslinks, generating a larger osmotic pressure that causes the hydrogel to increasingly swell. As the hydrogel swells more, the particle spacing of the embedded 2DPC array increases. This adenosine concentration-dependent response enables the use of these 2DPC hydrogels as adenosine sensors.

Since the particle spacing change depends on the amount of aptamer-adenosine binding, the dissociation constant ( $K_D$ ) of the adenosine-binding aptamer in our 2DPC hydrogel can be

estimated from the particle spacing data shown in Figure 3.6 (see Appendix A.1 for detailed calculation). The  $K_D$  was estimated to be  $\sim 68 \mu\text{M}$ , which is slightly larger than the reported  $K_D$  for the adenosine-binding aptamer in solution ( $\sim 10 \mu\text{M}$ ).<sup>79, 141</sup> We hypothesize that this decrease in binding affinity is caused by competitive binding of the aptamer with its complementary DNA and spatial restrictions that result from the aptamer's covalent attachment to the hydrogel network. Our estimated  $K_D$  is smaller than that reported for the duplexed adenosine-binding aptamer in solution ( $\sim 600 \mu\text{M}$ )<sup>83</sup>, suggesting the duplexed aptamer's binding affinity for adenosine has been largely preserved despite polymerization into the hydrogel network.

The concentration of adenosine can be determined from the particle spacing change at a short-fixed detection time of 30 min. The particle spacing change data at  $T = 30$  min were taken from Figure 3.6 and replotted in Figure 3.7 as a function of adenosine concentration. Figure 3.7 shows that the particle spacing change was proportional to the logarithm of adenosine concentration (20  $\mu\text{M}$  to 2 mM adenosine). The linear fit line can be used as a calibration curve for adenosine detection. The LoD was calculated to be 13.9  $\mu\text{M}$  ( $S/N = 3$ ).

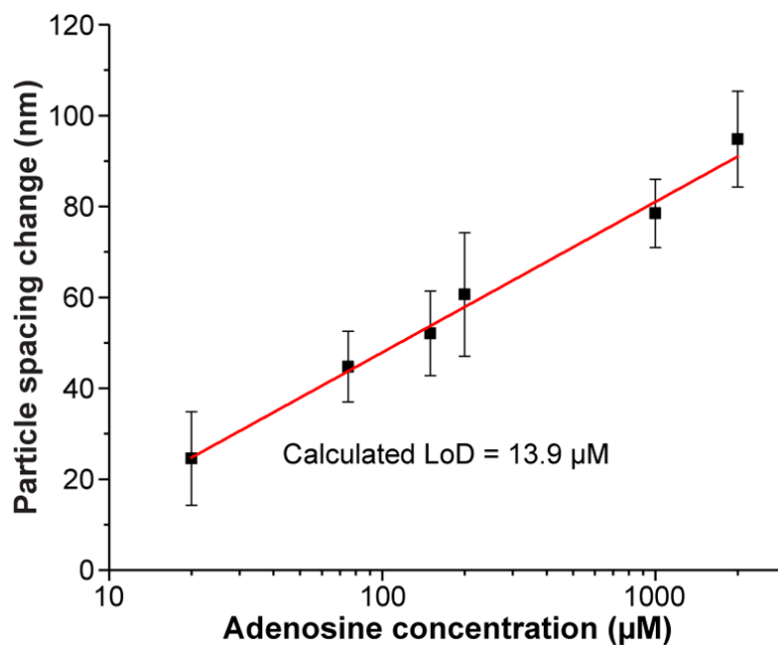


**Figure 3.7: Particle spacing changes' dependence on adenosine concentration in buffer solutions (detection time = 30 min). The X-axis is in a logarithmic scale. The red line shows a linear fit (adjusted R-Squared = 0.9874). Error bars indicate standard deviations (n = 3).**

### 3.3.4 Selectivity of Adenosine-Sensing 2DPC Hydrogels

Figure 3.8 shows data supporting the selectivity of the adenosine-sensing 2DPC hydrogels. To verify that adenosine actuated the 2DPC hydrogel response, we first measured the 2DPC particle spacing in a blank solution containing no adenosine. Compared to samples containing adenosine which showed a large increase in particle spacing, samples containing no adenosine showed negligible changes.

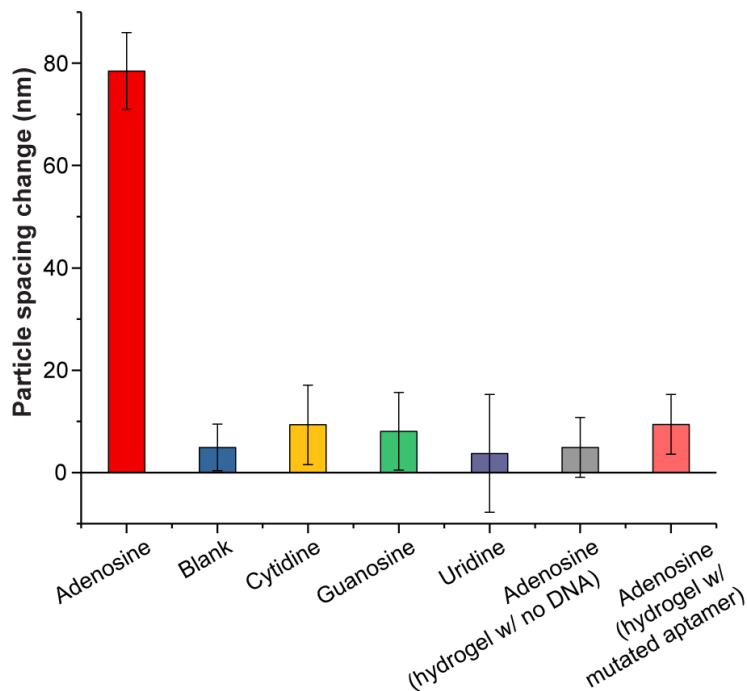


**Figure 3.8: Selectivity of adenosine-sensing 2DPC hydrogels.** 2DPC hydrogel particle spacing was measured in a blank sample containing no nucleosides, and in samples containing 1 mM concentration of adenosine, cytidine, guanosine, or uridine. Each 2DPC hydrogel contained the adenosine-binding aptamer, except for a control containing no DNA (“hydrogel w/ no DNA”) and a control containing a mutated aptamer that did not bind adenosine (“hydrogel w/ mutated aptamer”). The particle spacing change of each sample was measured after immersion in each solution for 30 min. Error bars indicate standard deviations (n = 3).

The adenosine aptamer used in our hydrogels has been reported to bind adenine derivatives like adenosine but not other nucleosides.<sup>79</sup> To verify this selectivity for adenosine, we measured the 2DPC particle spacing of samples containing 1 mM solutions of cytidine, guanosine, or uridine, respectively (Figure 3.8). Compared to the large response in 1 mM adenosine, these other nucleosides induced negligible particle spacing changes similar to that in the blank measurement. This indicates that the 2DPC hydrogel response was actuated by the selective adenosine-binding aptamer.

We further confirmed the selectivity of the adenosine-binding aptamer in actuating sensor response using two different controls (Figure 3.8). The first control hydrogel was fabricated with only acrylamide and MBAAm, and without DNA. This sample showed negligible particle spacing change in 1 mM adenosine solution because it did not have any target-recognition groups. The other control hydrogel contained DNA crosslinks (hybridized between DNA strands 2 and 3) and was nearly identical to the adenosine-sensing hydrogels (hybridized between DNA strands 1 and 2). However, in the control, double mutations occurred within the adenosine-binding site of DNA strand 1 which inactivated the mutant strand (DNA strand 3) to adenosine.<sup>83</sup> This control also showed negligible particle spacing change in adenosine solution, confirming the active adenosine-binding aptamer was required to actuate adenosine sensing

### 3.3.5 Adenosine Sensing in FBS

The response of the DNA-crosslinked 2DPC hydrogels was validated in a complex matrix, FBS. Based on preliminary data, serum proteins were removed to minimize interference. The protein-removed FBS solutions were diluted to 50% with the serum diluting buffer (40 mM Tris, pH 7.5; 19 mM MgCl<sub>2</sub>; 450 mM NaCl) to maintain the optimal adenosine-binding conditions. As with measurements in buffer solutions, 2DPC hydrogel particle spacing changes were monitored after 30 min in serum solutions spiked with adenosine.

Figure 3.9 shows that, as in pure buffer, the particle spacing change was proportional to the logarithm of adenosine concentration (20  $\mu$ M to 2 mM adenosine). Notably, the adenosine-induced particle spacing changes were slightly less in FBS solutions than in pure buffer. We hypothesize that this decrease in responsivity was caused by interferences in the serum matrix that inhibited the aptamer-adenosine binding. The calculated LoD was 26.7  $\mu$ M adenosine (S/N = 3).

While this LoD is greater than that in pure buffer (LoD = 13.9  $\mu\text{M}$ ), it is of the same order of magnitude. This indicates that the hydrogel sensor responsivity has been largely preserved and that our DNA-crosslinked 2DPC hydrogels can be used for adenosine detection in complex matrices.

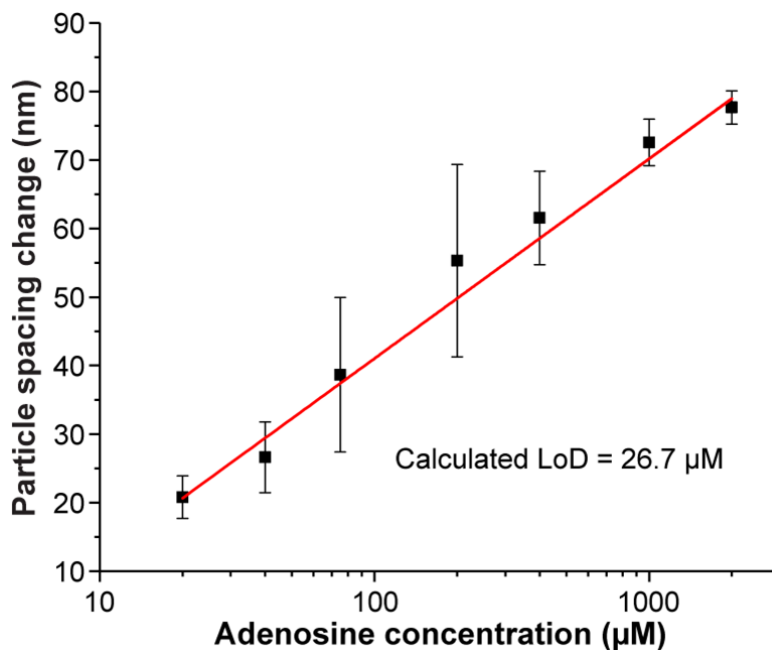


**Figure 3.9: Particle spacing changes' dependence on adenosine concentration in 50% protein-removed FBS (detection time = 30 min). The X-axis is in a logarithmic scale. The red line shows a linear fit (adjusted R-Squared = 0.9936). Error bars indicate standard deviations (n = 3).**

### 3.4 Conclusion

We report the first fabrication of a DNA-crosslinked 2DPC hydrogel sensor that is actuated by a DNA aptamer. As proof-of-concept, we created an adenosine sensor using an adenosine-binding aptamer. When adenosine is introduced into the 2DPC hydrogel sensor, aptamer-adenosine binding occurs, breaking pre-formed DNA crosslinks and actuating the sensor response. As DNA

crosslinks break, the hydrogel swells, increasing the particle spacing of the embedded 2DPC array. A linear range was observed to be 20  $\mu\text{M}$  – 2 mM. The calculated LoDs are 13.9  $\mu\text{M}$  in adenosine-binding buffer and 26.7  $\mu\text{M}$  in 50% protein-removed FBS (detection time = 30 min).

The reported sensing motif using DNA-crosslinked 2DPC hydrogels is simple, rapid, and requires only a laser pointer. We expect that the sample volume required for testing can be greatly reduced by using smaller hydrogel pieces. Additionally, our group has previously demonstrated the use of 2DPC and 3DPC hydrogels for developing colorimetric sensors that give visual readouts similar to a pH strip.<sup>60</sup> Thus, while requiring additional studies, the aptamer-actuated hydrogels described in this work may have potential clinical applications, especially in resource-limited settings.

In future work, we plan to systematically investigate DNA-crosslinks in the system to further understand the sensing-mechanism and optimize sensor performance. It is possible that the length of DNA strands, the number of hybridized base pairs, and the placement of the aptamer sequence within the longer DNA strand will impact sensor response.<sup>83, 153</sup> We will test these properties along with the effect of DNA concentration on sensor performance.

While requiring further studies, we hypothesize that this sensing motif is generalizable and that other sensors can be easily fabricated by simply exchanging the aptamer that serves as a molecular recognition group. High-affinity aptamers for a variety of analytes, ranging from small molecules to whole cells, have been reported. New aptamers can be developed rapidly, enabling the fabrication of sensors for a wide range of targets with ultralow limits of detection. We are continuing to investigate the versatility of this novel sensing motif and are working to develop aptamer-actuated 2DPC hydrogel sensors that can detect proteins in solution.

### **3.4.1 Acknowledgements**

The authors acknowledge the University of Pittsburgh for providing instrumentation and financial support.

## 4.0 DNA-Crosslinked Photonic Crystal Hydrogel Sensors: Optimization of Fabrication and Function

This chapter is in preparation for submission to the journal *ACS Applied Materials and Interfaces*, authored by Westbay, J. H.; Jang, K.; Goda, S. A.; and Asher, S. A. J. H. W. conceived experiments with assistance from K. J. J. H. W. collected and analyzed data with assistance from S. A. G. The manuscript was prepared by J. H. W. with assistance from K. J., S. A. G., and S. A. A.

DNA-crosslinked hydrogels are responsive materials with wide-ranging utility, including as sensors. Though there have been recent, promising developments in the research and development of these materials, there is a need to better understand their tunable properties in order to standardize their fabrication and optimize their function. Recently, we reported the fabrication of a sensor that utilizes a DNA-crosslinked hydrogel embedded with a photonic crystal array to detect a small molecule, adenosine. In this present work, we use our hydrogel sensor as a model system to investigate tunable aspects of the fabrication and operation of DNA-crosslinked hydrogels. We explore the impact of different DNA annealing protocols, DNA concentrations, hydrogel sizes, sample volumes, and DNA sequences. Informed by these results, we fabricate an optimized photonic crystal hydrogel sensor. Our optimized sensor detects adenosine in serum solutions with a calculated detection limit of 20.5  $\mu\text{M}$ . This sensor is more responsive, requires fewer materials, and operates in smaller sample volumes than previously reported. These results may prove useful beyond sensing by elucidating how the response of DNA-crosslinked materials can be tuned for other applications.

## 4.1 Introduction

DNA-crosslinked, polyacrylamide hydrogels are responsive materials with wide-ranging utility, including as actuators<sup>154</sup>, drug delivery vesicles<sup>109</sup>, and sensors<sup>109, 110</sup>. In these hydrogels, complementary DNA strands are covalently attached to the polyacrylamide network and hybridize to form noncovalent crosslinks. These strands can break and rehybridize with changes in the hydrogel chemical environment, actuating unique changes to the physical properties of the hydrogel. For example, DNA-crosslinked hydrogels have been designed to dissolve in the presence of a chemical target, enabling the fabrication of highly specific sensors.<sup>109, 110</sup>

Despite promising advances in recent years, there is a need to further characterize these materials and understand how their properties can be tuned for different applications.<sup>111, 112</sup> For example, addition of non-DNA, covalent crosslinks improves hydrogel mechanical robustness, but also limits hydrogel swelling.<sup>113</sup> Attempts to fabricate and optimize DNA-actuated materials have been hindered by the use of distinct fabrication methodologies and a lack of characterization among different research groups.<sup>109, 113, 155</sup>

The Tan group designed DNA-crosslinked hydrogels with aptamer molecular recognition groups.<sup>109, 110</sup> Aptamers are short DNA or RNA strands that have been selected to sensitively and specifically bind a chemical target.<sup>65, 66</sup> In the presence of the aptamer's binding target, competitive aptamer-target binding causes DNA crosslinks to break, actuating hydrogel swelling and ultimately dissolution.<sup>109</sup> This volume change was later coupled to the release of nanoparticles<sup>109</sup> or an enzymatic reaction<sup>110</sup> to fabricate hydrogel sensors. While the Tan group demonstrated the generalizability of their sensing motif by fabricating hydrogel sensors for two small molecules and a protein, no extensive attempt was made to investigate the tunability of the hydrogels or characterize physical properties outside of the sensing response.

The Stokke group later designed DNA-crosslinked hydrogels to act as logic gates in the presence of oligonucleotide probes.<sup>155</sup> Using a homemade interferometric instrument setup based around an optical fiber, they characterized the degree of swelling and kinetics of their hydrogels in the presence of different combinations of oligonucleotide probes. Despite this extensive characterization, they report only a single hydrogel formulation, and thus did not investigate the tunable aspects of their hydrogels. Furthermore, while they suggest their instrument setup could be used as an alternative to conventional characterization methods, such a setup is not widely accessible to other researchers, thus limiting its utility.

To date, the Hill group has made the most comprehensive attempt to characterize DNA-crosslinked hydrogels and systematically investigate their tunable properties.<sup>111-113</sup> Using a variety of rheological techniques, they examined how properties like hydrogel composition, temperature, and the addition of covalent crosslinks impact hydrogel behavior. Using this data, the Hill group developed a theoretical model to describe the swelling behavior of DNA-crosslinked hydrogels. While an important contribution to the field, this model is nascent. Further investigation is needed to better understand the tunable properties of these materials, characterize them, and apply this understanding to real-world applications.

Recently, we reported a novel sensing motif that utilizes DNA-crosslinked hydrogels actuated by aptamer recognition groups.<sup>27</sup> As proof-of-concept, we fabricated sensors to detect a small molecule, adenosine. Our adenosine sensor utilizes a photonic crystal (PC) hydrogel. PC hydrogels were invented by the Asher group and consist of a PC array embedded into a stimuli-responsive hydrogel.<sup>18</sup> This couples the PC particle spacing to the hydrogel volume. Thus, changes in the chemical environment that actuate changes in the hydrogel volume cause the PC particle spacing to change and can be monitored through shifts in PC diffraction.

In our adenosine sensor, the hydrogel contains complementary DNA strands that hybridize to form crosslinks. One of the DNA strands contains the sequence of an adenosine-binding aptamer.<sup>79</sup> On addition of adenosine, competitive aptamer-adenosine binding causes hydrogel crosslinks to break, actuating swelling. This in turn increases the particle spacing of the embedded PC array, shifting PC diffraction. Thus, adenosine concentration can be monitored through PC diffraction shifts. Importantly, our DNA-crosslinked hydrogels contain stabilizing covalent crosslinks. These covalent crosslinks improve hydrogel mechanical robustness and prevent dissolution, elongating the shelf life of our sensors.

PC hydrogel particle spacing changes that correspond to hydrogel volume transitions can be monitored through changes in diffraction wavelength or angle.<sup>18, 61, 63</sup> For our sensors, we monitor changes in diffraction angle through measurement of Debye rings.<sup>27, 143</sup> These measurements require only a laser pointer and a ruler. This simple setup is more accessible relative to other spectroscopic techniques, and thus enables our approach to be used by other researchers.<sup>156-159</sup>

In this work, we use our adenosine sensor to characterize and investigate the tunable properties of DNA-crosslinked hydrogels. Through these investigations, we optimize our sensor for the detection of adenosine. We further highlight tunable properties and protocols that may prove useful beyond sensing applications.

Since we began preparing this work, the Zhang group reported a PC hydrogel sensor to detect a protein, human thrombin, that utilizes a very similar sensing motif involving DNA crosslinks and a thrombin-binding aptamer.<sup>159</sup> They report optimizing their sensor by altering hydrogel composition. Here, we report some findings in conflict with theirs. We hypothesize these discrepancies are due to subtle differences in the fabrication chemistries between our two works

and their much larger sensing target, the protein thrombin, relative to ours, the small molecule adenosine. These differences highlight the need for further exploration into the tunable properties of these materials.

## 4.2 Experimental Section

### 4.2.1 Materials

Acrydite-modified DNA strands (DNA 1: 5'-acrydite-AGA GAA CCT GGG GGA GTA TTG CGG AGG AAG GT-3', DNA 2: 5'-acrydite-CCC AGG TTC TCT-3', DNA 3: 5'-acrydite-ACC TTC CTC CGC AAT ACT CCC CCA GGT-3', purified with high performance liquid chromatography) were purchased from Integrated DNA Technologies. Stock solutions of DNA 1, 2, and 3 were prepared separately at 2 mM concentration in TE buffer (10 mM Tris, pH 8.0; 0.1 mM EDTA) and stored at -20 °C. Tris base ( $\geq 99.9\%$ ), magnesium chloride, HEPES (99%), sodium hydroxide pellets ( $\geq 97\%$ ), sodium styrene sulfonate (NaSS) ( $\geq 90\%$ ), 2,2'-Azobisisobutyronitrile (AIBN) (98%), styrene (99%), acrylamide ( $\geq 99\%$ ), N,N'-methylenebisacrylamide (MBAAm) (99%), ammonium persulfate (98%), tetramethylethylenediamine (TEMED) (99%), adenosine ( $\geq 99\%$ ) was purchased from Sigma-Aldrich. Ethylenediaminetetraacetic acid (EDTA) (99.5%) was purchased from JT Baker. Sodium chloride was purchased from EMD Millipore. Hydrochloric acid (36.5-38% w/w), potassium acetate (99%), methanol (99.8%), and 2-propanol ( $\geq 99.5\%$ ) were purchased from Thermo Fisher Scientific. Ethanol (200 proof) was purchased from Decon Labs, Inc. Quant-iT PicoGreen dsDNA Assay Kit was purchased from Invitrogen. Cover glass (thickness 1,  $24 \times 60 \text{ mm}^2$ ) and FBS were purchased from Corning. To remove serum proteins, FBS was

filtered using 10 kDa centrifugal filters. Microscope premium frosted glass slides ( $25 \times 75 \times 1 \text{ mm}^3$ ) were purchased from Fisher Scientific. All chemicals were used as received unless otherwise specified. Ultrapure water ( $18.2 \text{ m}\Omega \cdot \text{cm}$ ) obtained from a Milli-Q Reference A+ was used for all experiments.

#### 4.2.2 2DPC Hydrogel Fabrication

2DPC hydrogels were fabricated using described procedures.<sup>27</sup> Briefly, negatively charged polystyrene particles with diameter  $\sim 1.20 \text{ }\mu\text{m}$  were synthesized by a dispersion polymerization method described by Zhang et al.<sup>48</sup> These particles ( $\sim 15 \text{ }\% \text{w/w}$  in water) were mixed with 2-propanol in a 3:1 ratio and assembled into a hexagonally close-packed 2DPC array through the needle tip flow method.<sup>25</sup> The 2DPC array was deposited on a glass substrate ( $24 \times 60 \text{ mm}^2$ , cover glass, Corning) and dried at room temperature for 24 h. A polymerizable monomer solution was prepared that contained  $25 \text{ }\% \text{w/v}$  acrylamide in water,  $0.2 \text{ }\% \text{w/v}$  N,N'-methylenebisacrylamide (MBAAm) in water, and annealed DNA. The monomer solution was then degassed in a vacuum desiccator for 15 min. Two layers of tape were applied to the 2DPC array sectioning off  $0.048 \text{ cm}^2$  per  $1 \text{ }\mu\text{L}$  of monomer solution. After adding initiator solution ( $0.7 \text{ }\mu\text{L}$  of  $5\% \text{ (v/v)}$  TEMED in water and  $0.7 \text{ }\mu\text{L}$  of  $10\% \text{ (w/v)}$  ammonium persulfate in water), the monomer solution was stirred for 5 seconds and then deposited on the 2DPC array using a micropipette tip. A glass cover ( $25 \times 75 \times 1 \text{ mm}^3$ , microscope premium frosted glass slides, Fisher Scientific) was placed over the solution, and polymerization proceeded for 30 min in a vacuum desiccator. After polymerization, the glass substrates were placed in TMN buffer ( $20 \text{ mM}$  Tris,  $10 \text{ mM}$   $\text{MgCl}_2$ ,  $300 \text{ mM}$  NaCl; pH 7.5) for 10 min. The glass cover was then removed using a razor blade, and the PC hydrogel was gently peeled

from the glass substrate. The PC hydrogel was washed in TMN buffer for 3 min, cut into pieces, and refrigerated in a petri dish without buffer for storage.

### 4.2.3 2DPC Particle Spacing Measurements

PC hydrogel particle spacing changes were monitored by measuring changes in Debye ring diameter.<sup>61</sup> Equation 4.1 gives the condition for Bragg diffraction of a 2D hexagonally close-packed PC array, where  $m$  is the diffraction order,  $\lambda$  is the wavelength of light,  $d$  is the 2DPC lattice spacing,  $\alpha$  is the angle of incidence, and  $\beta$  is the angle of diffraction.

$$m\lambda = 2d(\sin \alpha + \sin \beta) \quad \text{Equation 4.1}$$

Figure 4.1 shows the set up for our Debye ring measurements. Briefly, the PC hydrogel is placed on an elevated stand, and a laser pointer is positioned along its normal ( $\alpha = 0$ ). This illuminates a Debye ring. By measuring the height between the Debye ring and the PC hydrogel,  $h$ , and the Debye ring diameter,  $D$ , the diffraction angle,  $\beta$ , can be determined using Equation 4.2.

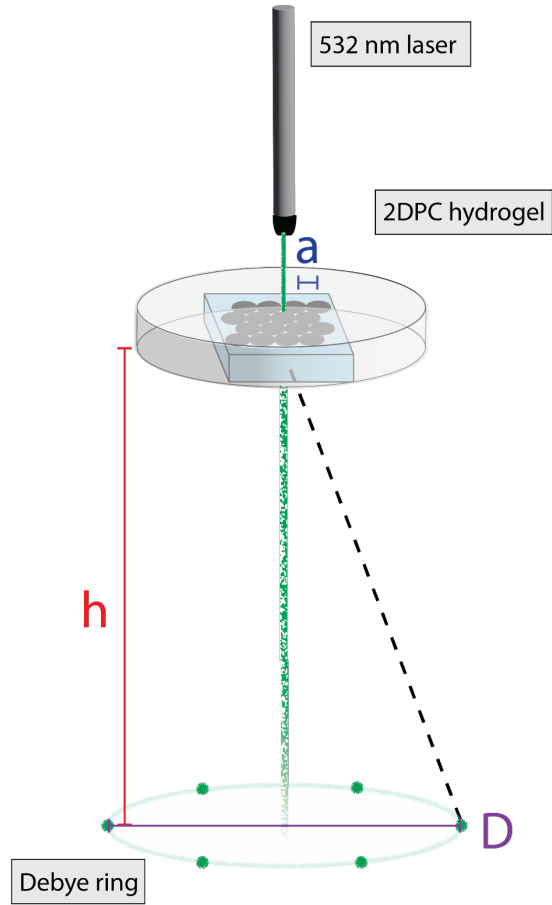


**Figure 4.1: Debye ring measurement setup.**

$$\beta = \tan^{-1}\left(\frac{D}{2h}\right) \quad \text{Equation 4.2}$$

The PC lattice spacing,  $d$ , is related to the PC particle spacing,  $a$ , through Equation 4.3.

$$d = \frac{\sqrt{3}a}{2} \quad \text{Equation 4.3}$$

Equations 4.2 and 4.3 can be substituted into Equation 4.1 to give Equation 4.4.

$$a = \frac{2\lambda}{\sqrt{3} \sin\left(\tan^{-1}\left(\frac{D}{2h}\right)\right)} \quad \text{Equation 4.4}$$

Since the wavelength of the laser pointer was known (532 nm), and the height between the PC hydrogel and Debye ring was fixed ( $h = 15 \text{ cm}$ ), PC hydrogel particle spacing changes were monitored by measuring changes in Debye ring diameter with a ruler. To calculate  $a$ , we measured and averaged  $D$  values at 5 different locations within each PC hydrogel piece.

#### 4.2.4 Adenosine Sensing

2DPC hydrogel particle spacing changes in adenosine solution were used to evaluate how changes in tunable properties impact PC hydrogel response. 2DPC hydrogel pieces were brought to room temperature and immersed in 10 mL of TMN buffer (20 mM Tris, 10 mM  $\text{MgCl}_2$ , 300 mM NaCl; pH 7.5). After 10 min, the initial particle spacing was measured. PC hydrogel pieces were then immersed in adenosine solutions of varying concentrations. After set intervals of time, the particle spacing of the PC hydrogel piece was measured. The initial particle spacing was subtracted from each measurement, and PC hydrogel response was analyzed as particle spacing changes. The average response of a blank sample measured in solution without adenosine was subtracted from each data point.

#### 4.2.5 PicoGreen Fluorescence Assay

A PicoGreen fluorescence assay was used to monitor DNA hybridization.<sup>27, 85</sup> Briefly, a 300  $\mu\text{L}$  solution of 1.6  $\mu\text{M}$  annealed DNA was prepared in TMN buffer (20 mM Tris, 10 mM  $\text{MgCl}_2$ , 300 mM NaCl; pH 7.5). A 300  $\mu\text{L}$  solution of 200 $\times$  diluted PicoGreen was prepared in the same buffer. These two solutions were combined and mixed by pipetting up and down 15 times with a micropipette. After 3 min, the sample was transferred to a quartz cuvette. Fluorescence spectra were measured in triplicate for each sample using a HORIBA Jobin Yvon Fluoromax-3 Spectrofluorometer with 480 nm excitation, 525 nm emission, and slit widths of 2 nm for excitation and emission. Blank measurements of PicoGreen in buffer without DNA were collected separately and subtracted from each measurement.

#### 4.2.6 DNA Annealing

Four annealing protocols were used to hybridize DNA for fluorescence analysis and PC hydrogel fabrication. For each protocol, a solution containing 200  $\mu\text{M}$  complementary DNA strands was prepared in duplex buffer (30 mM HEPES, 100 mM potassium acetate; pH 7.5) and mixed by pipetting up and down 20 times with a micropipette. The “Heating + Rapid Cooling” protocol is the annealing protocol we previously reported using.<sup>27</sup> This protocol involved heating the DNA solution to 95°C on a Corning LSE Digital Dry Bath Heater for 5 min and cooling the mixture on a bench top at room temperature for 30 min. The “Heating + Slow Cooling” protocol involved heating the DNA solution to 95°C on a Corning LSE Digital Dry Bath Heater for 5 min and cooling the mixture slowly on the dry bath for 2 h after turning off the dry bath. The “Room Temperature” protocol involved incubating the DNA mixture on a bench top at room temperature

for 30 min. The “No Treatment” protocol involved using the DNA solution immediately after mixing, with no time afforded for incubation.

DNA annealed using the “Heating + Rapid Cooling” and “Heating + Slow Cooling” protocols were used to fabricate PC hydrogels. For PC hydrogel fabrication, annealed DNA was dried on a Labconco Centrivap Concentrator (78100-00 A) for ~4.5 h. After drying, monomer solutions containing 0.80 mM DNA were used to fabricate PC hydrogels. After polymerization, PC hydrogels were cut into 0.4 cm × 0.4 cm pieces. PC hydrogel particle spacing change was measured in 10 mL of adenosine solution ranging from 0 (blank) to 2 mM adenosine. Particle spacing measurements were taken at time intervals of 5, 15, 30, and 60 min. Each measurement was repeated 3 times using a separate PC hydrogel piece.

#### **4.2.7 DNA Concentration**

Four DNA concentrations were used to fabricate PC hydrogels. We previously reported fabricating PC hydrogels using 0.80 mM DNA.<sup>27</sup> In this work, we also fabricated PC hydrogels using 1.60 mM, 0.40 mM, and 0.08 mM DNA. Prior to polymerization of the PC hydrogel, 200 μM DNA was annealed using the “Heating + Rapid Cooling” protocol and dried on a Labconco Centrivap Concentrator (78100-00 A) for ~4.5 h. Dried DNA was then diluted to the desired concentration with PC hydrogel monomer solution. After PC hydrogel fabrication, PC hydrogels were cut into 0.4 cm × 0.4 cm pieces. PC hydrogel particle spacing change was measured in 10 mL of adenosine solution ranging from 0 (blank) to 2 mM adenosine. Particle spacing measurements were taken at time intervals of 5, 15, 30, and 60 min. Each measurement was repeated 3 times using a separate PC hydrogel piece.

#### 4.2.8 Hydrogel Size and Sample Volume

PC hydrogels were fabricated with 0.40 mM DNA annealed using the “Heating + Rapid Cooling” protocol. After polymerization, PC hydrogels were cut into two different sizes, and PC hydrogel particle spacing change was measured in two different volumes. Previously, we reported using  $\sim 0.4 \text{ cm} \times 0.4 \text{ cm}$  PC hydrogel pieces in 10 mL solutions.<sup>27</sup> Here, we also use  $0.2 \text{ cm} \times 0.2 \text{ cm}$  PC hydrogel pieces and 1 mL sample volumes. After PC hydrogel fabrication, PC hydrogels were cut into the desired size (either  $0.2 \text{ cm} \times 0.2 \text{ cm}$  or  $0.4 \text{ cm} \times 0.4 \text{ cm}$ ), and incubated in adenosine solutions of the desired volume (either 1 mL or 10 mL). Particle spacing measurements were taken in solutions ranging from 0 (blank) to 2 mM adenosine, and at time intervals of 5 and 60 min. Each measurement was repeated 3 times using a separate PC hydrogel piece.

#### 4.2.9 DNA Sequence

PC hydrogels were fabricated with 0.80 mM DNA annealed using the “Heating + Rapid Cooling” protocol. After polymerization, PC hydrogels were cut into  $0.4 \text{ cm} \times 0.4 \text{ cm}$  pieces, and PC hydrogel particle spacing change was measured in 10 mL solutions with 0 (blank) to 4 mM adenosine. Particle spacing measurements were taken at time intervals of 5, 15, 30, and 60 min. Each measurement was repeated 3 times using a separate PC hydrogel piece. For heated-treated samples, initial particle spacing was measured after incubation for 10 min in 10 mL of TMN buffer (20 mM Tris, 10 mM  $\text{MgCl}_2$ , 300 mM NaCl; pH 7.5). PC hydrogels were then transferred to a centrifuge tube containing 1 mL of TMN buffer and heated to  $95^\circ\text{C}$  on a Corning LSE Digital Dry Bath Heater for 5 min. Particle spacing was measured after the PC hydrogels were cooled on a bench top at room temperature for 30 min.

#### **4.2.10 Adenosine Sensing in Bovine Serum using Optimized PC Hydrogels**

Optimized PC hydrogels were fabricated with 1.6 mM DNA annealed using the “Heating + Rapid Cooling” protocol. After polymerization, PC hydrogels were cut into 0.2 cm × 0.2 cm pieces. Protein-removed fetal bovine serum was diluted 50% using a serum-diluting buffer (40 mM Tris, 20 mM MgCl<sub>2</sub>, 450 mM NaCl; pH 7.5) so that the final concentration of the solution was similar to that of the pure TMN buffer (20 mM Tris, 10 mM MgCl<sub>2</sub>, 300 mM NaCl; pH 7.5). PC hydrogel pieces were immersed in 1 mL of 50% fetal bovine serum solution spiked with adenosine ranging in concentration from 0 (blank) to 2 mM. The particle spacing was measured after incubation for 60 min. Each measurement was repeated 3 times using a separate PC hydrogel piece.

### **4.3 Results and Discussion**

#### **4.3.1 DNA Annealing**

DNA annealing protocols are necessary to ensure complementary DNA strands are maximally and reproducibly hybridized. Despite their importance, there is no standard annealing protocol for DNA strands in DNA-crosslinked hydrogels, and evaluation of the effectiveness of annealing is rarely reported.<sup>109, 110, 155, 159</sup>

In our PC hydrogels, complementary DNA strands are annealed prior to polymerization. We sought to investigate how different annealing protocols impact DNA hybridization and how differences in hybridization impact sensor response.

We investigated four annealing protocols, as summarized in Table 4.1.

**Table 4.1: DNA Annealing Protocols**

<b>Annealing Protocol</b>	<b>Description</b>
<b>Heating + Rapid Cooling</b>	DNA mixed, heated to 95°C for 5 min, and rapidly cooled on a bench top for ~30 min.
<b>Heating + Slow Cooling</b>	DNA mixed, heated to 95°C for 5 min, and slowly cooled on a dry bath for ~2 h.
<b>Room Temperature</b>	DNA mixed and left on a bench top at room temperature for ~30 min.
<b>No Treatment</b>	DNA mixed and used immediately.

For each protocol, we used a PicoGreen fluorescence assay to evaluate DNA hybridization (see Appendix B.1).<sup>27, 85</sup> PicoGreen is an intercalating dye that becomes more fluorescent in the presence of double-stranded DNA relative to single-stranded DNA.<sup>151, 152</sup> Since hybridized DNA is double-stranded, PicoGreen will show enhanced fluorescence with greater amounts of hybridization. Thus, PicoGreen can be used to monitor DNA hybridization.

PicoGreen fluorescence was measured after each annealing treatment and compared, as shown in Figure 4.2. The measured fluorescence signals for each protocol were averaged. Samples that underwent the “Heating + Rapid Cooling” protocol showed the largest fluorescence. Each average signal was divided by the that for the “Heating + Rapid Cooling” protocol, and the results were evaluated in terms of relative fluorescence.

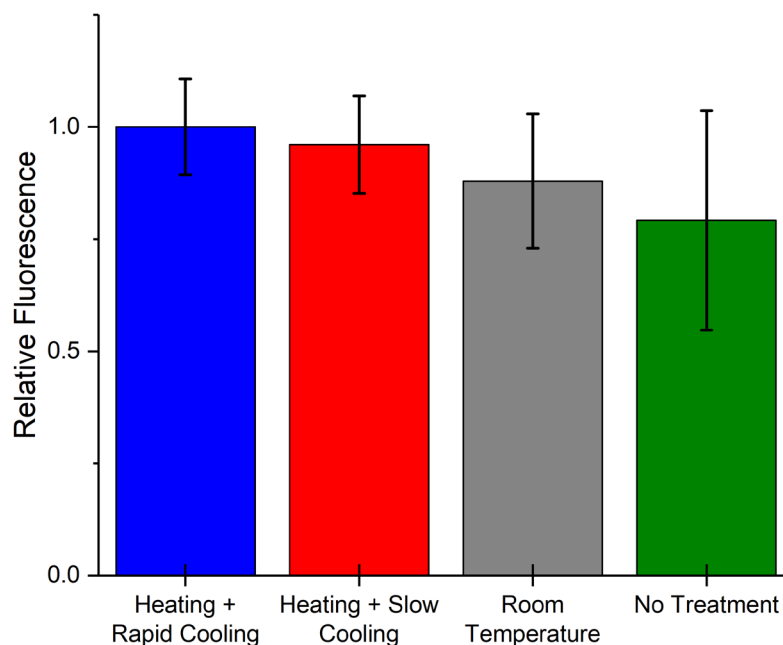


**Figure 4.2: Relative PicoGreen fluorescence for DNA annealing protocols. Each annealing protocol is described in Table 4.1. For each protocol, PicoGreen fluorescence of at least three different DNA samples were measured and averaged. Each average was divided by the largest average fluorescence signal, and the results reported as relative fluorescence. Larger relative fluorescence is indicative of greater hybridization, and thus more successful annealing. Error bars indicate standard deviations ( $n \geq 3$ ).**

The fluorescence measurements indicate that samples that underwent heat treatment hybridized the most (see Appendix B.2). Furthermore, samples that did not undergo heat treatment showed larger standard deviations, indicating greater variability in the amount of hybridization. Thus, to maximize the amount of hybridized DNA and ensure reproducibility between samples, an annealing protocol involving heat treatment should be utilized.

To further investigate the effect of cooling time after heat treatment, we fabricated PC hydrogel sensors with DNA prepared using two different annealing protocols. One group of sensors utilized DNA annealed via the “Heating + Rapid Cooling” protocol, while the other group utilized DNA annealed via the “Heating + Slow Cooling” protocol. The responsivity of these

sensors was evaluated by measuring the PC hydrogel particle spacing changes after 60 min in solutions with 75-2000  $\mu\text{M}$  adenosine, as shown in Figure 4.3.

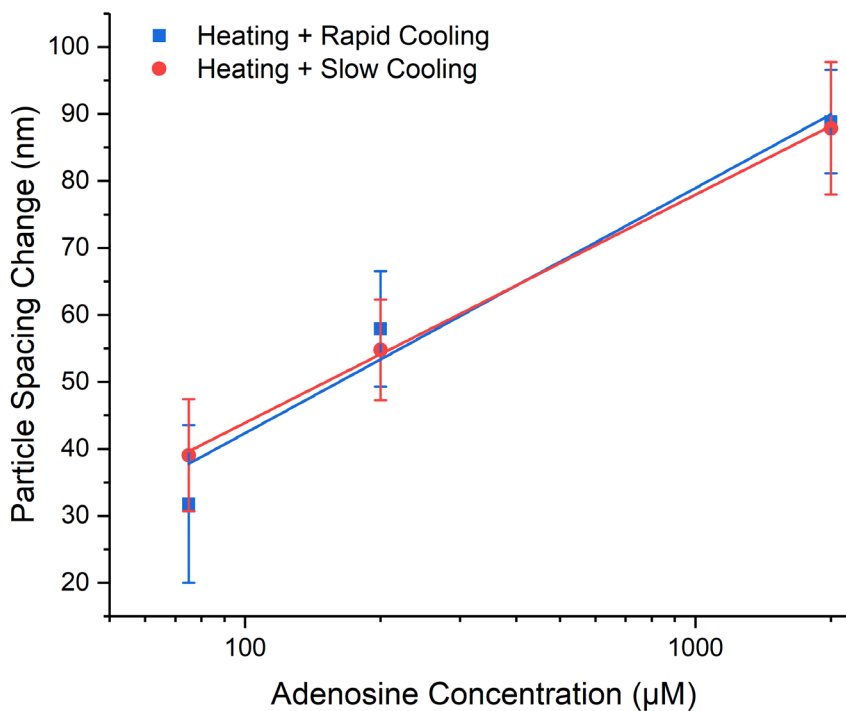


**Figure 4.3: Responsivity of PC hydrogel sensors utilizing DNA annealed by heating followed by different cooling times. Responsivity was evaluated by measuring PC hydrogel particle spacing changes in different concentrations of adenosine after 60 min. The average response of a blank sample measured in solution without adenosine was subtracted from each data point. Lines show linear fits for each protocol (see Appendix B.2). Error bars indicate standard deviations ( $n = 3$ ).**

The similar PC particle spacing changes suggest that cooling time after annealing does not significantly impact sensor responsivity. In practice, the rapid cooling protocol is preferable to conserve time.

### 4.3.2 DNA Concentration

We previously optimized the concentration of acrylamide monomer and methylenebisacrylamide covalent crosslinker in our PC hydrogel adenosine sensor.<sup>27</sup> We hypothesized that, since the sensing response depends on breaking DNA crosslinks, PC hydrogel responsivity would increase as the concentration of DNA increased.

We evaluated the impact of DNA concentration on sensor responsivity. We investigated three concentrations of DNA, as summarized in Table 4.2. The “Normal [DNA]” is the same concentration that we previously reported using (0.8 mM).<sup>27</sup> The “Higher [DNA]” is 2× the “Normal [DNA]” (1.6 mM), while the “Lower [DNA]” is  $\frac{1}{2}$  × the “Normal [DNA]” (0.4 mM).

**Table 4.2: Concentrations of DNA**

<b>Name</b>	<b>[DNA] (mM)</b>
<b>Normal [DNA]</b>	0.8
<b>Higher [DNA]</b>	1.6
<b>Lower [DNA]</b>	0.4

PC hydrogels were fabricated using each concentration of DNA, and sensor responsivity was evaluated by measuring PC hydrogel particle spacing changes after 60 min in solutions with 75-2000  $\mu$ M adenosine, as summarized in Figure 4.4.

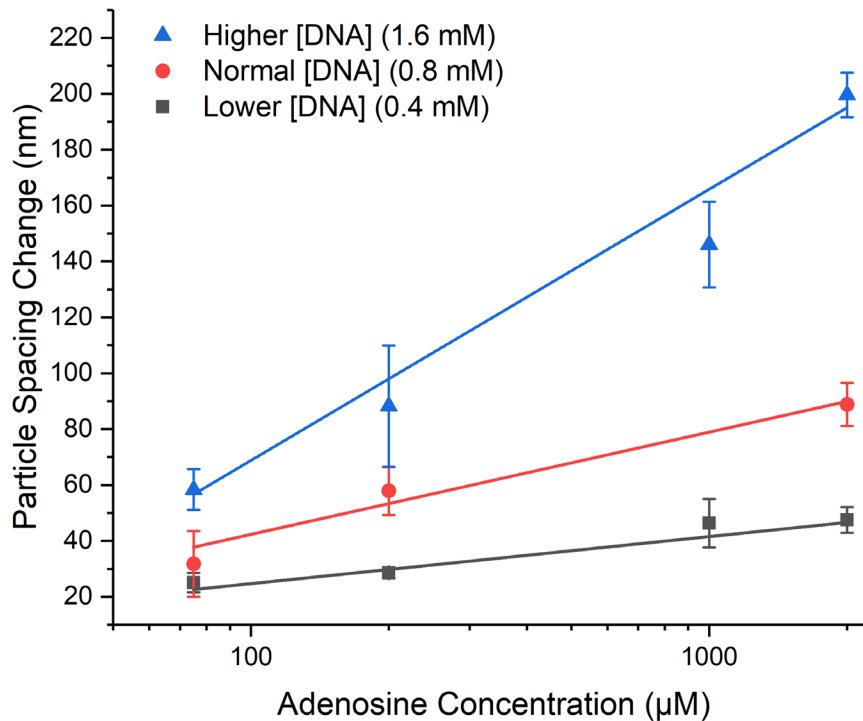


**Figure 4.4: Responsivity of PC hydrogel sensors with varying concentrations of DNA. Responsivity was evaluated by measuring PC hydrogel particle spacing changes in different concentrations of adenosine after 60 min. The average response of a blank sample measured in solution without adenosine was subtracted from each data point. Lines show linear fits for each concentration of DNA (see Appendix B.5). Error bars indicate standard deviations ( $n = 3$ ).**

We further analyzed PC hydrogels fabricated with  $\frac{1}{10} \times$  the “Normal [DNA]” (0.08 mM DNA) (see Appendix B.3). At this DNA concentration, we observed a small particle spacing change ( $< 15$  nm) in 2 mM adenosine after 60 min, so this dataset was excluded from Figure 4.4.

The results indicate that sensor responsivity scales with the concentration of DNA in the PC hydrogel. Thus, sensors with greater responsivity can be fabricated by simply increasing the concentration of DNA.

We also observed that the standard deviation of our particle spacing measurements generally increases with increasing concentration of DNA in the PC hydrogel (see Appendix B.4).

We hypothesize that this increase in variability is caused by the spontaneous breaking of crosslinks. Our sensor response relies on the breaking of DNA crosslinks actuated by the binding of adenosine to the adenosine-binding aptamer. However, over time, DNA crosslinks can spontaneously break even in the absence of adenosine, actuating non-specific swelling.<sup>27, 111, 113</sup> We hypothesize that the impact of spontaneous swelling becomes more pronounced with increasing concentrations of DNA, hence the trend towards increasing variability at higher DNA concentrations. These results indicate there is a tradeoff between sensor responsivity and variability, and researchers must carefully consider the optimal concentration of DNA when designing DNA-crosslinked materials.

These results are in conflict with those reported by the Zhang group.<sup>159</sup> When designing their aptamer-actuated, DNA-crosslinked PC hydrogel that detects a protein, thrombin, the Zhang group reported that fabrication with 100  $\mu\text{M}$  DNA optimized the responsivity of their sensor. They further observed that increasing the concentration of DNA above 100  $\mu\text{M}$  caused a decrease in sensor responsivity.<sup>159</sup> We hypothesize that this discrepancy is in part due to the different sensing targets. Adenosine is a small molecule that can quickly diffuse into the hydrogel network and easily access internal DNA strands.<sup>109</sup> Thrombin is a medium-sized protein with a molar mass  $\sim 135\times$  that of adenosine.<sup>160</sup> Thus, diffusion of thrombin into the PC hydrogel is significantly slower<sup>109</sup>, and the sensing response may be actuated disproportionately by interactions on the hydrogel surface<sup>58</sup>. If these surface interactions are saturated at 100  $\mu\text{M}$  DNA, increasing the concentration of DNA would not increase sensor responsivity.

The impact of surface interactions may be enhanced by the fabrication chemistry used by the Zhang group. In our PC hydrogels, DNA is capped with a phosphoramidite group that behaves like an acrylamide monomer.<sup>145</sup> The hybridized DNA can thus be thoroughly mixed into the pre-

gel monomer solution and incorporated into the hydrogel network through a single-step polymerization. Alternatively, the Zhang group uses EDC coupling to incorporate the DNA strands into the hydrogel network after the hydrogel has been polymerized. Since the hydrogel has already formed, it is more challenging to evenly distribute the DNA throughout the hydrogel network, and it is likely that DNA is concentrated on the hydrogel surface. This disproportionate concentration of DNA on the hydrogel surface may inhibit diffusion of thrombin into the hydrogel, limiting the sensing response.

### 4.3.3 Hydrogel Size and Sample Volume

The volume of solution a sensor will operate in is an important consideration when designing sensors. While larger solution volumes can be necessary to attain effective responsivity and sensitivity, collecting large volumes of samples can be prohibitive.<sup>161, 162</sup> For example, in our PC hydrogel sensor for adenosine, we reported using sample volumes on the order of 10-20 mL.<sup>27</sup> While this volume range is acceptable for certain samples, like urine or tap water, it is prohibitive for others, like blood or saliva. We previously hypothesized we could reduce sample volume while maintaining responsivity by manipulating the size of the PC hydrogel sensor.

We explored the relationship between PC hydrogel size and sample volume to determine how these properties affect sensor response. We examined the response of hydrogels of two sizes, 0.2 cm × 0.2 cm and 0.4 cm × 0.4 cm, in two sample volumes, 10 mL and 1 mL, at two concentrations of adenosine, as summarized in Table 4.3 and Figure 4.5.

**Table 4.3: PC Hydrogel Size and Sample Volume**

<b>Sample Name</b>	<b>PC Hydrogel Size (cm × cm)</b>	<b>Volume of Adenosine Solution (mL)</b>
<b>Large Gel, Large Sample Volume</b>	0.4 cm × 0.4 cm	10 mL
<b>Large Gel, Small Sample Volume</b>	0.4 cm × 0.4 cm	1 mL
<b>Small Gel, Large Sample Volume</b>	0.2 cm × 0.2 cm	10 mL
<b>Small Gel, Small Sample Volume</b>	0.2 cm × 0.2 cm	1 mL

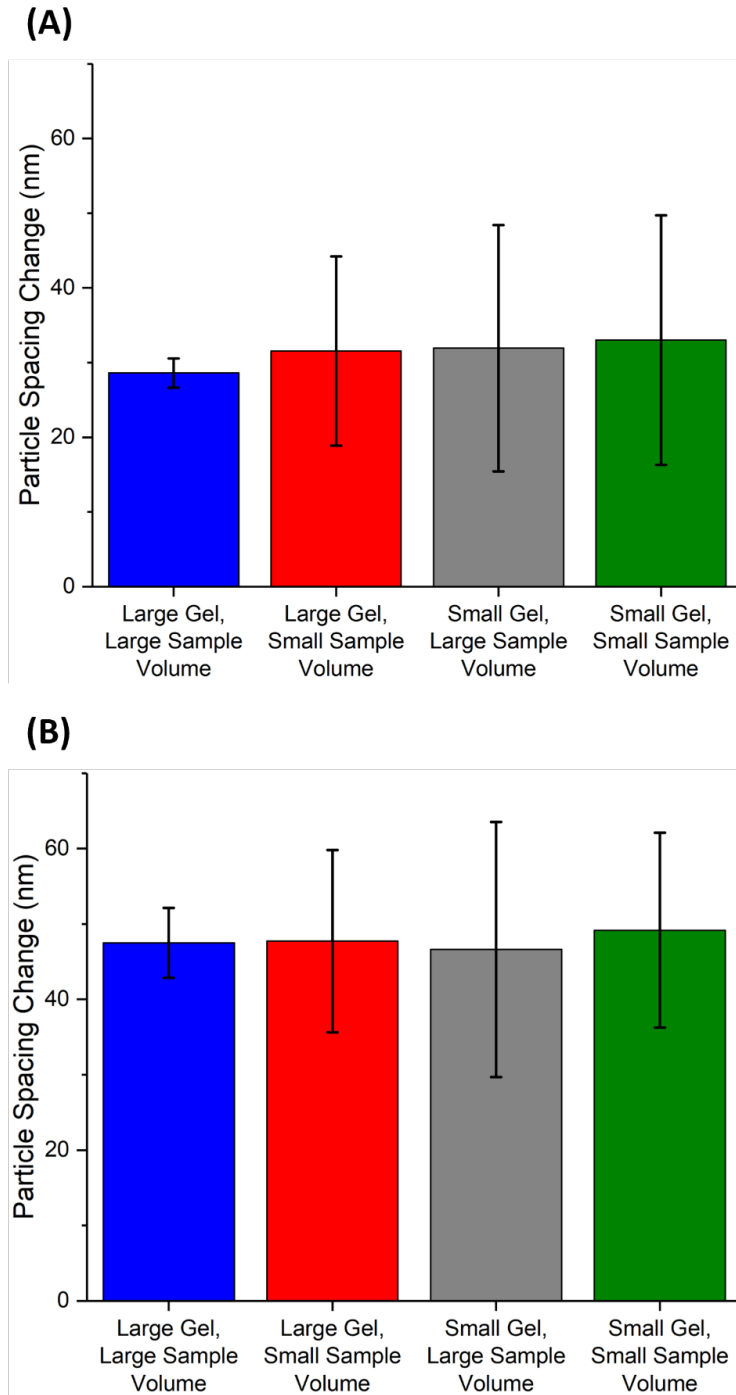


**Figure 4.5: Responsivity of PC hydrogels with varying size and sample volume in (A) 200  $\mu$ M and (B) 2 mM adenosine solution. Responsivity was evaluated by measuring PC hydrogel particle spacing changes after 60 min. PC hydrogels of two different sizes were analyzed in two different volumes of adenosine solution (Table 4.3). The average response of a blank sample measured in solution without adenosine was subtracted from each data point. Error bars indicate standard deviations ( $n \geq 3$ ).**

The results indicate that sensor responsivity is impacted by neither PC hydrogel size nor sample volume in the ranges analyzed (see Appendix B.6). This suggests that smaller PC hydrogels can be used in smaller sample volumes while maintaining responsivity, thus reducing the cost of fabrication and analysis.

The results further indicate that sensitivity is impacted by PC hydrogel size and the volume of solution the PC hydrogel operates in. Smaller PC hydrogels showed larger standard deviations in particle spacing measurements, regardless of sample volume. We hypothesize this is because smaller PC hydrogels have smaller areas with high-quality PC diffraction. 2DPC arrays fabricated using the needle tip flow method<sup>25</sup> contain random disordering.<sup>143</sup> Areas of the array are disordered further after polymerization of the hydrogel and while cutting the hydrogel into smaller pieces. These disordered areas reduce the quality of PC diffraction and cause variability in the PC hydrogel particle spacing measurements.<sup>143</sup> Since the disordered areas are distributed throughout the PC hydrogel, smaller PC hydrogels have smaller areas with high-quality diffraction, increasing variability in the particle spacing measurements.

In the larger PC hydrogels, we similarly observed increased variability in particle spacing changes measured in solutions with smaller volumes. We measured average particle spacing by measuring diffraction at five different spots on the PC hydrogel. Thus, particle spacing measurements are less variable when adenosine is evenly distributed throughout the hydrogel, and each spot where diffraction is measured is approximately the same volume. We hypothesize that for larger PC hydrogels in larger sample volumes, adenosine is more evenly distributed throughout the hydrogel network, and thus the hydrogel volume is more uniform between spots where measurements are taken, than for PC hydrogels in smaller sample volumes.

In contrast, smaller PC hydrogels show similar variability in particle spacing changes regardless of sample volume. We hypothesize this is because, due to the smaller size of the hydrogel, the distribution of adenosine throughout the hydrogel is similar in both 10 mL and 1 mL sample solutions. Thus, for smaller PC hydrogels, variability in particle spacing is due primarily to the size of the PC hydrogel rather than the volume of solution measurements are made in. In the future, we plan to continue to investigate the impact of PC hydrogel size and the sample volume in which measurements are made to confirm these hypotheses and further investigate the impact of these properties.

#### **4.3.4 DNA Sequence**

Aptamer-actuated materials utilize an aptamer sequence that has been selected to sensitively and specifically bind a chemical target. Additional, non-aptamer oligonucleotide sequences may be inserted into these materials to alter their physical properties. For example, in aptamer-actuated hydrogels, the addition of non-aptamer bases where the oligonucleotide is attached to the polymer network prior to the aptamer sequence improves aptamer flexibility and facilitates aptamer-target binding.<sup>109</sup>

The impact of non-aptamer sequences is more pronounced in systems that utilize hybridized DNA. In these systems, the amount of hybridization, presence of a single-stranded DNA tail, and specific placement of the aptamer sequence in a larger strand of DNA can all impact aptamer-target binding.<sup>153, 163</sup> Thus, the swelling response of DNA-crosslinked hydrogels containing an aptamer sequence can be tuned by altering the DNA sequence complementary to the aptamer.

In our original adenosine sensor, we utilized DNA strands that were 32 (DNA 1) and 12 bases (DNA 2), respectively, as summarized in Figure 4.6.<sup>27</sup> After annealing, the strands hybridize to form 12 base pairs, and were stable at room temperature. The aptamer sequence partially hybridizes, forming 7 base pairs and a 20-mer single-stranded tail. We hypothesized that this single-stranded tail shifted equilibrium towards aptamer-target binding in the presence of adenosine, and thus enhanced the response of our sensor.

To investigate the impact of altering the amount of hybridization in our PC hydrogels, we fabricated PC hydrogels utilizing DNA strands that contained 32 (DNA 1) and 27 (DNA 3) bases, respectively, as summarized in Figure 4.6. These DNA strands hybridize to form 27 base pairs, and there is no single-stranded tail that includes part of the aptamer.

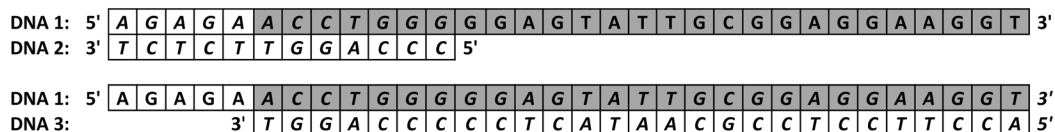


**Figure 4.6: DNA sequences used to fabricate PC hydrogels. Bases that make up the aptamer sequence are shaded. Complementary sequences are aligned and italicized.**

A PicoGreen fluorescence assay was used to verify DNA hybridization. As shown in Figure 4.7, PicoGreen fluorescence was measured after annealing DNA 1+2 (partially complementary), and DNA 1+3 (fully complementary).

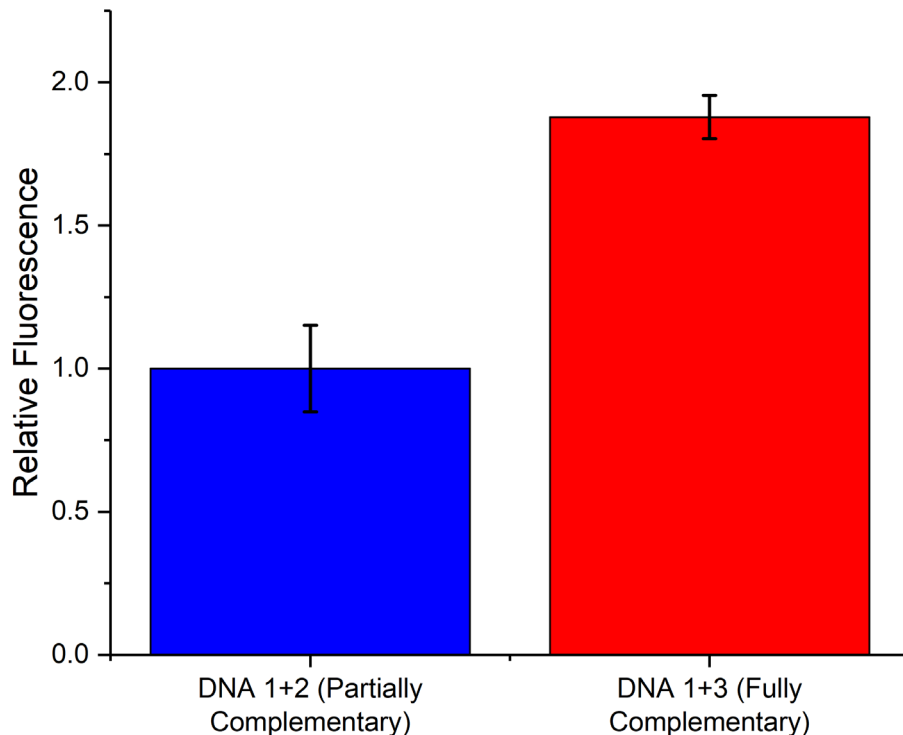


**Figure 4.7: PicoGreen fluorescence of DNA 1+2 (partially complementary) and DNA 1+3 (fully complementary). For each pair of DNA strands, PicoGreen fluorescence was measured at least three times and averaged. Each average was divided by the average fluorescence of DNA 1+2, and results were reported as relative fluorescence. Error bars indicate standard deviations ( $n \geq 3$ ).**

Since PicoGreen is fluorescently enhanced in the presence of double-stranded DNA, DNA strands with more base pairs should show greater relative PicoGreen fluorescence. DNA 1+3 (27 base pairs) has approximately  $2\times$  the number of base pairs as DNA 1+2 (12 base pairs). As expected, PicoGreen fluorescence in the presence of DNA 1+3 was approximately  $2\times$  that of DNA 1+2, confirming a greater amount of hybridization.

To determine the impact of more hybridization on PC hydrogel response, DNA 1+3 was used to fabricate PC hydrogels. PC hydrogel particle spacing changes were then monitored in solutions containing 0, 2, and 4 mM adenosine. As summarized in Figure 4.8, unlike hydrogels

fabricated with DNA 1+2, PC hydrogels containing DNA 1+3 did not respond after incubation for 60 min in adenosine solution.

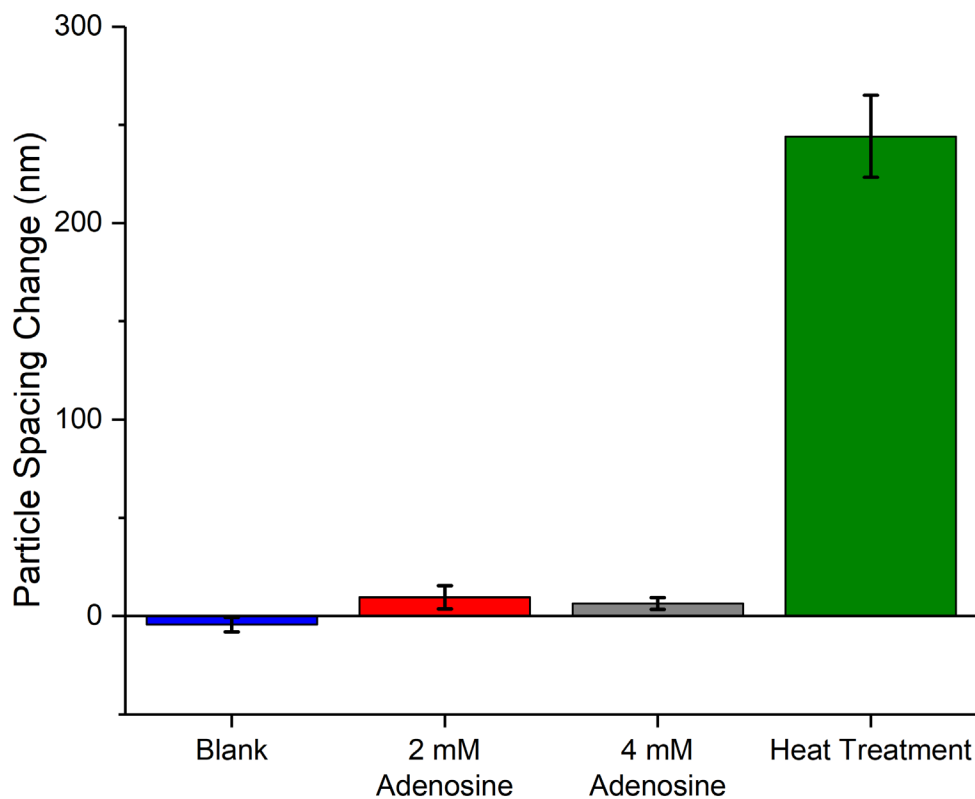


**Figure 4.8: Particle spacing changes for PC hydrogels fabricated using DNA 1+3 (fully complementary). PC hydrogel particle spacing changes were measured after 60 min in solutions containing 0 (blank), 2, and 4 mM adenosine (n=3), and after heat treatment (n=2). Error bars represent standard deviations.**

To verify that DNA crosslinks had successfully been incorporated into the PC hydrogel, PC hydrogel pieces were heated to 95°C. At 95°C, DNA melts and becomes unhybridized.<sup>147</sup> Thus, if DNA crosslinks are present, the PC hydrogel should swell significantly after being heated to this temperature. As shown in Figure 4.8, PC hydrogels fabricated with DNA 1+3 swelled > 200 nm after heat treatment, suggesting that DNA crosslinks had been successfully incorporated.

These results indicate that responsivity of DNA-crosslinked PC hydrogels is impacted by the degree of DNA hybridization. We found that the response to adenosine was eliminated when the amount of hybridization with the aptamer sequence was increased from 7 to 27 base pairs. The increase in DNA hybridization also resulted in a decrease in the length of the single-stranded tail from 20 to 0 bases. This observation supports reports that the presence of a single-stranded tail improves the responsivity of DNA-crosslinked hydrogels.<sup>106, 109</sup>

DNA-crosslinked hydrogels can suffer from spontaneous swelling, even in the absence of a chemical target.<sup>27, 113</sup> While increasing DNA hybridization decreased responsivity to adenosine in our PC hydrogels, it also reduced spontaneous swelling. Thus, increasing the amount of DNA hybridization may be a useful strategy in reducing spontaneous swelling of DNA-crosslinked hydrogels. In the future, hydrogels with intermediate degrees of hybridization should be analyzed to further characterize the tradeoff between responsivity and spontaneous swelling.

#### **4.3.5 Adenosine Sensing in Bovine Serum using Optimized PC Hydrogels**

To demonstrate real-world viability, the response of PC hydrogels fabricated using optimized procedures was evaluated in a complex matrix, 50% protein-removed fetal bovine serum. These PC hydrogels were fabricated with DNA annealed through the “Heating + Rapid Cooling” protocol, which was found to result in the greatest amount of hybridization with minimal time for cooling. To maximize responsivity, PC hydrogels were fabricated with 1.60 mM DNA. To minimize cost, PC hydrogels were cut into 0.2 cm × 0.2 cm pieces and analyzed in 1 mL solutions of diluted serum spiked with adenosine. As shown in Figure 4.9, we analyzed the particle spacing changes of this optimized sensor in serum solutions with 20-2000 μM adenosine.

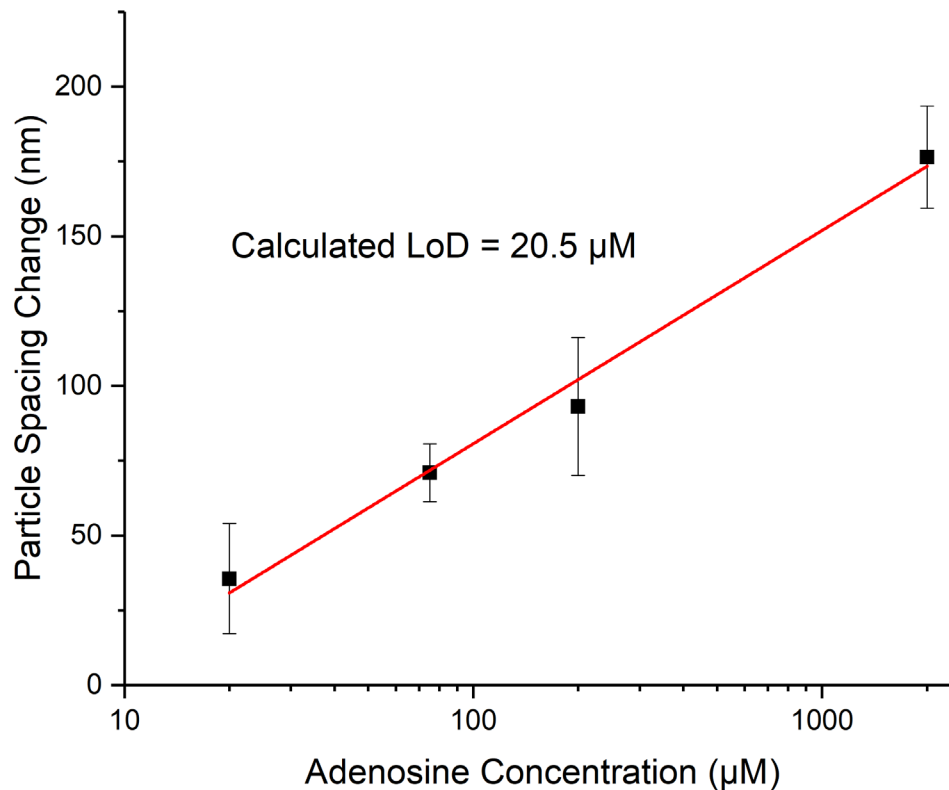


**Figure 4.9: Dependence of particle spacing change on adenosine concentration for optimized PC hydrogels. Particle spacing measurements were made after 60 mins in solutions of diluted fetal bovine serum spiked with adenosine. The average response of a blank sample measured in solution without adenosine was subtracted from each data point. The red line shows a linear fit (adjusted  $R$ -squared = 0.9898). Error bars indicate standard deviations ( $n=3$ ).**

We previously reported an aptamer-actuated PC hydrogel that can detect adenosine in diluted serum solutions.<sup>27</sup> Those PC hydrogels were 0.4 cm × 0.5 cm and incubated in 10 mL of adenosine-spiked serum solutions. In comparison, our optimized PC hydrogel sensors are smaller, operate in  $\frac{1}{10}$ <sup>th</sup> the sample volume, and are more responsive. Specifically, we found the particle spacing change of our optimized sensor to be  $\sim 1.8\times$  greater in 2 mM adenosine and  $\sim 1.2\times$  greater in 20 μM adenosine. We further estimate a limit of detection of 20.5 μM adenosine ( $S/N = 3$ ) for our optimized sensor, compared to 26.7 μM adenosine in our previously reported PC hydrogel.<sup>27</sup>

## 4.4 Conclusion

We report tunable aspects in the fabrication of aptamer-actuated, DNA-crosslinked PC hydrogels and their impact on responsivity. Our results indicate that annealing protocols should include a heat treatment, while cooling time is less important to maximize DNA hybridization; that responsivity scales with DNA concentration, but there is a simultaneous tradeoff with variability in particle spacing; and that responsivity is unimpacted by PC hydrogel size and sample volume, but that variability in particle spacing increases as PC hydrogel size and sample volume decrease. We further show that responsivity is impacted by DNA hybridization, and that increasing the amount of hybridization decreases responsivity while simultaneously decreasing spontaneous swelling.

Informed by these results, we fabricated an optimized PC hydrogel sensor to detect adenosine in diluted serum solutions. Compared to our previously reported sensor, our optimized sensor is smaller, requires a smaller sample volume, shows increased responsivity, and has a lower limit of detection.

These results may prove useful beyond sensing applications. For example, DNA-crosslinked hydrogels have been proposed as drug delivery vesicles.<sup>109</sup> To function properly, these vesicles have to swell in response to specific stimuli in the body. In this work, we have shown that the volume response can be tuned during hydrogel fabrication.

Studies of DNA-crosslinked and aptamer-actuated materials suffer from a lack of characterization, with research groups utilizing different techniques and frequently failing to report crucial aspects of their fabrication procedure. These shortcomings inhibit the application of these materials beyond research laboratories. Here, we report methodology and data to better understand

fundamental properties of these materials. We hope studies like this will activate further investigations and communication among researchers.

#### **4.4.1 Acknowledgements**

The authors acknowledge the University of Pittsburgh for providing instrumentation and financial support.

## **5.0 Aptamer-Actuated Two-Dimensional Photonic Crystal Hydrogel Sensor for Detection of Human Thrombin**

This chapter is in preparation for submission to the journal *Sensors & Diagnostics*, authored by Westbay, J. H.; Jang, K.; Goda, S. A.; and Asher, S. A. J. H. W. and K. J. conceived experiments. J. H. W. collected and analyzed data with assistance from K. J. and S. A. G. The manuscript was prepared by J. H. W. with assistance from K. J., S. A. G., and S. A. A.

There is a need to develop versatile sensing motifs that can be used in resource-limited settings. Ideally, sensors can be easily adapted to detect a wide variety of targets. We recently reported the development of a 2D photonic crystal (2DPC) hydrogel sensor that utilizes aptamer recognition groups to detect a small molecule, adenosine. Here, we extend that sensing motif to detect a protein, human thrombin. Our protein sensor is a 2DPC hydrogel with DNA crosslinks. DNA crosslinks are formed by hybridized DNA strands attached to the hydrogel network. One of the DNA strands contains a thrombin-binding aptamer sequence. On addition of thrombin, competitive aptamer-thrombin binding causes crosslinks to break, actuating hydrogel swelling. This, in turn, causes the particle spacing of the attached 2DPC array to increase, shifting PC diffraction. Thus, thrombin concentration can be monitored by measuring changes in 2DPC diffraction. Our thrombin sensor can detect thrombin in buffer and serum solutions at physiologically relevant concentrations, with calculated detection limits of 191 nM and 441 nM, respectively. These results demonstrate the generalizability of our aptamer-actuated 2DPC hydrogel sensing motif and suggest that sensors for other targets can be fabricated by simply exchanging the sequences of the attached DNA strands used during detection. We further

investigate the physical phenomena that actuate the observed response to better understand the aptamer-actuated sensing mechanism.

## 5.1 Introduction

There is a need to develop novel sensing technologies that are deliverable to end-users.<sup>1</sup> Recently, there has been significant progress in the development of sensors.<sup>164-169</sup> However, gold-standard technologies still suffer from the need for expensive equipment, trained personnel, and other limitations that inhibit their widespread use.<sup>1, 170</sup> Ideal sensors can be used in resource-limited settings and have wide-ranging utility, including to monitor environmental<sup>171-173</sup>, agricultural<sup>174-176</sup>, and military<sup>9, 177</sup> hazards, and as diagnostic devices<sup>165, 170, 173, 178, 179</sup>. Sensing motifs that are generalizable can be easily adapted to detect new targets and enable the rapid development of novel sensors.

Aptamers have emerged as a promising component of sensors. Aptamers are short DNA or RNA strands that have been selected using the systematic evolution of ligands by exponential enrichment (SELEX) process to sensitively and specifically bind a chemical target.<sup>65, 66</sup> Aptamers are analogous to antibodies, but tend to be more stable and cheaper to produce, thus enabling them to function as convenient molecular recognition agents.<sup>67</sup> Sensors that incorporate aptamers are categorized as aptasensors. Aptasensors have been incorporated into a variety of colorimetric<sup>28, 69, 82</sup>, fluorometric<sup>83-85</sup>, and electrochemical<sup>86, 87</sup> assays.

Photonic crystal (PC) hydrogels are a sensing platform invented by the Asher research group.<sup>18</sup> PC hydrogels consist of a PC array embedded into a stimuli-responsive hydrogel. This couples the PC particle spacing to the hydrogel volume. Changes in the chemical environment that

actuate hydrogel volume changes cause the PC particle spacing to change and can be monitored through shifts in PC diffraction. PC hydrogels are inexpensive to fabricate, require minimal to no sample preparation, and have a simple, colorimetric readout, enabling them to be used in resource-limited settings. PC hydrogels have been used to fabricate sensors for a variety of targets, including ions<sup>57, 127</sup>, small molecules<sup>28, 172</sup>, proteins<sup>63</sup>, and whole cells<sup>58</sup>.

Recently, we reported the development of a novel two-dimensional (2D) PC hydrogel aptasensor for a small molecule, adenosine.<sup>27</sup> In our aptasensor, the hydrogel contains noncovalent crosslinks formed by hybridized DNA. One of the DNA strands contains an adenosine-binding aptamer. On addition of adenosine, competitive aptamer-adenosine binding breaks hydrogel crosslinks. The breaking of crosslinks generates an osmotic pressure, causing the hydrogel to swell. This, in turn, increases the 2DPC particle spacing, shifting PC diffraction. Thus, adenosine concentration can be monitored by measuring changes in PC diffraction. Our sensor can detect adenosine in buffer and serum solutions, with detection limits of 13.9  $\mu\text{M}$  and 26.7  $\mu\text{M}$ , respectively.<sup>27</sup>

Subsequently, the Zhang group reported the development of a 2DPC hydrogel aptasensor to detect a protein target, human thrombin.<sup>159</sup> Thrombin is a serine protease involved in blood coagulation.<sup>160</sup> This aptasensor similarly relies on the breaking of DNA crosslinks actuated by a thrombin-aptamer binding. Despite utilizing a similar sensing motif as our adenosine aptasensor, the Zhang group reports a different fabrication procedure.

Here, we report the development of a novel aptamer-actuated 2DPC hydrogel sensor to detect human thrombin. We fabricated a thrombin aptasensor in the same way as our adenosine aptasensor, save that a thrombin-binding aptamer was used in place of the adenosine-binding aptamer.<sup>73</sup> On addition of thrombin, competitive aptamer-thrombin binding breaks hydrogel

crosslinks. As was the case in our adenosine sensor, the breaking of crosslinks generates an osmotic pressure, causing the hydrogel to swell. This actuates changes to the PC particle spacing, shifting PC diffraction. Thus, thrombin concentration can be monitored by measuring changes in PC diffraction. We calculate detection limits of 191 nM thrombin in thrombin-binding buffer, and 441 nM thrombin in protein-removed fetal bovine serum.

Our thrombin sensor is fabricated using the same methodology as our adenosine sensor, and thus demonstrates the generalizability of our aptamer-actuated 2DPC hydrogel sensing motif. Like our adenosine sensor, our thrombin sensor requires minimal sample preparation and equipment to use, ideally positioning it for use in resource-limited settings. This indicates that sensors can be fabricated for other targets by simply exchanging the aptamer molecular recognition group. We further highlight differences between the response of our thrombin sensor and that reported by the Zhang group<sup>159</sup> to better elucidate the mechanisms that actuate the sensing response.

## **5.2 Experimental Section**

### **5.2.1 Materials**

Acrydite-modified DNA strands (DNA 1: 5'-acrydite-ACT GTG GTT GGT GTG GTT GG-3', DNA 2: 5'-acrydite-ACC AAC CAC AGT-3', purified with high performance liquid chromatography) were purchased from Integrated DNA Technologies. Stock solutions of DNA 1, and 2 were prepared separately at 2 mM concentration in TE buffer (10 mM Tris, pH 8.0; 0.1 mM EDTA) and stored at -20 °C. Tris base ( $\geq 99.9\%$ ), magnesium chloride, HEPES (99%), sodium

hydroxide pellets ( $\geq 97\%$ ), sodium styrene sulfonate (NaSS) ( $\geq 90\%$ ), 2,2'-Azobisisobutyronitrile (AIBN) (98%), styrene (99%), acrylamide ( $\geq 99\%$ ), N,N'-methylenebisacrylamide (MBAAm) (99%), ammonium persulfate (98%), tetramethylethylenediamine (TEMED) (99%), bovine serum albumin, and myoglobin was purchased from Sigma-Aldrich. Ethylenediaminetetraacetic acid (EDTA) (99.5%) was purchased from JT Baker. Sodium chloride and thrombin (human plasma, high activity) (see Appendix C.1 for concentration determination) was purchased from EMD Millipore. Hydrochloric acid (36.5-38% w/w), potassium acetate (99%), calcium chloride, methanol (99.8%), and 2-propanol ( $\geq 99.5\%$ ) were purchased from Thermo Fisher Scientific. Potassium chloride was purchased from Spectrum Chemical. Ethanol (200 proof) was purchased from Decon Labs, Inc. Cover glass (thickness 1,  $24 \times 60 \text{ mm}^2$ ) and FBS were purchased from Corning. To remove serum proteins, FBS was filtered using 10 kDa centrifugal filters. Microscope premium frosted glass slides ( $25 \times 75 \times 1 \text{ mm}^3$ ) were purchased from Fisher Scientific. All chemicals were used as received unless otherwise specified. Ultrapure water ( $18.2 \text{ m}\Omega \cdot \text{cm}$ ) obtained from a Milli-Q Reference A+ was used for all experiments.

### 5.2.2 2DPC Hydrogel Fabrication

2DPC hydrogels were fabricated using described procedures, as summarized in Figure 1.<sup>27</sup> Briefly, negatively charged polystyrene particles with diameter  $\sim 1.20 \mu\text{m}$  were synthesized by a dispersion polymerization method described by Zhang et al.<sup>48</sup> These particles ( $\sim 15 \text{ \%w/w}$  in water) were mixed with 2-propanol in a 3:1 ratio and assembled into a hexagonally close-packed 2DPC array through the needle tip flow method.<sup>25</sup> The 2DPC array was deposited on a glass substrate ( $24 \times 60 \text{ mm}^2$ , cover glass, Corning) and dried at room temperature for 24 h. A polymerizable monomer solution was prepared that contained 25  $\text{ \%w/v}$  acrylamide in water, 0.2  $\text{ \%w/v}$  N,N'-

methylenebisacrylamide (MBAAm) in water, and annealed DNA. DNA was annealed by heating a solution containing 200  $\mu\text{M}$  of DNA 1 and 2 in duplex buffer (30 mM HEPES, 100 mM potassium acetate; pH 7.5) to 95  $^{\circ}\text{C}$  on a Corning LSE Digital Dry Bath Heater for 5 min and cooling the mixture on a bench top at room temperature for 30 min. The annealed DNA was then dried for  $\sim 4.5$  h on a Labconco Centrivap Concentrator (78100-00 A). The final concentration of DNA in the monomer solution was 0.8 mM. The monomer solution was then degassed in a vacuum desiccator for 15 min. Two layers of tape were applied to the 2DPC array sectioning off 0.048  $\text{cm}^2$  per 1  $\mu\text{L}$  of monomer solution. After adding initiator solution (0.7  $\mu\text{L}$  of 5% (v/v) TEMED in water and 0.7  $\mu\text{L}$  of 10% (w/v) ammonium persulfate in water), the monomer solution was stirred for 5 seconds and then deposited on the 2DPC array using a micropipette tip. A glass cover (25  $\times$  75  $\times$  1  $\text{mm}^3$ , microscope premium frosted glass slides, Fisher Scientific) was placed over the solution, and polymerization proceeded for 30 min in a vacuum desiccator. After polymerization, the glass substrates were placed in thrombin-binding buffer (20 mM Tris, 140 mM NaCl, 4 mM KCl, 1 mM  $\text{CaCl}_2$ , 1 mM  $\text{MgCl}_2$ ; pH 7.4) for 10 min. The glass cover was then removed using a razor blade, and the PC hydrogel was gently peeled from the glass substrate. The PC hydrogel was washed in thrombin-binding buffer for 3 min, cut into  $\sim 0.25 \times 0.25 \text{ cm}^2$  pieces, and refrigerated in a petri dish without buffer for storage. Figure 5.1 summarizes this fabrication process.

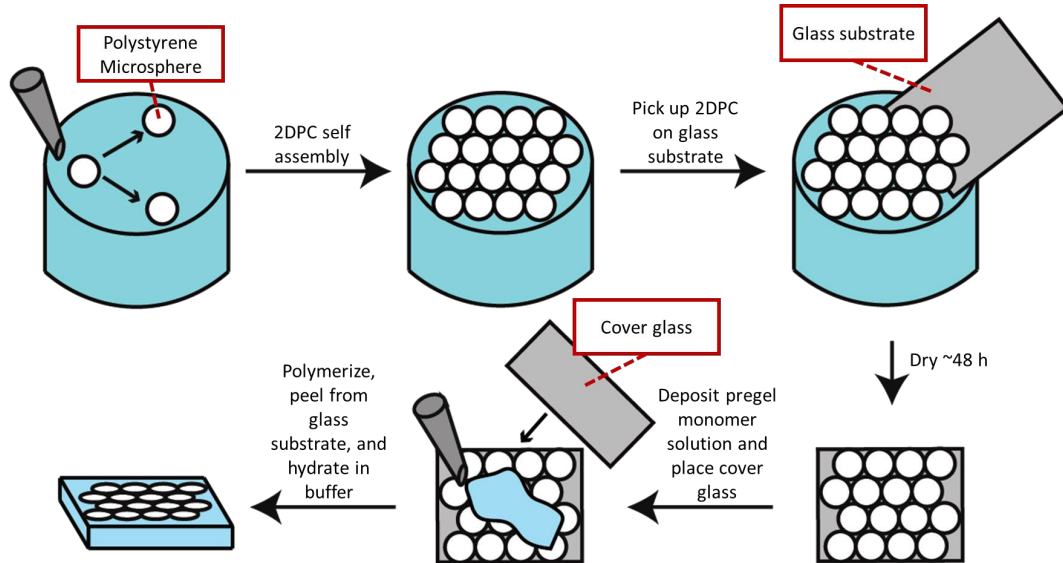


**Figure 5.1: 2DPC hydrogel fabrication procedure.** A 2DPC array is fabricated through a self-assembly process by injecting polystyrene particles onto the surface of water. The array is picked up on a glass substrate and dried. A monomer solution containing acrylamide, methylenebisacrylamide, DNA, and initiator is deposited onto the dried 2DPC array. A glass cover is placed over the monomer solution. After polymerization, the 2DPC hydrogel is peeled from the glass substrate, washed in buffer, and cut into pieces.

### 5.2.3 2DPC Particle Spacing Measurements

2DPC hydrogel particle spacing changes were monitored by measuring changes in Debye ring diameter.<sup>61</sup> Equation 5.1 gives the condition for Bragg diffraction of a 2D hexagonally close-packed PC array, where  $m$  is the diffraction order,  $\lambda$  is the wavelength of light,  $a$  is the 2DPC lattice spacing,  $\alpha$  is the angle of incidence, and  $\beta$  is the angle of diffraction.

$$m\lambda = \frac{\sqrt{3}}{2} a(\sin \alpha + \sin \beta) \quad \text{Equation 5.1}$$

Figure 5.2 shows a schematic of the set up for our Debye ring measurements. Briefly, the PC hydrogel is placed on an elevated stand, and a laser pointer is positioned along its normal ( $\alpha = 0$ ). This illuminates a Debye ring. By measuring the height between the Debye ring and the PC hydrogel,  $h$ , and the Debye ring diameter,  $D$ , the diffraction angle,  $\beta$ , can be determined using Equation 5.2.

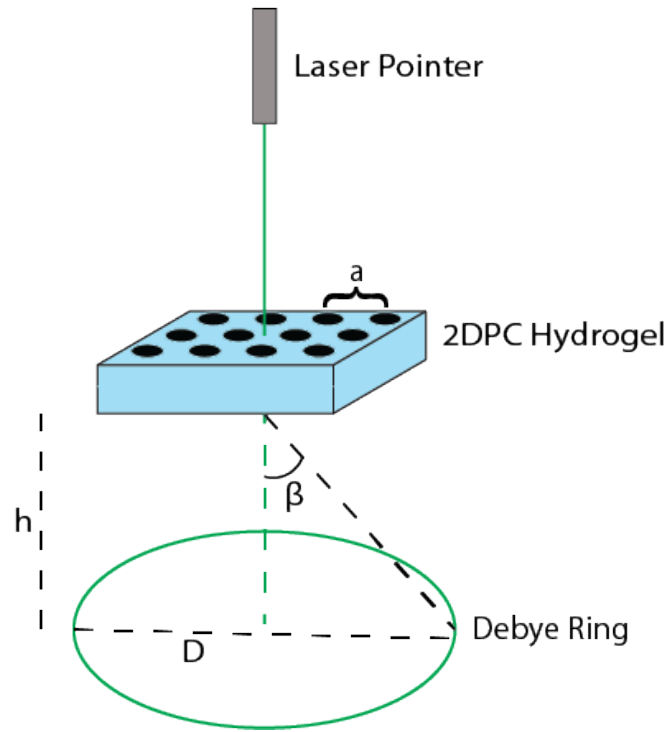


Figure 5.2: 2DPC hydrogel particle spacing measurement setup.

$$\beta = \tan^{-1}\left(\frac{D}{2h}\right)$$

Equation 5.2

Equations 5.1 and 5.2 can be combined to give Equation 5.3.

$$a = \frac{2\lambda}{\sqrt{3} \sin\left(\tan^{-1}\left(\frac{D}{2h}\right)\right)} \quad \text{Equation 5.3}$$

Since the wavelength of the light source is known (532 nm), and the height between the PC hydrogel and Debye ring is kept constant ( $h=15$  cm), PC hydrogel particle spacing changes can be monitored by simply measuring the Debye ring diameter,  $D$ , with a ruler. To calculate  $a$ , we measured and averaged  $D$  values at 5 different locations within each PC hydrogel piece.

#### 5.2.4 Thrombin Sensing in Buffer Solution

2DPC hydrogel pieces were brought to room temperature and immersed in 5 mL of thrombin-binding buffer (20 mM Tris, 140 mM NaCl, 4 mM KCl, 1 mM CaCl<sub>2</sub>, 1 mM MgCl<sub>2</sub>; pH 7.4). After 10 min, the initial particle spacing change was measured. PC hydrogel pieces were then immersed in 1 mL of thrombin-binding buffer solutions containing 0 (blank), 250, 500, 750, 1000, or 2000 nM thrombin. Particle spacing measurements were taken at time intervals of 30, 60, 90, and 120 min. Each measurement was repeated 3 times using a separate PC hydrogel piece.

#### 5.2.5 Changing the Buffer System

2DPC hydrogel pieces were brought to room temperature and immersed in 5 mL of alternate buffer (20 mM Tris, 150 mM NaCl, 10 mM MgCl<sub>2</sub>, 1 mM EDTA; pH 7.4). After 10 min, the initial particle spacing change was measured. PC hydrogel pieces were then immersed in 1 mL of alternate buffer solutions containing 0 (blank), 500, 1000, 1500 or 2000 nM thrombin. Particle

spacing measurements were taken at time intervals of 30, 60, 90, and 120 min. Each measurement was repeated 3 times using a separate PC hydrogel piece.

### **5.2.6 DNA Concentration Optimization**

2DPC hydrogels were fabricated using procedures described in Chapter 5.2.2, except that the concentration of DNA in the monomer solution was varied. PC hydrogels were fabricated using 0.1 mM, 0.8 mM, and 1.067 mM DNA.

After polymerization, 2DPC hydrogel pieces were brought to room temperature and immersed in 5 mL of thrombin-binding buffer (20 mM Tris, 140 mM NaCl, 4 mM KCl, 1 mM CaCl<sub>2</sub>, 1 mM MgCl<sub>2</sub>; pH 7.4). After 10 min, the initial particle spacing change was measured. PC hydrogel pieces were then immersed in 1 mL of thrombin-binding buffer solutions containing 0 (blank) or 1000 nM thrombin. Particle spacing measurements were taken after incubation for 120 min. Each measurement was repeated 3 times using a separate PC hydrogel piece.

### **5.2.7 Thrombin Sensing in Fetal Bovine Serum**

2DPC hydrogel pieces were brought to room temperature and immersed in 5 mL of thrombin-binding buffer. After 10 min, the initial particle spacing change was measured. Protein-removed fetal bovine serum was diluted 50% using a serum-diluting buffer (40 mM Tris, 210 mM NaCl, 8 mM KCl, 2 mM CaCl<sub>2</sub>, 2 mM MgCl<sub>2</sub>; pH 7.4) so that the final concentration of the solution was similar to that of the pure thrombin-binding buffer (20 mM Tris, 140 mM NaCl, 4 mM KCl, 1 mM CaCl<sub>2</sub>, 1 mM MgCl<sub>2</sub>; pH 7.4). PC hydrogel pieces were immersed in 1 mL of 50% fetal bovine serum solution spiked with 0 (blank), 500, 750, or 1000 nM thrombin. The particle spacing

was measured after incubation for 120 min. Each measurement was repeated 3 times using a separate PC hydrogel piece.

### **5.2.8 Selectivity Measurements**

PC hydrogel pieces were brought to room temperature and immersed in 5 mL of thrombin-binding buffer. After 10 min, the initial particle spacing change was measured. PC hydrogel pieces were then immersed in thrombin-binding buffer solutions containing 0 (blank) or 1000 nM thrombin, bovine serum albumin, or myoglobin. Particle spacing was measured after incubation for 120 min. PC hydrogels without DNA were fabricated using procedures described in Chapter 5.2.2, save that no DNA was added to the monomer solution. Each measurement was repeated 3 times using a separate PC hydrogel piece.

### **5.2.9 Free Energy of Mixing Measurements**

PC hydrogels were fabricated using procedures described in Chapter 5.2.2 with minor adjustments. For PC hydrogels with dangling, single-stranded DNA, only DNA 1 was added to the monomer solution. For PC hydrogels with melted DNA crosslinks, after polymerization, PC hydrogel pieces were transferred to centrifuge tubes containing 1 mL of thrombin-binding buffer. These tubes were sealed, heated to 95 °C on a Corning LSE Digital Dry Bath Heater for 5 min, and cooled to room temperature on a lab bench for 30 min. All PC hydrogel pieces were brought to room temperature and immersed in 5 mL of thrombin-binding buffer. After 10 min, the initial particle spacing change was measured. PC hydrogel pieces were then immersed in thrombin-binding buffer solutions containing 0 (blank) or 1000 nM thrombin, and particle spacing was

measured after 120 min. Each measurement was repeated 3 times using a separate PC hydrogel piece.

## **5.3 Results and Discussion**

### **5.3.1 Aptamer-Actuated 2DPC Hydrogel Sensing Motif for Detection of Thrombin**

Our sensing motif for detection of thrombin is based on that of our reported adenosine sensor.<sup>27</sup> As summarized in Figure 5.3, hydrogels were copolymerized with acrylamide, MBAAm, and annealed DNA strands. MBAAm formed covalent crosslinks that enhanced the mechanical robustness of the hydrogel and prevented dissolution. Annealed DNA strands were capped with an acrydite group (Figure 5.3). Acrydite is a phosphoramidite that has similar reactivity to an acrylamide monomer.<sup>145</sup> Thus, we were able to incorporate DNA into the hydrogel network with a single-step polymerization.

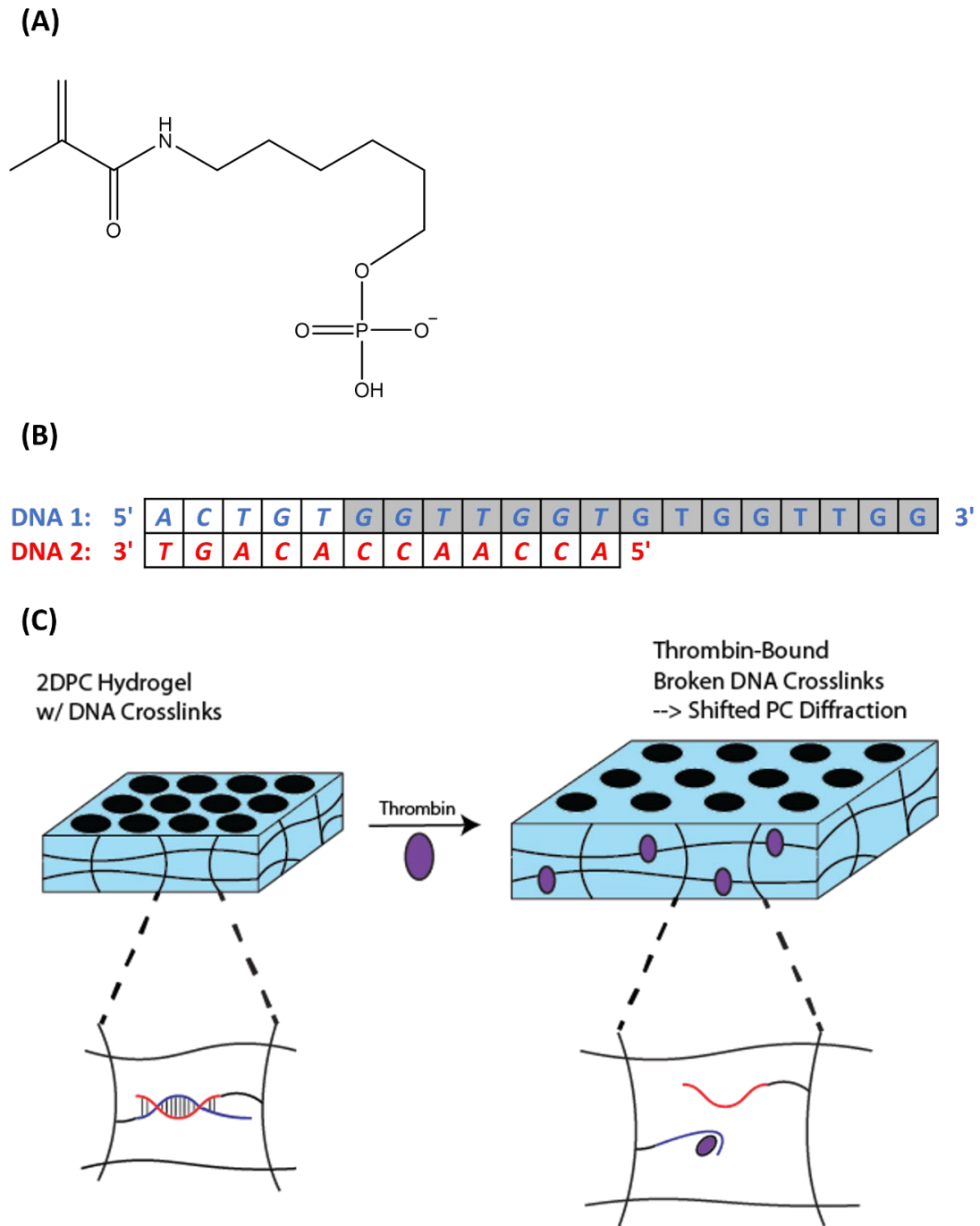


Figure 5.3: (A) Structure of acrydite. (B) DNA sequences used to fabricate PC hydrogels. Bases that make up the aptamer sequence are shaded. Complementary sequences are aligned and italicized. (C) The thrombin-sensing mechanism using a DNA-crosslinked 2DPC hydrogel. DNA 1 (blue) and 2 (red) are attached to the polyacrylamide hydrogel network, and competitive aptamer-thrombin binding actuates the sensing response.

Within the hydrogel, hybridized DNA forms non-covalent crosslinks. The hybridized DNA consists of a 15-mer thrombin-binding aptamer<sup>73</sup> and a 12-mer strand with bases complementary to the thrombin-binding aptamer. On addition of thrombin, competitive thrombin-aptamer binding breaks hydrogel crosslinks. This alters the elastic free energy of the hydrogel, generating an osmotic pressure.<sup>55</sup> The hydrogel swells to relieve this pressure, in turn increasing the particle spacing of the embedded PC array, shifting PC diffraction. Thrombin concentration was monitored by measuring 2DPC hydrogel Bragg diffraction shifts.

### **5.3.2 Thrombin Detection in Buffer Solution**

The sensing response of our thrombin-binding 2DPC hydrogels was monitored by measuring the 2DPC hydrogel particle spacing change of each  $0.25 \times 0.25 \text{ cm}^2$  piece immersed in buffer solutions. 2DPC hydrogels were first immersed in thrombin-binding buffer (20 mM Tris, 140 mM NaCl, 4 mM KCl, 1 mM CaCl<sub>2</sub>, 1 mM MgCl<sub>2</sub>; pH 7.4) that was blank and did not contain thrombin. After 10 min, the initial particle spacing was measured. Then, each hydrogel was immersed in a buffer solution containing 0 to 2000 nM thrombin.

Figure 5.4 shows the 2DPC hydrogel particle spacing changes over time in different concentrations of thrombin. Particle spacing change was evaluated by subtracting the initial particle spacing (at time = 0 min) from each subsequent measurement. Over time, hydrogels in larger concentrations of thrombin swelled more quickly and to a greater extent.

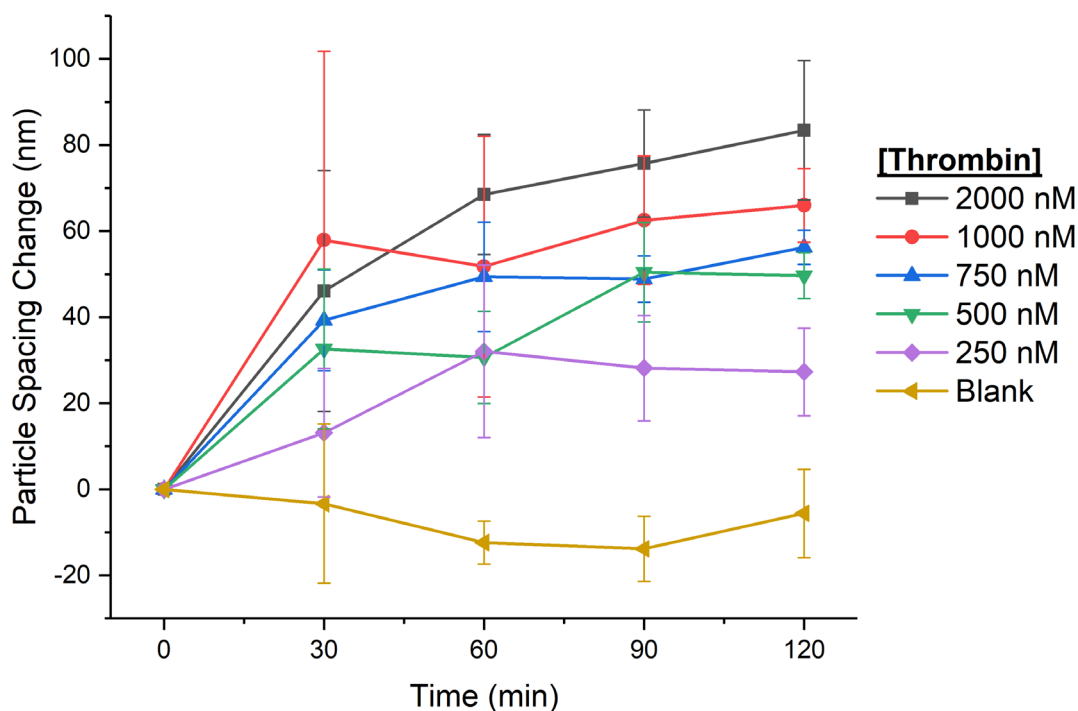


**Figure 5.4: 2DPC hydrogel particle spacing changes over time in different concentrations of thrombin solution. Error bars indicate standard deviations (n=3).**

The 2DPC hydrogel particle spacing changes depend on the concentration of thrombin because, as explained in Chapter 5.3.1, aptamer-thrombin binding actuates the response. Larger amounts of thrombin cause more aptamer-thrombin binding. This breaks a greater amount of DNA crosslinks, generating a larger osmotic pressure that causes more swelling. Since the 2DPC hydrogel particle spacing is proportional to the hydrogel volume, more swelling causes a larger particle spacing change.

Since the particle spacing change is actuated by aptamer-thrombin binding, particle spacing measurements can be used to estimate the aptamer dissociation constant ( $K_D$ ) (see Appendix C.2). The  $K_D$  was estimated to be  $\sim 369$  nM, which is slightly larger than the reported  $K_D$  for the thrombin-binding aptamer in solution ( $\sim 100$  nM)<sup>73</sup>. We hypothesize this slight decrease in binding affinity is caused by competitive binding of the aptamer to its complementary DNA, and by spatial

restrictions due to the attachment of the aptamer to the hydrogel polymer network. Interestingly, the estimated  $K_D$  of our adenosine-sensing PC hydrogels (68  $\mu\text{M}$ ) was also of the same order of magnitude as the reported  $K_D$  of the adenosine-binding aptamer ( $\sim 10 \mu\text{M}$ ).<sup>27</sup> This indicates that the response of our aptamer-actuated sensors is limited by aptamer-target equilibrium binding.

Particle spacing changes after 120 min were used to generate a calibration curve, as shown in Figure 5.5. Prior to 120 min, we observed large variability in particle spacing measurements, as indicated by the large standard deviations in Figure 5.4. We hypothesize that at these early time points, the PC hydrogel had not yet reached an equilibrium volume. After 120 min, we observed that 2DPC hydrogels swelled significantly in blank solutions without thrombin. To make the calibration curve, the average particle spacing change in blank solutions without thrombin was subtracted from that at each concentration of thrombin and plotted against thrombin concentration. A best fit line can be used to estimate thrombin concentration. Using the calibration curve, we calculated a detection limit of 191 nM (S/N=3). This detection limit is below reported physiologic concentrations of free thrombin found in the body during blood coagulation ( $> 500 \text{ nM}$ ) and demonstrates real-world viability.<sup>180</sup>

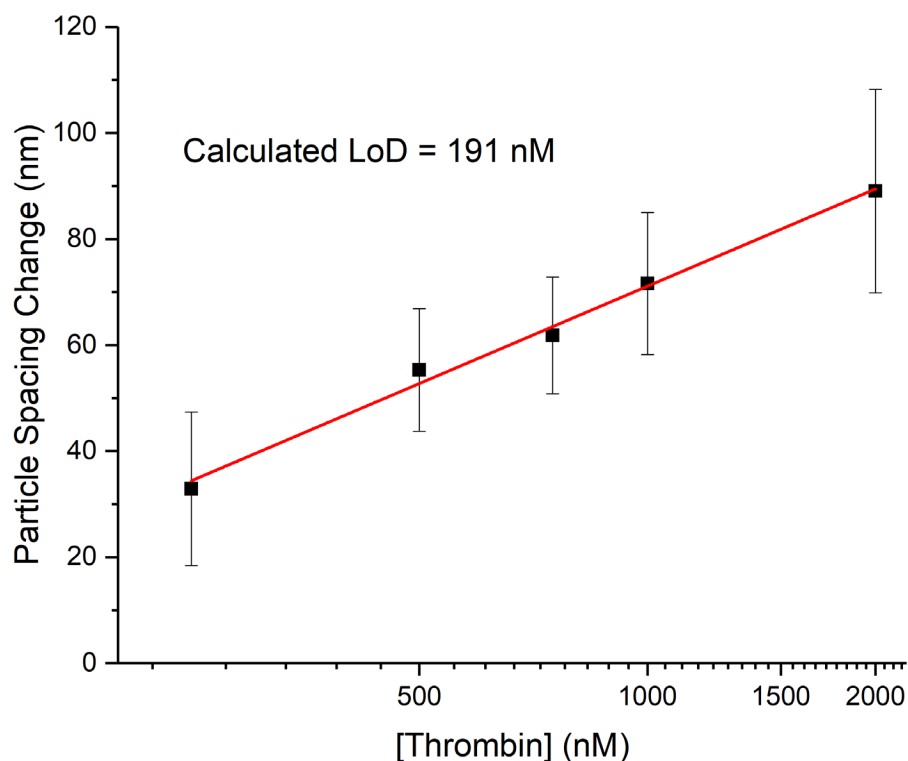


**Figure 5.5:** Dependence of particle spacing changes on thrombin concentration in buffer solutions at  $t=120$  min. The average particle spacing change in blank solution without thrombin was subtracted from each data point. The red line shows a linear fit (see Appendix C.3). Error bars indicate standard deviations ( $n=3$ ).

### 5.3.3 Changing the Buffer System

DNA conformation is impacted by buffer conditions in the surrounding environment.<sup>147,</sup>  
<sup>148</sup> Thus, buffer conditions can impact aptamer binding and stability. Despite the impact of buffer on aptamer-thrombin binding, several different buffer conditions have been reported in studies that utilize the same thrombin-binding aptamer as our 2DPC hydrogels.<sup>73, 85, 109, 181</sup> Researchers rarely comment on why a specific buffer system was utilized.

Ideally, buffer conditions are independently optimized for systems that utilize aptamer-target binding. However, optimization experiments require additional resources that can be

prohibitive. When designing our adenosine sensor, we optimized buffer conditions for aptamer-adenosine binding using a fluorescence assay.<sup>27, 85</sup> In contrast to adenosine, thrombin is more expensive and less stable. Thus, we were unable to utilize a fluorescence assay to optimize buffer conditions when designing our thrombin sensor.

In the absence of buffer optimization, it is best practice to utilize the buffer conditions reported during selection of the aptamer.<sup>118</sup> While different systems may have different optimal buffer conditions—for example, the optimal conditions for aptamer-target binding in solution may be different than the optimal conditions for aptamer-target binding in a hydrogel—absent other data, the original selection conditions are more likely to maximize aptamer-target binding than conditions that have not been tested.

For this study, we selected a buffer system similar to that initially reported during selection of the thrombin-binding aptamer.<sup>73</sup> To support this selection, we measured 2DPC hydrogel particle spacing changes in an alternate buffer system. This alternate buffer (20 mM Tris, 150 mM NaCl, 10 mM MgCl<sub>2</sub>, 1 mM EDTA; pH 7.4) was based on that utilized for our adenosine-sensing PC hydrogels (20 mM Tris, 10 mM MgCl<sub>2</sub>, 300 mM NaCl; pH 7.5).<sup>27</sup> Compared to the buffer used for our adenosine-sensing system, this alternate buffer contains less NaCl and a slightly lower pH, since these conditions are reported to be favorable for thrombin-aptamer binding.<sup>73</sup> We also included a small amount of EDTA to assist in stability of thrombin during storage. Figure 5.6 shows the particle spacing changes over time for 2DPC hydrogel pieces in this alternate buffer system with varying concentrations of thrombin.

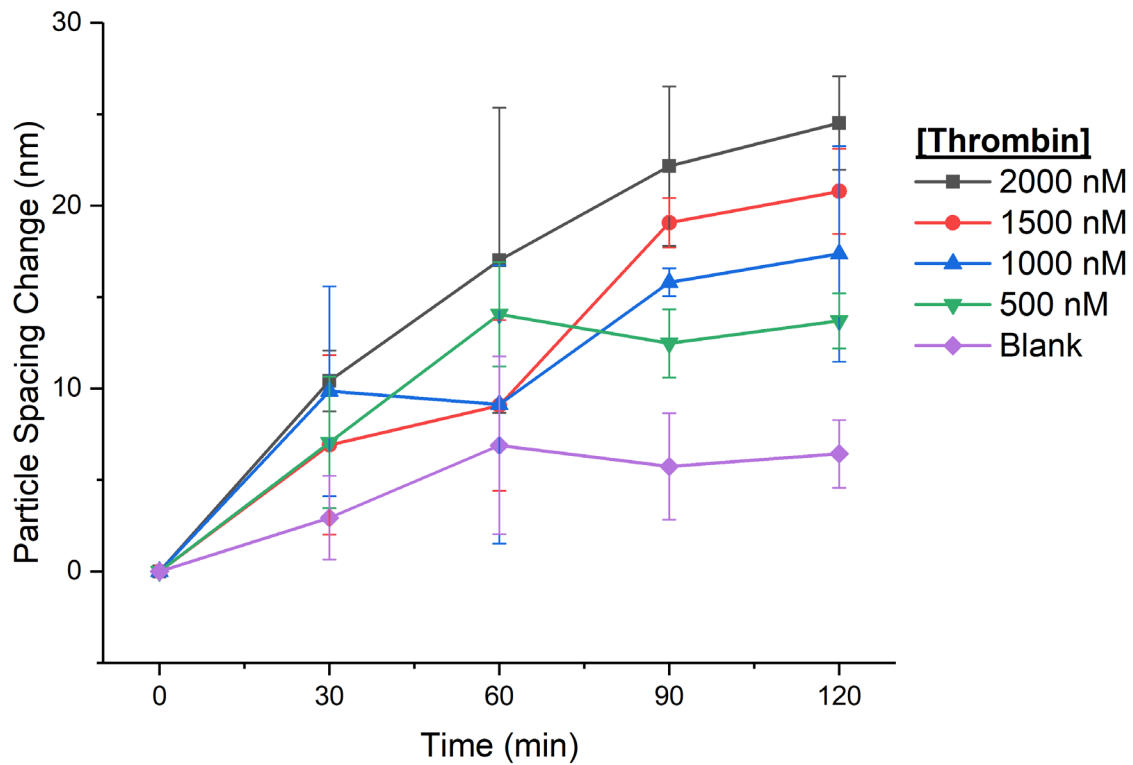


**Figure 5.6: 2DPC hydrogel particle spacing changes over time in an alternate buffer system with varying concentrations of thrombin. Error bars indicate standard deviations (n=3).**

Particle spacing changes after 120 min were used to generate a calibration curve, as shown in Figure 5.7.

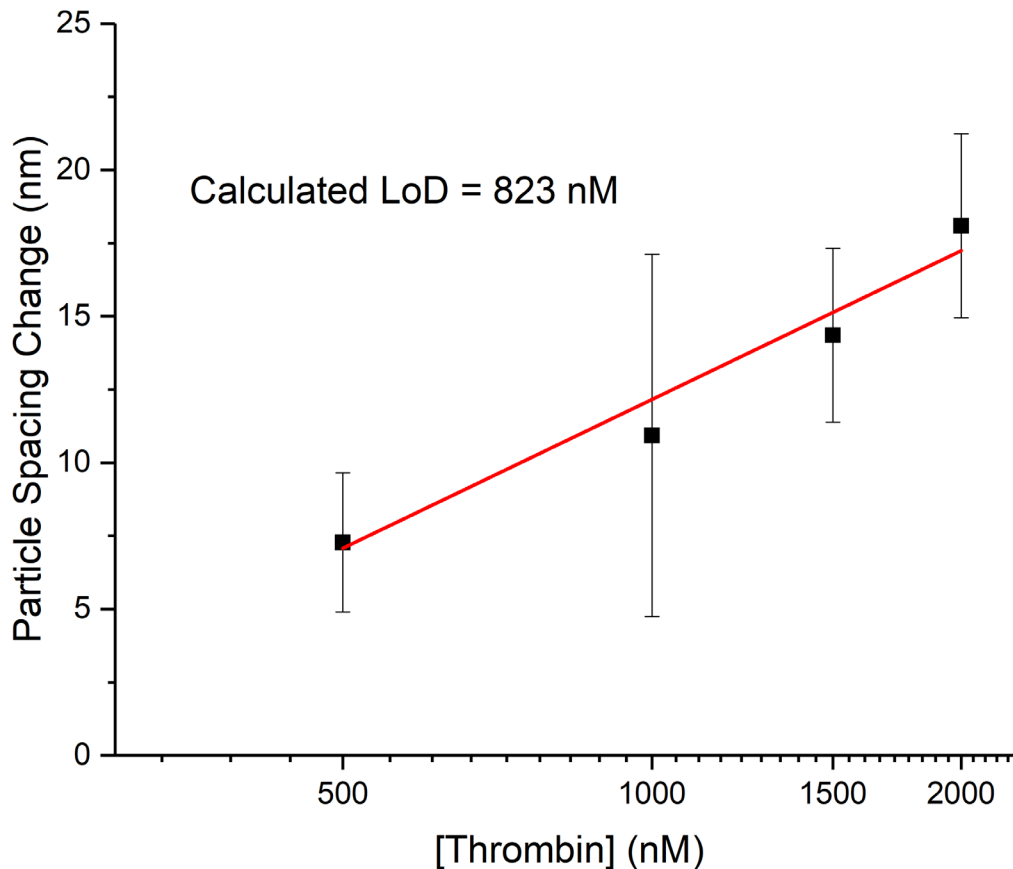


**Figure 5.7:** Dependence of particle spacing changes on thrombin concentration in an alternate buffer system at  $t=120$  min. The average particle spacing change in blank solution without thrombin was subtracted from each data point. The red line shows a linear fit (see Appendix C.4). Error bars indicate standard deviations ( $n=3$ ).

These results indicate that our 2DPC hydrogels are less responsive in alternate buffer compared to thrombin-binding buffer. For example, after 120 min in solutions with 2000 nM thrombin, the particle spacing change in alternate buffer is  $\sim 65$  nm smaller than that in the thrombin-binding buffer system. Furthermore, we calculated a detection limit of 823 nM ( $S/N=3$ ), which is over  $4\times$  that calculated in the thrombin-binding buffer system, indicating a significant decrease in sensitivity.

We hypothesize that this decrease in responsivity and sensitivity is caused by a decrease in aptamer-thrombin binding in the alternate buffer system. It is possible that KCl and CaCl<sub>2</sub>, which are absent in the alternate buffer but present in the thrombin-binding buffer, are necessary for the aptamer to fold into the proper conformation to bind thrombin.<sup>147, 148, 182</sup> It is also possible that EDTA, which is present in the alternate buffer but absent in the thrombin-binding buffer, inhibits aptamer-thrombin binding. For example, EDTA complexes with divalent metal ions. If the aptamer must interact with divalent ions to fold into the proper conformation for aptamer-thrombin binding, the EDTA-divalent ion complexes may inhibit interaction of the divalent ions with the aptamer, thus inhibiting aptamer-thrombin binding. Further investigation should be done to determine the impact of each component of the buffer system and optimize conditions for detection of thrombin.

#### **5.3.4 Optimization of DNA Concentration**

We investigated the impact of DNA concentration on 2DPC hydrogel particle spacing changes to optimize response to thrombin. Originally, we began studying 2DPC hydrogels with 800  $\mu\text{M}$  DNA.<sup>27</sup> Here, we also fabricated hydrogels using 100  $\mu\text{M}$  and 1067  $\mu\text{M}$  DNA. As summarized in Figure 5.8, PC hydrogels fabricated with different amounts of DNA were immersed in buffer solutions with 1000 nM thrombin, and particle spacing changes were measured after 120 min.

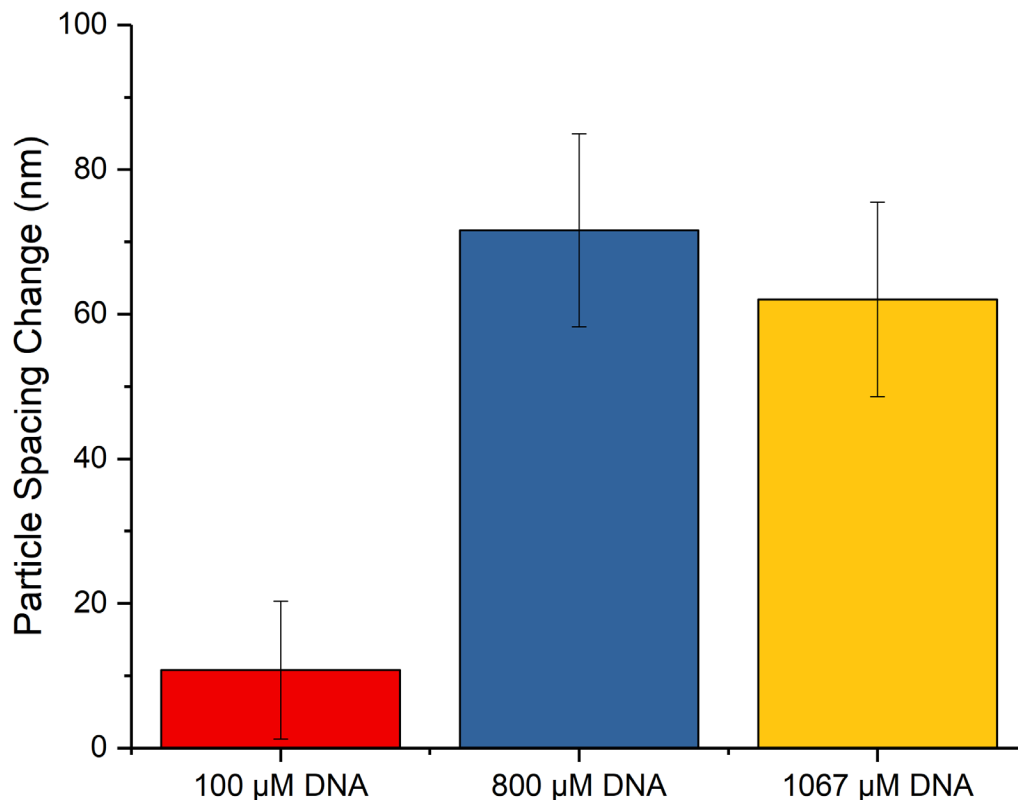


**Figure 5.8: Particle spacing changes of 2DPC hydrogels fabricated with different amounts of DNA in buffer solutions with 1000 nM thrombin after 120 min. The average particle spacing change in blank solution without thrombin was subtracted from each data point. Error bars indicate standard deviations (n=3).**

The results indicate that 2DPC hydrogel response depends on DNA concentration. In our 2DPC hydrogels, particle spacing changes are actuated by aptamer-thrombin binding. We hypothesized that 2DPC hydrogel response can be increased by increasing the concentration of DNA, since this would increase the amount of aptamer, and thus the amount of aptamer-thrombin binding. The data suggests this is true for DNA concentrations at and below 800  $\mu\text{M}$ . Thus, 2DPC hydrogel responsivity can be tuned by altering the concentration of DNA between 0 and 800  $\mu\text{M}$ .

At concentrations above 800  $\mu\text{M}$ , the observed particle spacing change decreases. We hypothesize this is because increasing the concentration of DNA above 800  $\mu\text{M}$  limits diffusion of thrombin into the hydrogel. In our sensors, DNA is dispersed throughout the hydrogel, and there

are aptamer strands both on the hydrogel surface and in the internal polymer network. Initially, thrombin binds to aptamer strands on the hydrogel surface. Over time, thrombin diffuses into the hydrogel, accessing internal aptamer strands that increase the amount of aptamer-thrombin binding and thus the response of the sensor. Increasing the concentration of DNA increases the concentration of aptamer strands on the hydrogel surface. It is possible that at DNA concentrations above 800  $\mu\text{M}$ , the amount of aptamer-thrombin binding on the surface of the hydrogel inhibits further diffusion of thrombin into the hydrogel network, limiting the sensing response.

Our results indicate that the response of our sensor is maximized when hydrogels are fabricated with 800  $\mu\text{M}$  DNA. In contrast, the Zhang group reports an optimal DNA concentration of 100  $\mu\text{M}$  for their thrombin-binding 2DPC hydrogel sensor.<sup>159</sup> They further report that increasing the concentration of DNA in their hydrogel above 100  $\mu\text{M}$  decreases response to thrombin.<sup>159</sup> We hypothesize that this difference in optimal DNA concentration is due to different fabrication chemistries.

We fabricate our sensors with acrydite-capped DNA. As explained in Chapter 5.3.1, acrydite has similar reactivity to the acrylamide monomer. We thoroughly mix the acrydite-capped DNA into our pre-gel monomer solution and fabricate hydrogels with a single-step polymerization. In contrast, the Zhang group utilizes DNA capped with an amine group. They incorporate amine-capped DNA using EDC coupling after their hydrogels have been polymerized.<sup>159</sup> Since the hydrogel has already been polymerized, it is more difficult to evenly distribute the DNA throughout the hydrogel polymer network, and it is likely that DNA is concentrated on the surface of the hydrogel. Since DNA is concentrated on the surface of the hydrogel, thrombin will bind more at the surface of the hydrogel. The accumulation of thrombin on the hydrogel surface may

limit diffusion of thrombin into the hydrogel network and could account for the observed decrease in responsivity when hydrogels are polymerized with more than 100  $\mu\text{M}$  DNA.

We also fabricated PC hydrogels with 100  $\mu\text{M}$  DNA and compared the sensing response to that reported by the Zhang group. Despite using the same concentration of DNA, we observed a smaller response to thrombin. This observation supports the hypothesis that DNA is concentrated on the surface of the hydrogels reported by the Zhang group. In PC hydrogels, when a molecular recognition group is concentrated on the surface of the hydrogel, analyte-recognition group interactions at the surface disproportionately actuate the sensing response.<sup>58</sup> Thus, accumulation of DNA on the surface of the hydrogel could explain why the Zhang group observed a larger response to thrombin despite fabricating hydrogels with the same amount of DNA. While this may be advantageous for larger sensing targets that diffuse slowly into the hydrogel, it may limit the detection of smaller targets, thus diminishing the generalizability of the fabrication methodology reported by the Zhang group.

### **5.3.5 Thrombin Detection in Fetal Bovine Serum**

The response of our 2DPC hydrogels was validated in a complex matrix, protein-removed fetal bovine serum (FBS). This is the same complex matrix used to validate our adenosine sensor.<sup>27</sup> Protein was removed from FBS through centrifugal filtration and diluted with buffer such that the buffer system conditions were similar to those reported in Chapter 5.3.2.

Figure 5.9 shows the response of our 2DPC hydrogels in FBS solutions spiked with different amounts of thrombin after incubation for 120 min. The thrombin-induced particle spacing changes were slightly smaller than those reported in pure thrombin-binding buffer solution. We hypothesize that this is due to interferents in the serum matrix that inhibit aptamer-thrombin

binding. We further calculated a detection limit of 441 nM ( $S/N=3$ ),  $\sim 2.3\times$  larger than that reported in pure thrombin-binding buffer. This decrease in sensitivity is greater than that observed for our adenosine sensor in FBS.<sup>27</sup> We hypothesize this greater decrease is due to the larger size of thrombin compared to adenosine. Larger molecules are more limited by diffusion. Thus, the impact of interferents that inhibit diffusion of analyte into the hydrogel will be more pronounced in the detection of thrombin when compared to adenosine.

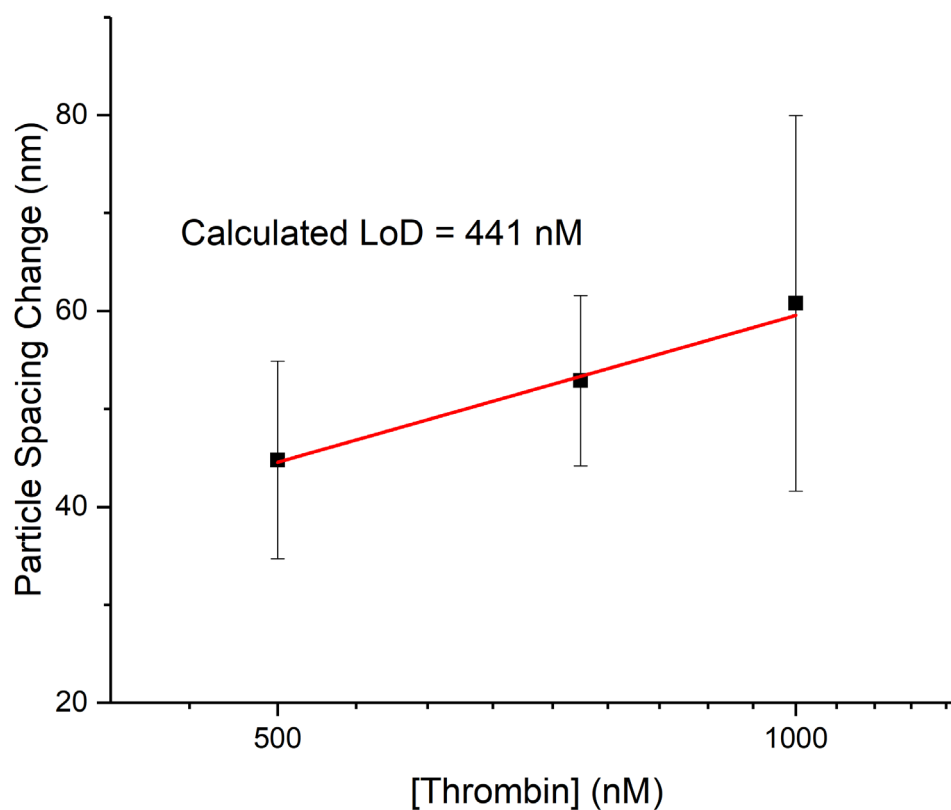


**Figure 5.9: Dependence of particle spacing changes on thrombin concentration in protein-removed FBS solutions at  $t=120$  min. The average particle spacing change in blank solution without thrombin was subtracted from each data point. The red line shows a linear fit (see Appendix C.5). Error bars indicate standard deviations ( $n=3$ ).**

Despite the decrease in responsivity and sensitivity, this calculated detection limit is of the same order of magnitude as the reported  $K_D$  of the thrombin-binding aptamer and is within the physiologically relevant range of free thrombin found in the human body.<sup>180</sup> This indicates that the sensing response has been largely preserved in FBS and demonstrates real-world viability. While these preliminary results are promising, further testing should be done to investigate the response of our thrombin sensor in complex matrices, particularly matrices with comparably sized proteins. Chapter 6.2 of this dissertation details further strategies to aid in these investigations.

### **5.3.6 Selectivity of Thrombin-Sensing 2DPC Hydrogels**

To investigate the selectivity of our thrombin sensor, we measured 2DPC hydrogel particle spacing changes in solutions spiked with proteins that do not bind the thrombin-binding aptamer. As summarized in Figure 5.10, only 2DPC hydrogels in solutions with thrombin swelled significantly after incubation for 120 min. We further measured the response of a 2DPC hydrogel fabricated without DNA, and thus without the thrombin-binding aptamer, in thrombin solution and observed a negligible change. These results confirm that the response of our sensor is actuated by aptamer-thrombin binding.

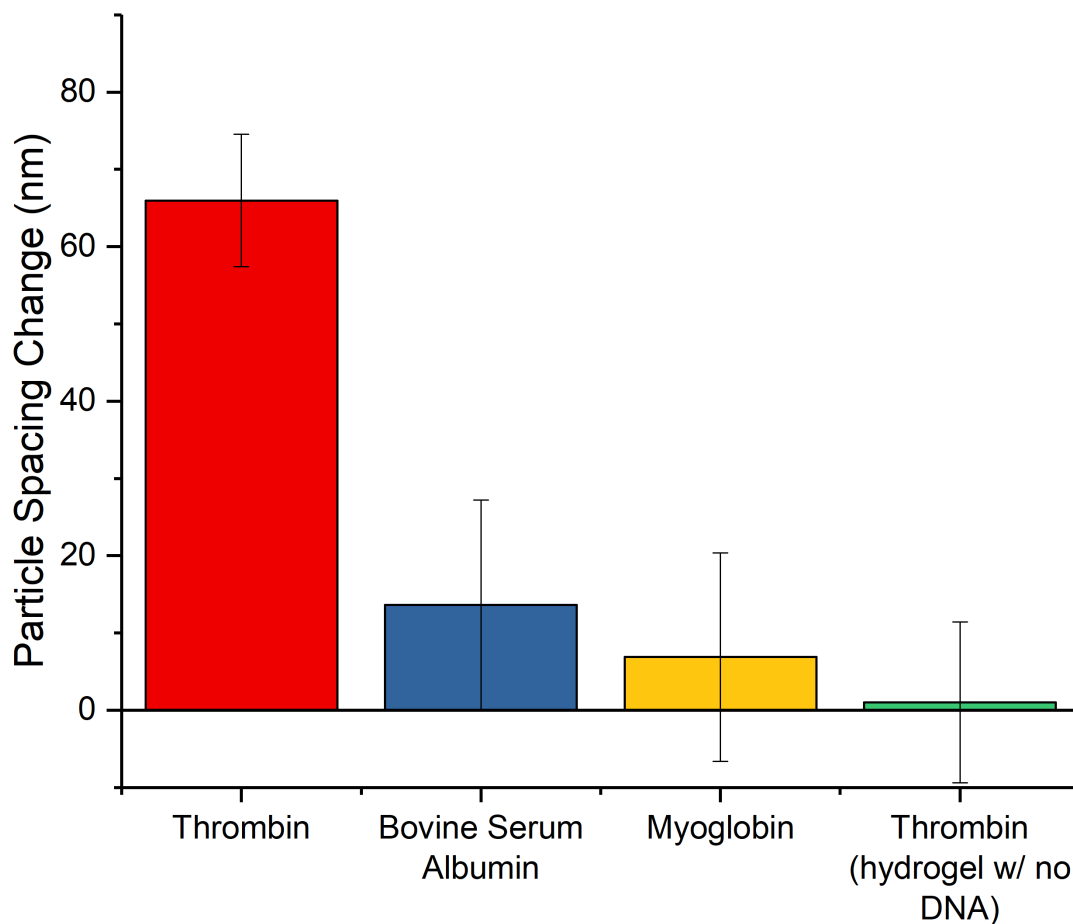


**Figure 5.10: Selectivity measurements for thrombin-binding 2DPC hydrogels. Particle spacing change was measured after 120 min in buffer solutions spiked with 0 (blank) or 1000 nM protein. The response of a 2DPC hydrogel without DNA (labeled “hydrogel w/ no DNA”) in 1000 nM thrombin was also measured. The average response in a blank solution without protein was subtracted from each data point. Error bars indicate standard deviations (n=3).**

### 5.3.7 Investigation of Free Energy of Mixing Phenomena

In their work, the Zhang group hypothesized that changes in the free energy of mixing contribute to the response of their thrombin sensor.<sup>159</sup> However, they provide no data to

specifically confirm this hypothesis. It is possible that aptamer-thrombin binding alters the free energy of mixing of the hydrogel. Free energy of mixing phenomena arise from interactions between the hydrogel polymer network and surrounding mobile phase.<sup>55</sup> Briefly, aptamer-thrombin binding effectively incorporates thrombin into the hydrogel polymer network. If interactions between thrombin and the hydrogel mobile phase are energetically favorable, the hydrogel will take in more mobile phase and swell. Contrarily, if these interactions are energetically unfavorable, the hydrogel will expel mobile phase and shrink. The Zhang group observed a swelling response, thus suggesting that thrombin-mobile phase interactions are energetically favorable.

To investigate the impact of free energy of mixing phenomena on the observed sensing response, we measured particle spacing changes of 2DPC hydrogels without DNA crosslinks. If no DNA crosslinks are present, there will be no changes to the elastic free energy of the hydrogel on addition of thrombin, and thus changes in the hydrogel volume are actuated by changes in the free energy of mixing.<sup>55</sup>

We utilized two strategies to investigate free energy of mixing phenomena. First, as summarized in Figure 5.11, we heated our DNA-crosslinked PC hydrogels, cooled them to room temperature, and then immersed them in solutions containing thrombin. Heating breaks DNA crosslinks. Since the DNA crosslinks are broken, aptamer-thrombin binding will not cause changes to the elastic free energy of the system, and observed volume changes are actuated by free energy of mixing phenomena.

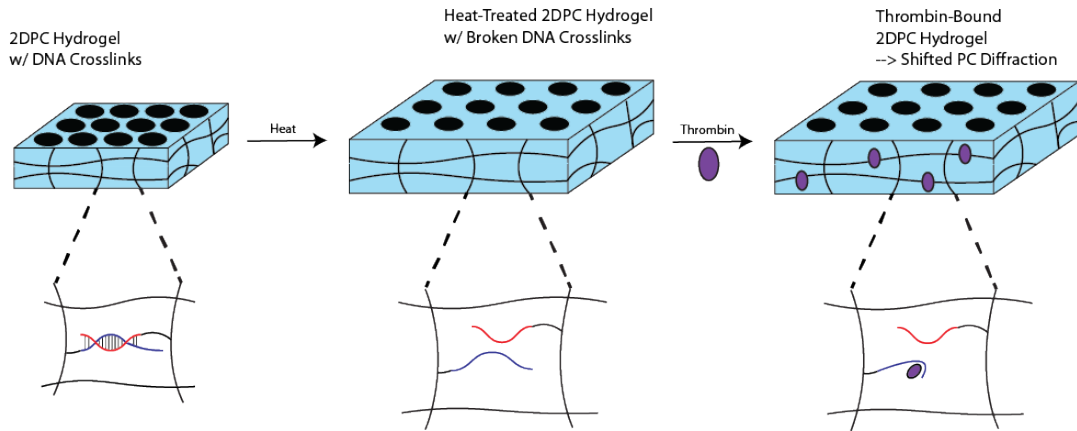


**Figure 5.11: Thrombin-sensing mechanism using a 2DPC hydrogel with melted DNA crosslinks to investigate the effect of free energy of mixing phenomena. The PC hydrogels are first heated to break DNA crosslinks, and then immersed in solutions containing thrombin. If aptamer-thrombin binding causes a change in the free energy of mixing of the system, the PC hydrogel will swell or shrink, shifting PC diffraction.**

Next, we fabricated 2DPC hydrogels without DNA crosslinks, as summarized in Figure 5.12. These hydrogels contained dangling, single-stranded DNA with the thrombin-binding aptamer sequence. Since there are no DNA crosslinks, aptamer-thrombin binding will not cause changes to the elastic free energy of the system, and observed volume changes are caused by changes to the free energy of mixing.

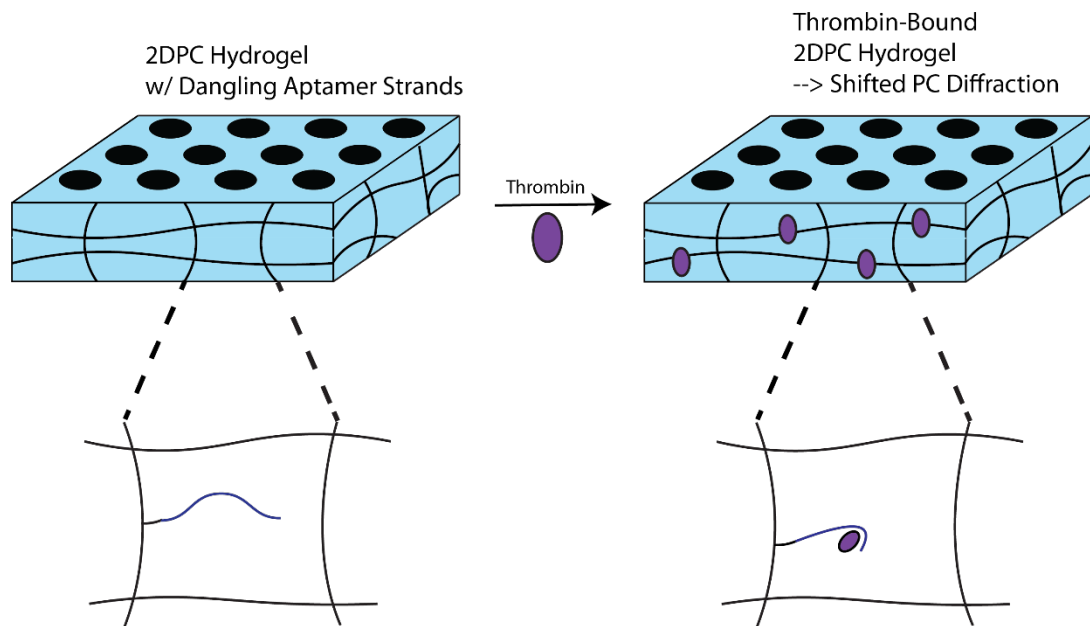


**Figure 5.12: Thrombin-sensing mechanism using a 2DPC hydrogel to investigate the effect of free energy of mixing phenomena. The PC hydrogels contain a dangling, single-stranded aptamer instead of hybridized DNA crosslinks. If aptamer-thrombin binding causes a change in the free energy of mixing of the system, the PC hydrogel will swell or shrink, shifting PC diffraction.**

2DPC hydrogel pieces fabricated using these strategies were immersed in buffer solutions with 1000 nM thrombin, and the response was compared to those containing DNA crosslinks, as shown in Figure 5.13.

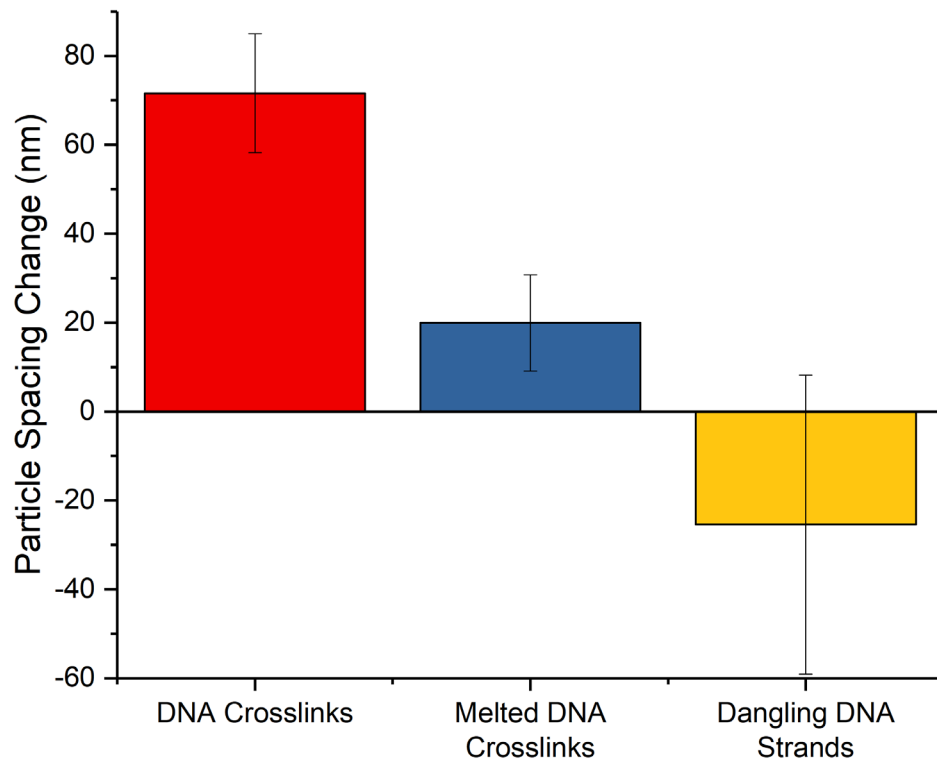


**Figure 5.13: Particle spacing changes of 2DPC hydrogels to investigate free energy of mixing phenomena. Particle spacing changes were measured after 120 min incubation in buffer solutions with 1000 nM thrombin. 2DPC hydrogels with DNA crosslinks (“DNA Crosslinks”), crosslinks broken by heating (“Melted DNA Crosslinks”), and dangling, single-stranded aptamer sequences (“Dangling DNA Strands”) were analyzed. The average particle spacing change in blank solution without thrombin was subtracted from each data point. Error bars indicate standard deviations (n=3).**

2DPC hydrogels with DNA crosslinks swelled significantly more in thrombin solution than those with melted crosslinks and those with dangling single-stranded DNA. This confirms that changes to the elastic free energy are primarily responsible for the observed sensing response. 2DPC hydrogels with melted DNA crosslinks showed a ~20 nm increase in particle spacing after immersion in 1000 nM thrombin. It is possible that this response is actuated by changes to the free energy of mixing of the hydrogel. However, we hypothesize it is more likely this response is due to the breaking of a small number of DNA crosslinks actuated by thrombin-aptamer binding.

Although the hydrogels were heated prior to exposure to thrombin to break DNA crosslinks, it is possible that a small number of crosslinks reformed as the hydrogels were cooled to room temperature. Thus, the breaking of a small number of DNA crosslinks could account for the observed sensing response.

This hypothesis is supported by the response of PC hydrogels fabricated without DNA crosslinks. These hydrogels contained dangling, single-stranded aptamer sequences, and thus the observed response was not actuated by breaking crosslinks. When compared to the response in blank solution without thrombin, these PC hydrogels appeared to shrink. This suggests that incorporation of thrombin into the hydrogel polymer network causes unfavorable changes to the free energy of mixing of the hydrogel. This shrinking response caused by changes to free energy of mixing would counteract swelling caused by changes to the elastic free energy, in contrast to what the Zhang group hypothesized. These results further suggest that the response of our sensor is actuated predominately by changes to the elastic free energy of the hydrogel.

It should be noted that our measurements utilizing PC hydrogels with dangling, single-stranded DNA were highly variable, as indicated by the large standard deviation in Figure 5.13. We hypothesize this variability is due to the smaller number of crosslinks in PC hydrogels with dangling, single-stranded DNA. Prior to immersion in thrombin solution, all PC hydrogels were equilibrated in buffer for 10 min. Samples with DNA crosslinks contained both covalent MBAAm crosslinks and non-covalent DNA crosslinks, totaling to a crosslinker concentration of  $\sim 2.1$  mM. Samples with dangling, single-stranded DNA did not contain DNA crosslinks, and the total crosslinker concentration was  $\sim 1.3$  mM. Hydrogels with larger concentrations of crosslinker swell less at equilibrium.<sup>55</sup> We hypothesize that 10 min incubation is enough time for the PC hydrogels with 2.1 mM crosslinker to reach an initial equilibrium volume, but not enough time for PC

hydrogels with 1.3 mM crosslinker to reach an initial equilibrium volume. This caused significant variability in the initial particle spacing measurements of PC hydrogels with dangling, single-stranded DNA, thus causing variability in the measured particle spacing changes.

In the future, we plan to fabricate more hydrogels with dangling, single-stranded thrombin-binding aptamers and fully investigate the effect of changes to the free energy of mixing of the hydrogel on measured particle spacing changes.

#### **5.4 Conclusion**

We report a novel aptamer-actuated 2DPC hydrogel sensor that detects a protein, human thrombin. Our sensor is user-friendly, requiring only a laser pointer and ruler to operate, specific for thrombin, and sensitive, with calculated detection limits of 191 nM in buffer solution and 441 nM in diluted serum.

The sensing motif described herein is based on that of our reported adenosine-sensing PC hydrogels. The only differences between our thrombin sensor and adenosine sensor are the DNA sequences attached to the hydrogel and the buffer conditions during sensor operation. Thus, these results suggest our motif is generalizable, and sensors for diverse targets can be fabricated by exchanging the attached DNA sequences and buffer system used during detection.

We further investigated the physical phenomena that actuate the response of our sensor. We found that changes to the elastic free energy predominantly cause changes in the PC hydrogel particle spacing rather than changes to the free energy of mixing. In future work, we plan to further investigate the impact of changes to the free energy of mixing.

### **5.4.1 Acknowledgements**

The authors acknowledge the University of Pittsburgh for providing instrumentation and financial support.

## 6.0 Summary of Conclusions and Future Works

### 6.1 Conclusions

In this dissertation, we report a novel aptamer-actuated, 2DPC hydrogel sensing motif. Chapters 1 and 2 provide pertinent background and the theoretical justification for our novel sensing mechanism. To fabricate sensors, a 2DPC array is embedded into a DNA-crosslinked hydrogel. In the hydrogel, hybridized DNA strands form non-covalent crosslinks. One of the DNA strands contains an aptamer sequence. On addition of the aptamer's binding target, competitive aptamer-target binding breaks crosslinks. This alters the elastic free energy of the hydrogel, actuating swelling. Hydrogel swelling causes the 2DPC particle spacing to increase, shifting 2DPC diffraction. Thus, the aptamer's binding target can be quantified by monitoring shifts in 2DPC diffraction.

2DPC hydrogel diffraction shifts can be simply quantified using a laser pointer and ruler. Thus, our novel sensing motif is user-friendly, requires minimal equipment to operate, and is ideally positioned for use in resource-limited settings.

In Chapter 3, we report our proof-of-concept work using this novel sensing motif to fabricate a sensor to detect a small molecule, adenosine. This is the first reported aptamer-actuated, DNA-crosslinked 2DPC hydrogel sensor. Our adenosine sensor responds in less than 60 min, is selective, and sensitive, with calculated detection limits  $< 30 \mu\text{M}$ . The sensor is versatile and can quantify adenosine in both buffer and serum solutions with similar sensitivity.

In Chapter 4, we investigate the tunable properties of our aptamer-actuated sensor. By monitoring shifts in 2DPC hydrogel diffraction, we systematically characterized how properties

like the concentration and sequence of DNA, and hydrogel size impact the aptamer-actuated hydrogel volume response. We further demonstrate how experimental details often ignored in literature, such as the protocol for annealing DNA, impact hydrogel behavior, and emphasize the importance of reporting these procedures. By optimizing these tunable properties for the detection of adenosine, we reduced the cost of fabricating our sensors, increased responsivity to adenosine, and lowered the detection limit in serum by > 20%. These investigations are impactful beyond sensing applications, as volume-responsive, aptamer-actuated hydrogels have been used as drug-delivery vesicles, actuators, and tissue scaffolds.

In Chapter 5, we use our aptamer-actuated sensing motif to fabricate sensors for a protein, human thrombin. Our thrombin sensor responds in 120 min, is selective, and sensitive, with detection limits < 500 nM in both buffer and serum solutions. These detection limits are within the physiologically relevant range for thrombin and demonstrate real-world viability.

The sensors reported here are easy to fabricate, selective, specific, respond rapidly, require minimal equipment to operate, and have user-friendly readouts. These properties ideally position them for use outside of the laboratory.

Importantly, our sensors for adenosine, a small molecule, and thrombin, a protein, are fabricated in the exact same way, save for the utilized sequences of DNA. This indicates that the sensing motif and reported fabrication methodology are generalizable, and sensors for other targets can be fabricated by simply exchanging the DNA strands in the 2DPC hydrogel network. Aptamers have been reported for a wide range of chemical targets, including ions<sup>57</sup>, small molecules<sup>28, 62</sup>, proteins<sup>63, 64</sup>, and whole cells<sup>58</sup>, enabling the fabrication of a multitude of sensors. This is the first work to report an aptamer-actuated PC hydrogel sensing motif that can detect chemically diverse targets.

For both sensors, we estimate that the dissociation constant of the aptamer in the 2DPC hydrogel is of the same order of magnitude as the reported dissociation constant of the aptamer in solution. This indicates that the sensing response is limited by aptamer-binding equilibrium, regardless of the sensing target. Recently, aptamers with < nM dissociation constants have been reported, suggesting that we can fabricate sensors with ultra-low limits of detection.<sup>73, 79</sup>

## **6.2 Future Works**

### **6.2.1 Alternative Aptamer-Actuated, DNA-Crosslinked 2DPC Hydrogel Sensing Motifs for Protein Detection**

The 2DPC hydrogel sensing response reported in this dissertation relies on the breaking of DNA crosslinks actuated by aptamer-target binding. In Chapter 5.3.7, we investigated an alternative aptamer-actuated sensing motif to detect the protein thrombin. Briefly, we fabricated 2DPC hydrogels with dangling DNA aptamer strands. In theory, on addition of thrombin, aptamer-thrombin binding effectively incorporates thrombin into the hydrogel network. This could alter the free energy of mixing of the hydrogel, actuating a volume change that can be monitored through shifts in PC diffraction. We observed a modest shrinking response. However, the large standard deviation of those measurements indicates a need for further testing.

Sensors for other proteins can be fabricated using a similar sensing motif. Changes to the free energy of mixing are actuated by changes to the hydrogel polymer-mobile phase interactions.<sup>55</sup> Hydrogel polymer-mobile phase interactions are related to the solubility of the polymer in the mobile phase. When hydrogels contain dangling aptamer sequences, aptamer-target

binding effectively incorporates the target into the hydrogel polymer network. If incorporation of a protein into the hydrogel polymer network significantly alters that solubility of the polymer in the mobile phase, the free energy of mixing of the hydrogel will change, actuating swelling or shrinking that can be monitored through an attached PC array. Thus, we hypothesize 2DPC hydrogels with dangling aptamer strands are a generalizable platform to detect proteins that alter the solubility of the hydrogel polymer on aptamer-protein binding.

We also hypothesize that a third generalizable aptamer-actuated 2DPC hydrogel sensing motif can be developed using two different aptamer sequences. Aptamers that bind proteins bind specific domains in the protein. For example, in the case of thrombin, there is a 15-mer aptamer that binds exosite I<sup>73</sup> and a 29-mer aptamer that binds exosite II<sup>183</sup>. As summarized in Figure 6.1, these distinct aptamers can be used in concert to fabricate a 2DPC hydrogel sensor for thrombin.

Briefly, 2DPC hydrogels can be fabricated with both the 15-mer<sup>73</sup> and 29-mer<sup>183</sup> thrombin-binding aptamers. On addition of thrombin, these aptamers will bind different exosites of thrombin. Simultaneous binding of each aptamer to its exosite will create effective hydrogel crosslinks. This will alter the elastic free energy of the system, actuating shrinking, that in turn causes shifts in the diffraction of the attached 2DPC array. Thus, thrombin concentration can be monitored through 2DPC diffraction shifts.

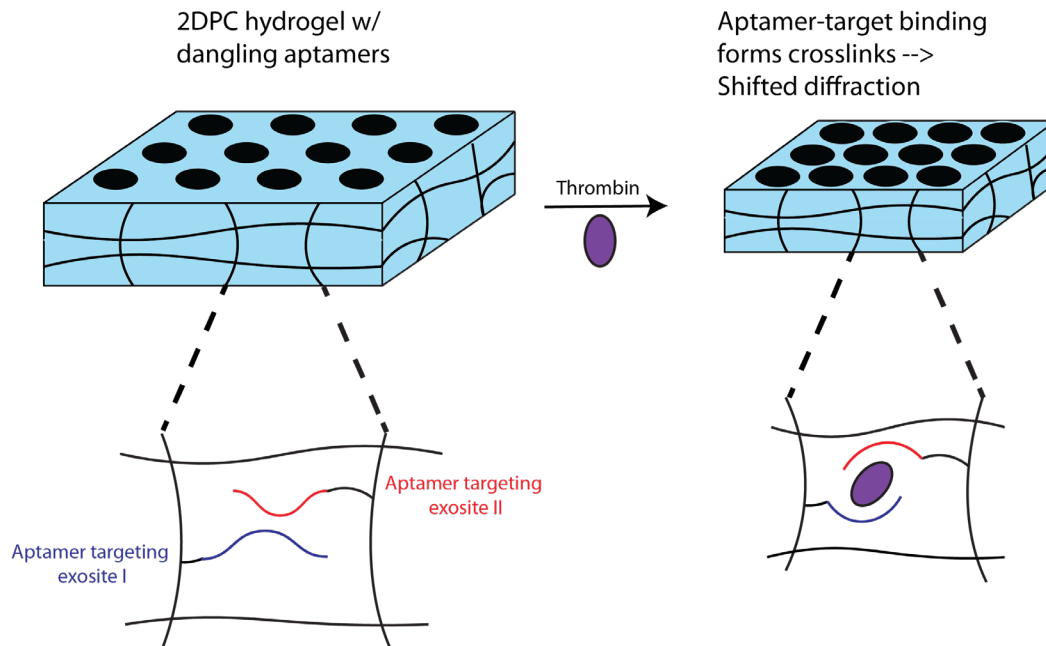


**Figure 6.1: Alternative thrombin sensing motif. 2DPC hydrogels are fabricated with two different aptamers that bind different sites on thrombin. On addition of thrombin, each aptamer binds to a unique binding site, creating effective hydrogel crosslinks. This causes the hydrogel to shrink, shifting 2DPC diffraction.**

We hypothesize that this sensing motif is generalizable to any protein for which there exists at least two aptamers that bind distinct sites on the protein.

### **6.2.2 Further Investigation of Tunable Properties of Aptamer-Actuated PC Hydrogels**

The tunable properties of aptamer-actuated PC hydrogels explored in Chapter 4 can be investigated further to attain a more robust understanding of how these properties impact the sensing response. PC hydrogel particle spacing measurements are a convenient way to systematically examine how altering aspects of the fabrication and operation of hydrogel materials impacts the hydrogel volume response, and may be useful beyond sensing applications.



### 6.2.3 Reversibility of Aptamer-Actuated 2DPC Hydrogels

The reversibility of the reported DNA-crosslinked hydrogel sensors can be investigated. Reversibility of our sensors requires two steps: (1) Removing the aptamer-bound target; and (2) Reforming the hybridized DNA crosslinks.

Removing the aptamer-bound target can be achieved through enzymatic reactions that selectively alter the chemistry of the target. For example, in the case of adenosine, the enzyme adenosine deaminase converts adenosine to inosine.<sup>28</sup> Since inosine does not bind the adenosine-binding aptamer, inosine will detach from the hydrogel and can be removed through rinsing.

Reformation of broken DNA crosslinks in an aptamer-actuated PC hydrogel has not yet been reported. In preliminary investigations, we attempted reforming DNA crosslinks by repeating our annealing protocol on swollen hydrogels. However, we found no evidence that DNA crosslinks had reformed. We hypothesize that this is because, in a swollen hydrogel, the DNA strands have been spatially separated from their complementary pairs. Since the DNA is attached to the hydrogel network, it does not have the spatial freedom to find its complementary pair and rehybridize. Thus, the hydrogel must first shrink before DNA crosslinks can reform. Strategies that may enable hydrogel shrinking include exchanging the hydrogel mobile phase<sup>184</sup> and polymerizing an interpenetrating network that can be used to manipulate the hydrogel volume<sup>185</sup>.

### 6.2.4 Aptamer-Actuated 2DPC Hydrogel Sensors for Novel Targets

This work demonstrates the generalizability of our aptamer-actuated 2DPC hydrogel sensing motif through fabrication of sensors for two distinct targets—a small molecule and a protein. This sensing motif can be applied to detect other targets. For example, aptamers have been

reported that bind ions<sup>57</sup> and whole cells<sup>58</sup>, enabling fabrication of sensors for these distinct chemical species.

Fabricating sensors for whole-cell targets may prove challenging because these targets can be larger than the pore size of the acrylamide hydrogel network, inhibiting diffusion into the hydrogel. However, we have demonstrated that interactions of large targets at the surface of a hydrogel are sufficient to actuate measurable volume responses.<sup>58</sup> Thus, we hypothesize we can fabricate sensors for large targets, even if those targets do not diffuse into the hydrogel. Sensors for whole-cell targets should be fabricated utilizing the methodology described herein to verify this hypothesis.

## Appendix A Supporting Information for Chapter 3

### Appendix A.1 Calculating dissociation constant of adenosine-binding aptamer

The fraction of bound aptamer,  $f_{bound}$ , is defined as:

$$f_{bound} = \frac{[aptamer \cdot adenosine]}{[free aptamer] + [aptamer \cdot adenosine]}$$

Where  $[aptamer \cdot adenosine]$  is the concentration of adenosine-bound aptamer and  $[free aptamer]$  is the concentration of aptamer that has not bound adenosine. Dividing the numerator and denominator by  $[aptamer \cdot adenosine]$  gives:

$$f_{bound} = \frac{1}{\frac{[free aptamer]}{[aptamer \cdot adenosine]} + 1}$$

The dissociation constant,  $K_D$ , of the adenosine-binding aptamer is:

$$K_D = \frac{[free aptamer][free adenosine]}{[aptamer \cdot adenosine]}$$

Where  $[free adenosine]$  is the concentration of adenosine that the aptamer has not bound.

Thus,  $f_{bound}$  can be written as:

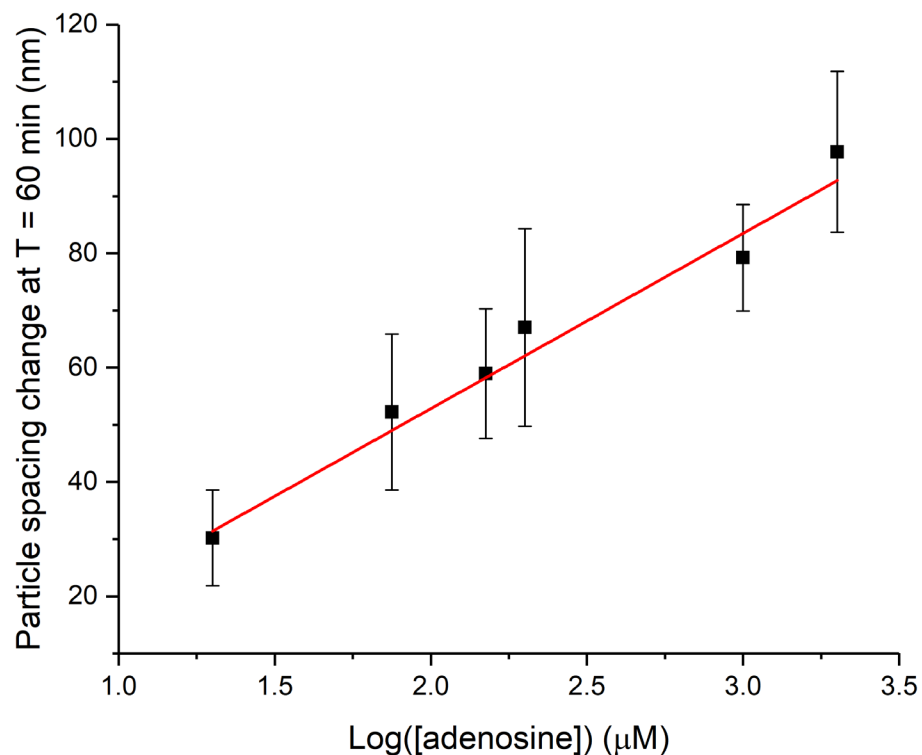
$$f_{bound} = \frac{1}{\frac{K_D}{[free\ adenosine]} + 1}$$

Multiplying the numerator and denominator by  $[free\ adenosine]$  gives:

$$f_{bound} = \frac{[free\ adenosine]}{K_D + [free\ adenosine]}$$

If  $K_D = [free\ adenosine]$ , then  $f_{bound} = \frac{1}{2}$ . Assuming the particle spacing change is proportional to  $f_{bound}$ , and the concentration of adenosine added is equal to  $[free\ adenosine]$ ,  $K_D$  can be estimated as the concentration of adenosine when the particle spacing change is at half-maximum.

Using measured particle spacing changes at  $t = 60$  min, we constructed a calibration curve relating  $\log([adenosine])$  to particle spacing change and generated a linear fit using the software OriginLab (Appendix Figure 1). We observed a maximum particle spacing change of 97.746 nm at an adenosine concentration of 2000  $\mu\text{M}$ . The half-maximum particle spacing was thus 48.873 nm. The linear fit was then used to calculate an adenosine concentration of 74.36  $\mu\text{M}$ , which was taken as the estimated  $K_D$  of the adenosine-binding aptamer.



**Appendix Figure 1: Log ([adenosine]) vs. particle spacing change. A weighted-least square method in OriginLab was used to generate a linear fit of  $y = 30.65366x - 8.49099$  (adjusted R-Squared = 0.9746).**

### **Appendix A.2 Optimizing acrylamide (AAM) monomer and MBAAM crosslinker concentrations in 2DPC hydrogel fabrication**

To find the optimal 2DPC hydrogel fabrication conditions for this proof-of-concept study, we systematically varied the concentrations of AAM monomer and MBAAM crosslinker. 2DPC hydrogels are expected to be more sensitive to adenosine if a lower amount of crosslinker is used, as the sensor response is induced by altering the crosslinking density of the hydrogel. However, hydrogels cannot embed a 2DPC array into the network if they do not have sufficient mechanical

robustness. It is important that the 2DPC array fully embeds into the hydrogel because it affects the quality of light diffraction that is used to monitor particle spacing changes in 2DPC hydrogels. Thus, the main goal was to minimize the amount of MBAAm, while ensuring appropriate mechanical robustness of the 2DPC hydrogels. After fabricating 2DPC hydrogels with different recipes, we visually evaluated how much of the 2DPC array was successfully embedded into the hydrogel. A recipe was deemed successful if over 90% of the 2DPC array was embedded in the corresponding hydrogel.

As summarized in Appendix Table 1 below, 2DPC hydrogels with 25% (w/v) AAm and 0.02% (w/v) MBAAm successfully embedded a 2DPC array with the lowest amount of MBAAm crosslinker. Thus, this composition was adopted to fabricate DNA-crosslinked 2DPC hydrogels. We will continue to investigate hydrogel formulations in future studies by systematically altering DNA concentration in addition to AAm and MBAAm.

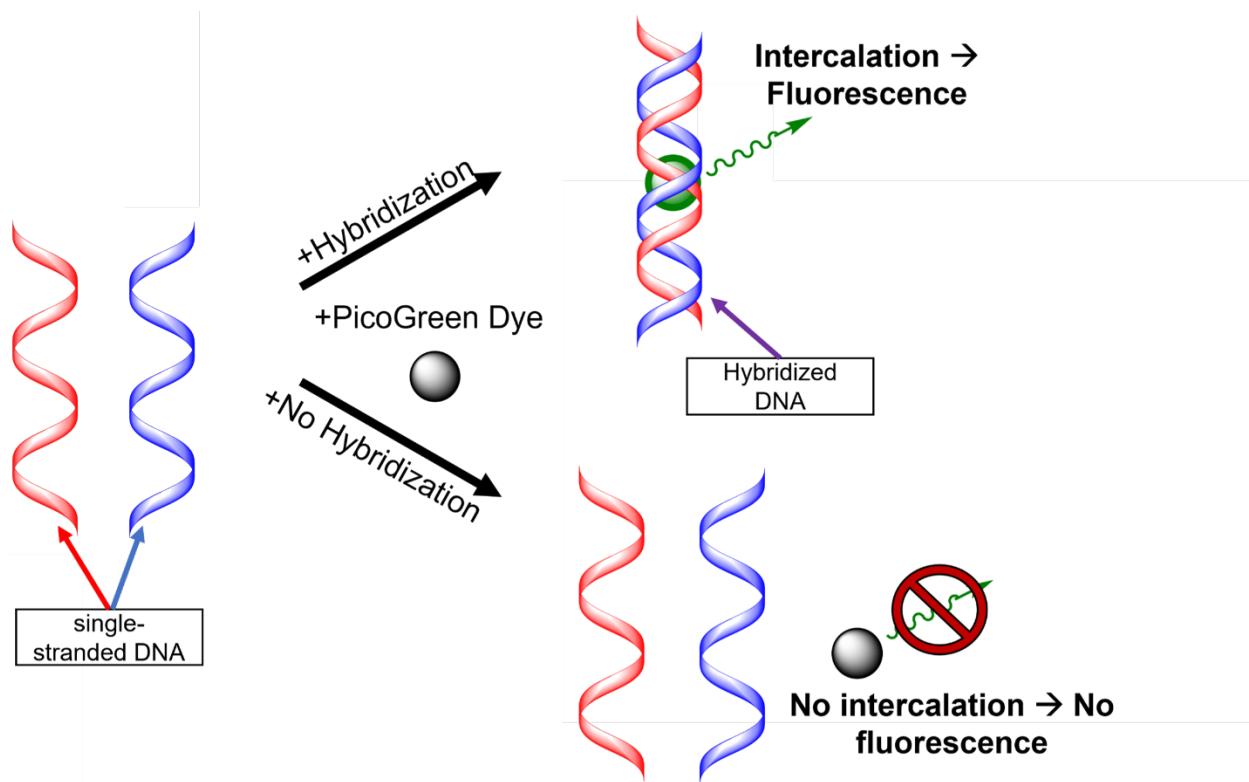
**Appendix Table 1: Concentrations of AAm and MBAAm used in preparation of 2DPC hydrogels**

AAm concentration (%, w/v)	MBAAm concentration (%, w/v)	Was >90% of 2DPC array embedded in the 2DPC hydrogel?
20	0.03	✓
20	0.02	✗
25	0.03	✓
25	0.02	✓
25	0.01	✗

## **Appendix B Supporting Information for Chapter 4**

### **Appendix B.1 PicoGreen Assay**

PicoGreen (PG) is a fluorescent dye that can be used to monitor DNA hybridization, as shown in Appendix Figure 2. In the free state in solution, the intramolecular dynamic fluctuations of PG quench its fluorescence.<sup>152</sup> In the presence of double-stranded DNA, PG intercalates between the hybridized DNA strands. This intercalation and electrostatic interactions between the DNA and PG immobilize the dye and inhibit the self-quenching mechanism, resulting in intense increases in fluorescence. PG has negligible binding interactions with single-stranded DNA and RNA. Thus, in the presence of single-stranded DNA and RNA, the PG self-quenching mechanism is uninhibited, and fluorescence remains negligible.<sup>151, 152</sup> In this way, PG fluorescence can be used to monitor DNA hybridization, as larger PG fluorescence indicates more double-stranded DNA.



Appendix Figure 2: Log ([adenosine]) vs. particle spacing change. A weighted-least square method in OriginLab was used to generate a linear fit of  $y = 30.65366x - 8.49099$  (adjusted R-Squared = 0.9746).

## Appendix B.2 Statistical analysis and linear fit data for annealing protocols

Appendix Table 2: t statistics for PG fluorescence measurements investigating annealing protocols

DNA Annealing Protocol	Heating + Rapid Cooling	Heating + Slow Cooling	Room Temperature	No Treatment
Heating + Rapid Cooling		1.31948	3.1803	4.0368
Heating + Slow Cooling	1.31948		2.07276	3.23716
Room Temperature	3.1803	2.07276		1.51999
No Treatment	4.0368	3.23716	1.51999	

A two-sample t test was used to compare the mean PG fluorescence signals of DNA annealed using different annealing protocols (Figure 4.2). Due to limited sample size, equal variance was not assumed. The t statistic for each two-sample test is reported in the cross section of the applicable samples. t statistics that indicate significantly different means at 0.05 level are colored red, while t statistics that do not indicate significantly different means at 0.05 level are colored green. Analysis was performed using the software OriginLabs.

**Appendix Table 3: Linear fit data for annealing protocols**

Annealing Protocol	Adjusted R-squared	Slope	Y-intercept
Heating + Rapid Cooling	0.9379	$36.58 \pm 6.55$	$-30.83 \pm 17.89$
Heating + Slow Cooling	0.9981	$34.06 \pm 1.04$	$-24.24 \pm 2.56$

Linear fits were generated with a weighted least squares method using the software OriginLab.

### **Appendix B.3 Particle spacing change of PC hydrogels fabricated with 0.08 mM DNA**

**Appendix Table 4: Particle spacing change data for PC hydrogels fabricated with 0.08 mM DNA**

Time (min)	2 mM AD	
	Particle Spacing Change (nm)	Standard Deviation (nm)
0	0	0
5	1.2192	11.22229318
15	17.2532	17.0701236
30	14.1969	2.876323647
60	12.756	8.702457589

PC hydrogels were fabricated using 0.08 mM DNA and particle spacing changes were monitored in 2 mM adenosine solution using described procedures. Measurements were repeated 3 times and averaged. The average response of PC hydrogels fabricated in the same way in blank solutions without adenosine was subtracted from each data point. Since the response in 2 mM adenosine solution was much smaller than that of PC hydrogels fabricated using 0.4 mM DNA, these data were excluded from Figure 4.4.

#### Appendix B.4 Impact of increasing [DNA] on PC hydrogel response and variability

Appendix Table 5: Impact of increasing [DNA] on particle spacing change and standard deviation

[DNA]	Average Particle Spacing Change (nm)	% increase (from Lower [DNA])	% increase (from Normal [DNA])	Average Std Dev (nm)	% increase (from Lower [DNA])	% increase (from Normal [DNA])
Lower [DNA] (0.4 mM)	36.90			4.69		
Normal [DNA] (0.8 mM)	59.51	61.28		9.36	99.64	
Higher [DNA] (1.6 mM)	123.04	233.44	106.74	13.07	178.64	39.57

The particle spacing changes and standard deviations for PC hydrogels fabricated with different amounts of DNA were averaged and compared to elucidate the impact of increasing

[DNA]. Particle spacing change was used to evaluate responsivity, while standard deviations were used to evaluate variability.

### Appendix B.5 Linear fit data for changing [DNA]

**Appendix Table 6: Impact of increasing [DNA] on particle spacing change and standard deviation**

[DNA]	Adjusted R-squared	Slope	Y-intercept
Lower [DNA] (0.4 mM)	0.9092	$16.83 \pm 3.02$	$-8.95 \pm 7.22$
Normal [DNA] (0.8 mM)	0.9379	$36.58 \pm 6.55$	$-30.83 \pm 17.89$
Higher [DNA] (1.6 mM)	0.9808	$97.03 \pm 7.82$	$-125.27 \pm 20.73$

Linear fits were generated with a weighted least squares method using the software OriginLab.

**Appendix B.6 Statistical analysis for particle spacing measurements investigating hydrogel size and sample volume**

**Appendix Table 7: t statistics for particle spacing measurements investigating hydrogel size and sample volume in 200  $\mu$ M adenosine solutions**

Hydrogel Size, Sample Volume	Large Hydrogel, Large Sample Volume	Large Hydrogel, Small Sample Volume	Small Hydrogel, Large Sample Volume	Small Hydrogel, Small Sample Volume
Large Hydrogel, Large Sample Volume		-0.48563	-1.59309	1.05875
Large Hydrogel, Small Sample Volume	-0.48563		-0.06308	0.97169
Small Hydrogel, Large Sample Volume	-1.59309	-0.06308		1.83844
Small Hydrogel, Small Sample Volume	1.05875	0.97169	1.83844	

A two-sample t test was used to compare the mean particle spacing changes of hydrogels of varying sizes and in varying sample volumes in 200  $\mu$ M adenosine solutions (Figure 4.5 A). Due to limited sample size, equal variance was not assumed. The t statistic for each two-sample test is reported in the cross section of the applicable samples. t statistics that indicate significantly different means at 0.05 level are colored red, while t statistics that do not indicate significantly different means at 0.05 level are colored green. Analysis was performed using the software OriginLabs.

**Appendix Table 8: t statistics for particle spacing measurements investigating hydrogel size and sample volume in 2 mM adenosine solutions**

Hydrogel Size, Sample Volume	Large Hydrogel, Large Sample Volume	Large Hydrogel, Small Sample Volume	Small Hydrogel, Large Sample Volume	Small Hydrogel, Small Sample Volume
Large Hydrogel, Large Sample Volume		-0.03471	-0.29378	-0.36198
Large Hydrogel, Small Sample Volume	-0.03471		-0.13509	-0.21766
Small Hydrogel, Large Sample Volume	-0.29378	-0.13509		-0.14778
Small Hydrogel, Small Sample Volume	-0.36198	-0.21766	-0.14778	

A two-sample t test was used to compare the mean particle spacing changes of hydrogels of varying sizes and in varying sample volumes in 2 mM adenosine solutions (Figure 4.5 B). Due to limited sample size, equal variance was not assumed. The t statistic for each two-sample test is reported in the cross section of the applicable samples. t statistics that indicate significantly different means at 0.05 level are colored red, while t statistics that do not indicate significantly different means at 0.05 level are colored green. Analysis was performed using the software OriginLabs.

## Appendix C Supporting Information for Chapter 5

### Appendix C.1 Determination of thrombin concentration

Concentration of thrombin stock solution was determined using a Pierce Rapid Gold BCA protein assay kit. The manufacturer's protocol was followed using a BSA standard.<sup>186</sup> Samples were analyzed in 96-well plates in a SpectraMax M2 plate reader with absorbance at 480 nm.

### Appendix C.2 Calculating the dissociation constant ( $K_D$ ) of the thrombin-binding aptamer

$$fraction_{bound} = \frac{[aptamer \cdot thrombin]}{[free aptamer] + [aptamer \cdot thrombin]}$$

$$fraction_{bound} = \frac{1}{\frac{[free aptamer]}{[aptamer \cdot thrombin]} + 1}$$

$$K_D = \frac{[free aptamer][free thrombin]}{[aptamer \cdot thrombin]}, fraction_{bound} = \frac{1}{\frac{K_D}{[free thrombin]} + 1}$$

$$fraction_{bound} = \frac{[free thrombin]}{K_D + [free thrombin]}$$

Thus, when  $K_D = [\text{free thrombin}]$ ,  $\text{fraction}_{\text{bound}} = 1/2$ . Assuming  $\text{fraction}_{\text{bound}}$  is proportional to the 2DPC hydrogel particle spacing, and  $[\text{free thrombin}] =$  the concentration of thrombin in solution,  $K_D$  can be estimated as the thrombin concentration at half the maximum 2DPC hydrogel particle spacing.

### Appendix C.3 Linear fit data for calibration curve in thrombin-binding buffer

**Appendix Table 9: Linear fit data for calibration curve in thrombin-binding buffer**

Adjusted R-squared	Slope	Y-intercept
0.9836	$60.95 \pm 3.93$	$-111.74 \pm 11.10$

Linear fits were generated with a weighted least squares method using the software OriginLab.

### Appendix C.4 Linear fit data for calibration curve in alternate buffer

**Appendix Table 10: Linear fit data for calibration curve in alternate buffer**

Adjusted R-squared	Slope	Y-intercept
0.9663	$16.88 \pm 1.81$	$-38.47 \pm 5.44$

Linear fits were generated with a weighted least squares method using the software OriginLab.

## Appendix C.5 Linear fit data for calibration curve in diluted serum

Appendix Table 11: Linear fit data for calibration curve in diluted serum

Adjusted R-squared	Slope	Y-intercept
0.9787	$49.83 \pm 5.17$	$-89.94 \pm 14.60$

Linear fits were generated with a weighted least squares method using the software OriginLab.

## Bibliography

1. Mabey, D.; Peeling, R. W.; Ustianowski, A.; Perkins, M. D., Diagnostics for the developing world. *Nature Reviews Microbiology* **2004**, *2* (3), 231-240.
2. Younes, N.; Al-Sadeq, D. W.; Al-Jighefee, H.; Younes, S.; Al-Jamal, O.; Daas, H. I.; Yassine, H. M.; Nasrallah, G. K., Challenges in laboratory diagnosis of the novel coronavirus SARS-CoV-2. *Viruses* **2020**, *12* (6), 582.
3. Congress, U., HR 6074—Coronavirus Preparedness and Response Supplemental Appropriations Act, 2020. 2020.
4. Sharma, S.; Zapatero-Rodríguez, J.; Estrela, P.; O'Kennedy, R., Point-of-care diagnostics in low resource settings: present status and future role of microfluidics. *Biosensors* **2015**, *5* (3), 577-601.
5. Control, D.; Group, C. T. R., The effect of intensive treatment of diabetes on the development and progression of long-term complications in insulin-dependent diabetes mellitus. *New England journal of medicine* **1993**, *329* (14), 977-986.
6. Welch, R. D.; Ayaz, S. I.; Lewis, L. M.; Unden, J.; Chen, J. Y.; Mika, V. H.; Saville, B.; Tyndall, J. A.; Nash, M.; Buki, A.; Barzo, P.; Hack, D.; Tortella, F. C.; Schmid, K.; Hayes, R. L.; Vossough, A.; Sweriduk, S. T.; Bazarian, J. J., Ability of Serum Glial Fibrillary Acidic Protein, Ubiquitin C-Terminal Hydrolase-L1, and S100B To Differentiate Normal and Abnormal Head Computed Tomography Findings in Patients with Suspected Mild or Moderate Traumatic Brain Injury. *J Neurotrauma* **2016**, *33* (2), 203-214.
7. Khan, F. A.; Fatima, S. S.; Khan, G. M.; Shahid, S., Evaluation of kidney injury molecule-1 as a disease progression biomarker in diabetic nephropathy. *Pak J Med Sci* **2019**, *35* (4), 992-996.
8. Szilágyi, B.; Fejes, Z.; Pócsi, M.; Kappelmayer, J.; Nagy, B., Jr., Role of sepsis modulated circulating microRNAs. *EJIFCC* **2019**, *30* (2), 128-145.
9. Walker, J. P.; Asher, S. A., Acetylcholinesterase-based organophosphate nerve agent sensing photonic crystal. *Analytical chemistry* **2005**, *77* (6), 1596-1600.
10. John, S., Strong localization of photons in certain disordered dielectric superlattices. *Physical review letters* **1987**, *58* (23), 2486.
11. Yablonovitch, E., Inhibited spontaneous emission in solid-state physics and electronics. *Physical review letters* **1987**, *58* (20), 2059.
12. Kesavamoorthy, R.; Pan, G.; Asher, S. A., Thermally switchable laser diffracting gels. *Laser applications in material science and industry. New Delhi: Allied Publishers* **1997**, 265-273.

13. Pallares, I. G.; Rout, D.; Deering, T. J.; Hufziger, K. T.; Bykov, S. V.; Asher, S. A., Colloidal self-assembly of highly-ordered silica inverse opals for deep ultraviolet diffraction. *ACS Applied Nano Materials* **2020**, *3* (5), 4135-4146.
14. Angelakis, D. G.; Santos, M. F.; Yannopapas, V.; Ekert, A., A proposal for the implementation of quantum gates with photonic-crystal waveguides. *Physics Letters A* **2007**, *362* (5-6), 377-380.
15. Azuma, H., Quantum computation with Kerr-nonlinear photonic crystals. *Journal of Physics D: Applied Physics* **2007**, *41* (2), 025102.
16. Vigneron, J. P.; Simonis, P., Natural photonic crystals. *Physica B: Condensed Matter* **2012**, *407* (20), 4032-4036.
17. Chang, Y.; Xu, S.; Dong, B.; Wei, J.; Le, X.; Ma, Y.; Zhou, G.; Lee, C., Development of triboelectric-enabled tunable Fabry-Pérot photonic-crystal-slab filter towards wearable mid-infrared computational spectrometer. *Nano Energy* **2021**, *89*, 106446.
18. Holtz, J. H.; Asher, S. A., Polymerized colloidal crystal hydrogel films as intelligent chemical sensing materials. *Nature* **1997**, *389* (6653), 829-832.
19. Zhang, J.-T.; Wang, L.; Luo, J.; Tikhonov, A.; Kornienko, N.; Asher, S. A., 2-D Array Photonic Crystal Sensing Motif. *Journal of the American Chemical Society* **2011**, *133* (24), 9152-9155.
20. Fenzl, C.; Hirsch, T.; Wolfbeis, O. S., Photonic crystals for chemical sensing and biosensing. *Angewandte Chemie International Edition* **2014**, *53* (13), 3318-3335.
21. Hou, J.; Li, M.; Song, Y., Recent advances in colloidal photonic crystal sensors: materials, structures and analysis methods. *Nano Today* **2018**, *22*, 132-144.
22. Shen, P.; Zhang, Y.; Cai, Z.; Liu, R.; Xu, X.; Li, R.; Wang, J.-J.; Yang, D. a., Three-dimensional/two-dimensional photonic crystal hydrogels for biosensing. *Journal of Materials Chemistry C* **2021**, *9* (18), 5840-5857.
23. Joannopoulos, J. D.; Johnson, S. G.; Winn, J. N.; Meade, R. D., Molding the flow of light. *Princeton Univ. Press, Princeton, NJ [ua]* **2008**.
24. Armstrong, E.; O'Dwyer, C., Artificial opal photonic crystals and inverse opal structures—fundamentals and applications from optics to energy storage. *Journal of materials chemistry C* **2015**, *3* (24), 6109-6143.
25. Zhang, J. T.; Wang, L.; Lamont, D. N.; Velankar, S. S.; Asher, S. A., Fabrication of large-area two-dimensional colloidal crystals. *Angewandte Chemie* **2012**, *124* (25), 6221-6224.
26. Wang, C.; Xiao, F.; Chen, Q.; Wang, S.; Zhou, J.; Wu, Z., A two-dimensional photonic crystal hydrogel biosensor for colorimetric detection of penicillin G and penicillinase inhibitors. *Analyst* **2021**, *146* (2), 502-508.

27. Jang, K.; Westbay, J. H.; Asher, S. A., DNA-Crosslinked 2D Photonic Crystal Hydrogels for Detection of Adenosine Actuated by an Adenosine-Binding Aptamer. *ACS sensors* **2022**.
28. Shen, P.; Jang, K.; Cai, Z.; Zhang, Y.; Asher, S. A., Aptamer-functionalized 2D photonic crystal hydrogels for detection of adenosine. *Microchimica Acta* **2022**, *189* (11), 1-10.
29. Lee, K.; LaBianca, N.; Rishton, S.; Zolgharnain, S.; Gelorme, J.; Shaw, J.; Chang, T. P., Micromachining applications of a high resolution ultrathick photoresist. *Journal of Vacuum Science & Technology B: Microelectronics and Nanometer Structures Processing, Measurement, and Phenomena* **1995**, *13* (6), 3012-3016.
30. Campbell, M.; Sharp, D.; Harrison, M.; Denning, R.; Turberfield, A., Fabrication of photonic crystals for the visible spectrum by holographic lithography. *Nature* **2000**, *404* (6773), 53-56.
31. Deubel, M.; Von Freymann, G.; Wegener, M.; Pereira, S.; Busch, K.; Soukoulis, C. M., Direct laser writing of three-dimensional photonic-crystal templates for telecommunications. *Nature materials* **2004**, *3* (7), 444-447.
32. Seet, K. K.; Mizeikis, V.; Matsuo, S.; Juodkasis, S.; Misawa, H., Three-dimensional spiral-architecture photonic crystals obtained by direct laser writing. *Advanced Materials* **2005**, *17* (5), 541-545.
33. Blanco, A.; Chomski, E.; Grabtchak, S.; Ibsate, M.; John, S.; Leonard, S. W.; Lopez, C.; Meseguer, F.; Miguez, H.; Mondia, J. P., Large-scale synthesis of a silicon photonic crystal with a complete three-dimensional bandgap near 1.5 micrometres. *Nature* **2000**, *405* (6785), 437-440.
34. Ozin, G. A.; Yang, S., The race for the photonic chip: colloidal crystal assembly in silicon wafers. *Advanced Functional Materials* **2001**, *11* (2), 95-104.
35. Jiang, P.; McFarland, M. J., Large-scale fabrication of wafer-size colloidal crystals, macroporous polymers and nanocomposites by spin-coating. *Journal of the American Chemical Society* **2004**, *126* (42), 13778-13786.
36. Cai, Z.; Li, Z.; Ravaine, S.; He, M.; Song, Y.; Yin, Y.; Zheng, H.; Teng, J.; Zhang, A., From colloidal particles to photonic crystals: advances in self-assembly and their emerging applications. *Chemical Society Reviews* **2021**, *50* (10), 5898-5951.
37. Tikhonov, A.; Kornienko, N.; Zhang, J.-T.; Wang, L.; Asher, S. A., Reflectivity enhanced two-dimensional dielectric particle array monolayer diffraction. *Journal of Nanophotonics* **2012**, *6* (1), 063509.
38. Jiang, P.; Prasad, T.; McFarland, M. J.; Colvin, V. L., Two-dimensional nonclose-packed colloidal crystals formed by spincoating. *Applied physics letters* **2006**, *89* (1), 011908.
39. Kim, M. H.; Im, S. H.; Park, O. O., Rapid Fabrication of Two-and Three-Dimensional Colloidal Crystal Films Via Confined Convective Assembly. *Advanced functional materials* **2005**, *15* (8), 1329-1335.

40. Quint, S. B.; Pacholski, C., Extraordinary long range order in self-healing non-close packed 2D arrays. *Soft Matter* **2011**, *7* (8), 3735-3738.
41. Singh, G.; Pillai, S.; Arpanaei, A.; Kingshott, P., Highly Ordered Mixed Protein Patterns Over Large Areas from Self-Assembly of Binary Colloids. *Advanced materials* **2011**, *23* (13), 1519-1523.
42. Yu, J.; Yan, Q.; Shen, D., Co-self-assembly of binary colloidal crystals at the air– water interface. *ACS applied materials & interfaces* **2010**, *2* (7), 1922-1926.
43. Dai, Z.; Li, Y.; Duan, G.; Jia, L.; Cai, W., Phase diagram, design of monolayer binary colloidal crystals, and their fabrication based on ethanol-assisted self-assembly at the air/water interface. *Acs Nano* **2012**, *6* (8), 6706-6716.
44. Zhang, J.-T.; Wang, L.; Chao, X.; Asher, S. A., Periodicity-Controlled Two-Dimensional Crystalline Colloidal Arrays. *Langmuir* **2011**, *27* (24), 15230-15235.
45. Scriven, L.; Sternling, C., The marangoni effects. *Nature* **1960**, *187* (4733), 186-188.
46. Vogel, N.; Retsch, M.; Fustin, C.-A.; Del Campo, A.; Jonas, U., Advances in colloidal assembly: the design of structure and hierarchy in two and three dimensions. *Chemical reviews* **2015**, *115* (13), 6265-6311.
47. Reese, C. E.; Asher, S. A., Emulsifier-free emulsion polymerization produces highly charged, monodisperse particles for near infrared photonic crystals. *Journal of colloid and interface science* **2002**, *248* (1), 41-46.
48. Zhang, F.; Cao, L.; Yang, W., Preparation of Monodisperse and Anion-Charged Polystyrene Microspheres Stabilized with Polymerizable Sodium Styrene Sulfonate by Dispersion Polymerization. *Macromolecular Chemistry and Physics* **2010**, *211* (7), 744-751.
49. Hatton, B.; Mishchenko, L.; Davis, S.; Sandhage, K. H.; Aizenberg, J., Assembly of large-area, highly ordered, crack-free inverse opal films. *Proceedings of the National Academy of Sciences* **2010**, *107* (23), 10354-10359.
50. Wu, T.-Y.; Zrimsek, A. B.; Bykov, S. V.; Jakubek, R. S.; Asher, S. A., Hydrophobic collapse initiates the poly (N-isopropylacrylamide) volume phase transition reaction coordinate. *The Journal of Physical Chemistry B* **2018**, *122* (11), 3008-3014.
51. Carlson, R. J.; Asher, S. A., Characterization of optical diffraction and crystal structure in monodisperse polystyrene colloids. *Applied spectroscopy* **1984**, *38* (3), 297-304.
52. Rundquist, P. A.; Photinos, P.; Jagannathan, S.; Asher, S. A., Dynamical Bragg diffraction from crystalline colloidal arrays. *The Journal of chemical physics* **1989**, *91* (8), 4932-4941.
53. Asher, S. A.; Weissman, J. M.; Tikhonov, A.; Coalson, R. D.; Kesavamoorthy, R., Diffraction in crystalline colloidal-array photonic crystals. *Physical Review E* **2004**, *69* (6), 066619.

54. Kittel, C., *Introduction to solid state physics*. Wiley: Hoboken, NJ, 2005.
55. Flory, P., *Principles of Polymer Chemistry*. Ithaca, NY, 1953.
56. Li, Y.; Tanaka, T., Phase transitions of gels. *Annual Review of Materials Science* **1992**, *22* (1), 243-277.
57. Lee, K.; Asher, S. A., Photonic crystal chemical sensors: pH and ionic strength. *Journal of the American Chemical Society* **2000**, *122* (39), 9534-9537.
58. Cai, Z.; Kwak, D. H.; Punihaole, D.; Hong, Z.; Velankar, S. S.; Liu, X.; Asher, S. A., A photonic crystal protein hydrogel sensor for *Candida albicans*. *Angewandte Chemie International Edition* **2015**, *54* (44), 13036-13040.
59. Tanaka, T.; Fillmore, D.; Sun, S.-T.; Nishio, I.; Swislow, G.; Shah, A., Phase Transitions in Ionic Gels. *Physical Review Letters* **1980**, *45* (20), 1636-1639.
60. Cai, Z.; Smith, N. L.; Zhang, J.-T.; Asher, S. A., Two-dimensional photonic crystal chemical and biomolecular sensors. *Analytical chemistry* **2015**, *87* (10), 5013-5025.
61. Zhang, J.-T.; Chao, X.; Liu, X.; Asher, S. A., Two-dimensional array Debye ring diffraction protein recognition sensing. *Chemical Communications* **2013**, *49* (56), 6337-6339.
62. Jang, K.; Horne, W. S.; Asher, S. A., Human Serum Phenylpyruvate Quantification Using Responsive 2D Photonic Crystal Hydrogels via Chemoselective Oxime Ligation: Progress toward Developing Phenylalanine-Sensing Elements. *ACS Applied Materials & Interfaces* **2020**, *12* (35), 39612-39619.
63. Cai, Z.; Zhang, J.-T.; Xue, F.; Hong, Z.; Punihaole, D.; Asher, S. A., 2D Photonic Crystal Protein Hydrogel Coulometer for Sensing Serum Albumin Ligand Binding. *Analytical Chemistry* **2014**, *86* (10), 4840-4847.
64. Cai, Z.; Sasmal, A.; Liu, X.; Asher, S. A., Responsive photonic crystal carbohydrate hydrogel sensor materials for selective and sensitive lectin protein detection. *ACS sensors* **2017**, *2* (10), 1474-1481.
65. Ellington, A. D.; Szostak, J. W., In vitro selection of RNA molecules that bind specific ligands. *Nature* **1990**, *346* (6287), 818-822.
66. Tuerk, C.; Gold, L., Systematic Evolution of Ligands by Exponential Enrichment: RNA Ligands to Bacteriophage T4 DNA Polymerase. *Science* **1990**, *249* (4968), 505-510.
67. Li, J.; Mo, L.; Lu, C.-H.; Fu, T.; Yang, H.-H.; Tan, W., Functional nucleic acid-based hydrogels for bioanalytical and biomedical applications. *Chemical Society Reviews* **2016**, *45* (5), 1410-1431.
68. Wu, Y.; Belmonte, I.; Sykes, K. S.; Xiao, Y.; White, R. J., Perspective on the Future Role of Aptamers in Analytical Chemistry. *Analytical Chemistry* **2019**, *91* (24), 15335-15344.

69. Ye, B.-F.; Zhao, Y.-J.; Cheng, Y.; Li, T.-T.; Xie, Z.-Y.; Zhao, X.-W.; Gu, Z.-Z., Colorimetric photonic hydrogel aptasensor for the screening of heavy metal ions. *Nanoscale* **2012**, *4* (19), 5998-6003.
70. Song, K.-M.; Jeong, E.; Jeon, W.; Jo, H.; Ban, C., A coordination polymer nanobelt (CPNB)-based aptasensor for sulfadimethoxine. *Biosensors and Bioelectronics* **2012**, *33* (1), 113-119.
71. Stojanovic, M. N.; de Prada, P.; Landry, D. W., Fluorescent sensors based on aptamer self-assembly. *Journal of the American Chemical Society* **2000**, *122* (46), 11547-11548.
72. Stojanovic, M. N.; De Prada, P.; Landry, D. W., Aptamer-based folding fluorescent sensor for cocaine. *Journal of the American Chemical Society* **2001**, *123* (21), 4928-4931.
73. Bock, L. C.; Griffin, L. C.; Latham, J. A.; Vermaas, E. H.; Toole, J. J., Selection of single-stranded DNA molecules that bind and inhibit human thrombin. *Nature* **1992**, *355* (6360), 564-566.
74. Gopinath, S. C.; Sakamaki, Y.; Kawasaki, K.; Kumar, P. K., An efficient RNA aptamer against human influenza B virus hemagglutinin. *Journal of biochemistry* **2006**, *139* (5), 837-846.
75. Cho, S.-J.; Woo, H.-M.; Kim, K.-S.; Oh, J.-W.; Jeong, Y.-J., Novel system for detecting SARS coronavirus nucleocapsid protein using an ssDNA aptamer. *Journal of bioscience and bioengineering* **2011**, *112* (6), 535-540.
76. Chen, Z.; Wu, Q.; Chen, J.; Ni, X.; Dai, J., A DNA Aptamer Based Method for Detection of SARS-CoV-2 Nucleocapsid Protein. *Virologica Sinica* **2020**, *1*.
77. Rong, Y.; Chen, H.; Zhou, X.-F.; Yin, C.-Q.; Wang, B.-C.; Peng, C.-W.; Liu, S.-P.; Wang, F.-B., Identification of an aptamer through whole cell-SELEX for targeting high metastatic liver cancers. *Oncotarget* **2016**, *7* (7), 8282.
78. Dwivedi, H. P.; Smiley, R. D.; Jaykus, L.-A., Selection and characterization of DNA aptamers with binding selectivity to *Campylobacter jejuni* using whole-cell SELEX. *Applied microbiology and biotechnology* **2010**, *87* (6), 2323-2334.
79. Huizenga, D. E.; Szostak, J. W., A DNA Aptamer That Binds Adenosine and ATP. *Biochemistry* **1995**, *34* (2), 656-665.
80. Klußmann, S.; Nolte, A.; Bald, R.; Erdmann, V. A.; Fürste, J. P., Mirror-image RNA that binds D-adenosine. *Nature biotechnology* **1996**, *14* (9), 1112.
81. Mairal, T.; Cengiz Özalp, V.; Lozano Sánchez, P.; Mir, M.; Katakis, I.; O'Sullivan, C. K., Aptamers: molecular tools for analytical applications. *Analytical and Bioanalytical Chemistry* **2008**, *390* (4), 989-1007.
82. Yin, B.-C.; Ye, B.-C.; Wang, H.; Zhu, Z.; Tan, W., Colorimetric logic gates based on aptamer-crosslinked hydrogels. *Chemical Communications* **2012**, *48* (9), 1248-1250.

83. Nutiu, R.; Li, Y., Structure-Switching Signaling Aptamers. *Journal of the American Chemical Society* **2003**, *125* (16), 4771-4778.
84. Kong, L.; Xu, J.; Xu, Y.; Xiang, Y.; Yuan, R.; Chai, Y., A universal and label-free aptasensor for fluorescent detection of ATP and thrombin based on SYBR Green Idye. *Biosensors and Bioelectronics* **2013**, *42*, 193-197.
85. Lv, Z.; Liu, J.; Zhou, Y.; Guan, Z.; Yang, S.; Li, C.; Chen, A., Highly sensitive fluorescent detection of small molecules, ions, and proteins using a universal label-free aptasensor. *Chemical Communications* **2013**, *49* (48), 5465-5467.
86. Liu, Z.; Yuan, R.; Chai, Y.; Zhuo, Y.; Hong, C.; Yang, X.; Su, H.; Qian, X., Highly sensitive, reusable electrochemical aptasensor for adenosine. *Electrochimica Acta* **2009**, *54* (26), 6207-6211.
87. Zhang, K.; Zhu, X.; Wang, J.; Xu, L.; Li, G., Strategy to fabricate an electrochemical aptasensor: application to the assay of adenosine deaminase activity. *Analytical chemistry* **2010**, *82* (8), 3207-3211.
88. Chen, A.; Yang, S., Replacing antibodies with aptamers in lateral flow immunoassay. *Biosensors and bioelectronics* **2015**, *71*, 230-242.
89. Toh, S. Y.; Citartan, M.; Gopinath, S. C.; Tang, T.-H., Aptamers as a replacement for antibodies in enzyme-linked immunosorbent assay. *Biosensors and bioelectronics* **2015**, *64*, 392-403.
90. Lee, K. H.; Zeng, H., Aptamer-based ELISA assay for highly specific and sensitive detection of Zika NS1 protein. *Analytical chemistry* **2017**, *89* (23), 12743-12748.
91. Li, H.; Li, M.; Yang, Y.; Wang, F.; Wang, F.; Li, C., Aptamer-linked CRISPR/Cas12a-based immunoassay. *Analytical Chemistry* **2021**, *93* (6), 3209-3216.
92. Song, Y.; Song, J.; Wei, X.; Huang, M.; Sun, M.; Zhu, L.; Lin, B.; Shen, H.; Zhu, Z.; Yang, C., Discovery of aptamers targeting the receptor-binding domain of the SARS-CoV-2 spike glycoprotein. *Analytical chemistry* **2020**, *92* (14), 9895-9900.
93. Abrego-Martinez, J. C.; Jafari, M.; Chergui, S.; Pavel, C.; Che, D.; Siaj, M., Aptamer-based electrochemical biosensor for rapid detection of SARS-CoV-2: Nanoscale electrode-aptamer-SARS-CoV-2 imaging by photo-induced force microscopy. *Biosensors and Bioelectronics* **2022**, *195*, 113595.
94. Idili, A.; Parolo, C.; Alvarez-Diduk, R.; Merkoçi, A., Rapid and efficient detection of the SARS-CoV-2 spike protein using an electrochemical aptamer-based sensor. *ACS sensors* **2021**, *6* (8), 3093-3101.
95. Liu, N.; Liu, R.; Zhang, J., CRISPR-Cas12a-mediated label-free electrochemical aptamer-based sensor for SARS-CoV-2 antigen detection. *Bioelectrochemistry* **2022**, *146*, 108105.

96. Seeman, N. C., Nucleic acid junctions and lattices. *Journal of theoretical biology* **1982**, *99* (2), 237-247.
97. Seeman, N. C.; Kallenbach, N. R., Design of immobile nucleic acid junctions. *Biophysical journal* **1983**, *44* (2), 201-209.
98. Seeman, N. C., DNA in a material world. *Nature* **2003**, *421* (6921), 427-431.
99. Murakami, Y.; Maeda, M., Hybrid hydrogels to which single-stranded (ss) DNA probe is incorporated can recognize specific ssDNA. *Macromolecules* **2005**, *38* (5), 1535-1537.
100. Liu, J.; Lu, Y., Preparation of aptamer-linked gold nanoparticle purple aggregates for colorimetric sensing of analytes. *Nature protocols* **2006**, *1* (1), 246.
101. Baeissa, A.; Dave, N.; Smith, B. D.; Liu, J., DNA-Functionalized Monolithic Hydrogels and Gold Nanoparticles for Colorimetric DNA Detection. *ACS Applied Materials & Interfaces* **2010**, *2* (12), 3594-3600.
102. Jacobi, Z. E.; Li, L.; Liu, J., Visual detection of lead (II) using a label-free DNA-based sensor and its immobilization within a monolithic hydrogel. *Analyst* **2012**, *137* (3), 704-709.
103. Soontornworajit, B.; Zhou, J.; Shaw, M. T.; Fan, T.-H.; Wang, Y., Hydrogel functionalization with DNA aptamers for sustained PDGF-BB release. *Chemical communications* **2010**, *46* (11), 1857-1859.
104. Lee, J. B.; Peng, S.; Yang, D.; Roh, Y. H.; Funabashi, H.; Park, N.; Rice, E. J.; Chen, L.; Long, R.; Wu, M., A mechanical metamaterial made from a DNA hydrogel. *Nature nanotechnology* **2012**, *7* (12), 816-820.
105. Nagahara, S.; Matsuda, T., Hydrogel formation via hybridization of oligonucleotides derivatized in water-soluble vinyl polymers. *Polymer Gels and Networks* **1996**, *4* (2), 111-127.
106. Lin, D. C.; Yurke, B.; Langrana, N. A., Mechanical properties of a reversible, DNA-crosslinked polyacrylamide hydrogel. *Journal of biomechanical engineering* **2004**, *126* (1), 104-110.
107. Lin, D.; Yurke, B.; Langrana, N., Inducing reversible stiffness changes in DNA-crosslinked gels. *Journal of materials research* **2005**, *20* (6), 1456-1464.
108. Murakami, Y.; Maeda, M., DNA-responsive hydrogels that can shrink or swell. *Biomacromolecules* **2005**, *6* (6), 2927-2929.
109. Yang, H.; Liu, H.; Kang, H.; Tan, W., Engineering target-responsive hydrogels based on aptamer-target interactions. *Journal of the American Chemical Society* **2008**, *130* (20), 6320-6321.

110. Zhu, Z.; Wu, C.; Liu, H.; Zou, Y.; Zhang, X.; Kang, H.; Yang, C. J.; Tan, W., An aptamer cross-linked hydrogel as a colorimetric platform for visual detection. *Angewandte Chemie International Edition* **2010**, *49* (6), 1052-1056.
111. Du, C.; Hill, R. J., Complementary-DNA-strand cross-linked polyacrylamide hydrogels. *Macromolecules* **2019**, *52* (17), 6683-6697.
112. Du, C.; Hill, R. J., Linear viscoelasticity of weakly cross-linked hydrogels. *Journal of Rheology* **2019**, *63* (1), 109-124.
113. Du, C.; Hill, R. J., Swelling and Dissolution Transitions of DNA- and “Bis”-Cross-Linked Polyacrylamide. *Macromolecules* **2020**, *53* (12), 4845-4854.
114. Chen, Q.; Wang, S.; Huang, T.; Xiao, F.; Wu, Z.; Yu, R., Construction and research of multiple stimuli-responsive 2D photonic crystal DNA hydrogel sensing platform with double-network structure and signal self-expression. *Analytical Chemistry* **2022**, *94* (14), 5530-5537.
115. Murtaza, G.; Rizvi, A. S.; Xue, M.; Qiu, L.; Meng, Z., Consensus Receptor-Binding Domain-Targeted Aptamer Selection and Designing of a Photonic Crystal-Decorated Aptasensor for SARS-CoV-2. *Analytical chemistry* **2022**.
116. Rizvi, A. S.; Murtaza, G.; Zhang, W.; Xue, M.; Qiu, L.; Meng, Z., Aptamer-Linked Photonic Crystal Hydrogel Sensor for Rapid Point-of-Care Detection of Human Immuno-Deficiency Virus-1 (HIV-1). *Journal of Pharmaceutical and Biomedical Analysis* **2022**, 115104.
117. Gubala, V.; Harris, L. F.; Ricco, A. J.; Tan, M. X.; Williams, D. E., Point of Care Diagnostics: Status and Future. *Analytical Chemistry* **2012**, *84* (2), 487-515.
118. Cho, E. J.; Lee, J.-W.; Ellington, A. D., Applications of Aptamers as Sensors. *Annual Review of Analytical Chemistry* **2009**, *2* (1), 241-264.
119. Chi, C.-W.; Lao, Y.-H.; Li, Y.-S.; Chen, L.-C., A Quantum Dot-Aptamer Beacon Using a DNA Intercalating Dye as the FRET Reporter: Application to Label-Free Thrombin Detection. *Biosensors and Bioelectronics* **2011**, *26* (7), 3346-3352.
120. Zhu, Y.; Cai, Y.; Xu, L.; Zheng, L.; Wang, L.; Qi, B.; Xu, C., Building An Aptamer/Graphene Oxide FRET Biosensor for One-Step Detection of Bisphenol A. *ACS Appl. Mater. Interfaces* **2015**, *7* (14), 7492-7496.
121. Li, J.; Zhong, X.; Zhang, H.; Le, X. C.; Zhu, J.-J., Binding-Induced Fluorescence Turn-On Assay Using Aptamer-Functionalized Silver Nanocluster DNA Probes. *Analytical Chemistry* **2012**, *84* (12), 5170-5174.
122. Xu, W.; Lu, Y., Label-Free Fluorescent Aptamer Sensor Based on Regulation of Malachite Green Fluorescence. *Analytical Chemistry* **2010**, *82* (2), 574-578.
123. Subramanian, P.; Lesniewski, A.; Kaminska, I.; Vlandas, A.; Vasilescu, A.; Niedziolka-Jonsson, J.; Pichonat, E.; Happy, H.; Boukherroub, R.; Szunerits, S., Lysozyme Detection on

Aptamer Functionalized Graphene-Coated SPR Interfaces. *Biosensors and Bioelectronics* **2013**, *50*, 239-243.

124.Zhu, Z.; Feng, M.; Zuo, L.; Zhu, Z.; Wang, F.; Chen, L.; Li, J.; Shan, G.; Luo, S.-Z., An Aptamer Based Surface Plasmon Resonance Biosensor for the Detection of Ochratoxin A in Wine and Peanut Oil. *Biosensors and Bioelectronics* **2015**, *65*, 320-326.

125.Kuang, H.; Chen, W.; Xu, D.; Xu, L.; Zhu, Y.; Liu, L.; Chu, H.; Peng, C.; Xu, C.; Zhu, S., Fabricated Aptamer-Based Electrochemical “Signal-Off” Sensor of Ochratoxin A. *Biosensors and Bioelectronics* **2010**, *26* (2), 710-716.

126.Liu, Y.; Tuleouva, N.; Ramanculov, E.; Revzin, A., Aptamer-Based Electrochemical Biosensor for Interferon Gamma Detection. *Analytical Chemistry* **2010**, *82* (19), 8131-8136.

127.Xu, X.; Goponenko, A. V.; Asher, S. A., Polymerized polyHEMA photonic crystals: pH and ethanol sensor materials. *Journal of the American Chemical Society* **2008**, *130* (10), 3113-3119.

128.Tian, E.; Ma, Y.; Cui, L.; Wang, J.; Song, Y.; Jiang, L., Color-Oscillating Photonic Crystal Hydrogel. *Macromolecular Rapid Communications* **2009**, *30* (20), 1719-1724.

129.Du, X.; Zhai, J.; Li, X.; Zhang, Y.; Li, N.; Xie, X., Hydrogel-Based Optical Ion Sensors: Principles and Challenges for Point-of-Care Testing and Environmental Monitoring. *ACS Sensors* **2021**, *6* (6), 1990-2001.

130.Asher, S. A.; Alexeev, V. L.; Goponenko, A. V.; Sharma, A. C.; Lednev, I. K.; Wilcox, C. S.; Finegold, D. N., Photonic Crystal Carbohydrate Sensors: Low Ionic Strength Sugar Sensing. *J. Am. Chem. Soc.* **2003**, *125* (11), 3322-3329.

131.Sharma, A. C.; Jana, T.; Kesavamoorthy, R.; Shi, L.; Virji, M. A.; Finegold, D. N.; Asher, S. A., A General Photonic Crystal Sensing Motif: Creatinine in Bodily Fluids. *J. Am. Chem. Soc.* **2004**, *126* (9), 2971-2977.

132.Hu, X.; Li, G.; Li, M.; Huang, J.; Li, Y.; Gao, Y.; Zhang, Y., Ultrasensitive Specific Stimulant Assay Based on Molecularly Imprinted Photonic Hydrogels. *Advanced Functional Materials* **2008**, *18* (4), 575-583.

133.Rizvi, A. S.; Murtaza, G.; Yan, D.; Irfan, M.; Xue, M.; Meng, Z. H.; Qu, F., Development of Molecularly Imprinted 2D Photonic Crystal Hydrogel Sensor for Detection of L-Kynurenine in Human Serum. *Talanta* **2020**, *208*, 120403.

134.Peng, H.; Wang, S.; Zhang, Z.; Xiong, H.; Li, J.; Chen, L.; Li, Y., Molecularly Imprinted Photonic Hydrogels as Colorimetric Sensors for Rapid and Label-Free Detection of Vanillin. *Journal of Agricultural and Food Chemistry* **2012**, *60* (8), 1921-1928.

135.Reese, C. E.; Baltusavich, M. E.; Keim, J. P.; Asher, S. A., Development of an Intelligent Polymerized Crystalline Colloidal Array Colorimetric Reagent. *Analytical Chemistry* **2001**, *73* (21), 5038-5042.

136. Ye, B.; Wang, H.; Ding, H.; Zhao, Y.; Pu, Y.; Gu, Z., Colorimetric logic response based on aptamer functionalized colloidal crystal hydrogels. *Nanoscale* **2015**, *7* (17), 7565-7568.
137. Lin, C. H.; Patei, D. J., Structural Basis of DNA Folding and Recognition in an AMP-DNA Aptamer Complex: Distinct Architectures but Common Recognition Motifs for DNA and RNA Aptamers Complexed to AMP. *Chem. Biol.* **1997**, *4* (11), 817-832.
138. Liu, J.; Lu, Y., Fast colorimetric sensing of adenosine and cocaine based on a general sensor design involving aptamers and nanoparticles. *Angewandte Chemie International Edition* **2006**, *45* (1), 90-94.
139. Li, F.; Zhang, J.; Cao, X.; Wang, L.; Li, D.; Song, S.; Ye, B.; Fan, C., Adenosine Detection by Using Gold Nanoparticles and Designed Aptamer Sequences. *Analyst* **2009**, *134* (7), 1355-1360.
140. Helwa, Y.; Dave, N.; Froidevaux, R.; Samadi, A.; Liu, J., Aptamer-Functionalized Hydrogel Microparticles for Fast Visual Detection of Mercury(II) and Adenosine. *ACS Applied Materials & Interfaces* **2012**, *4* (4), 2228-2233.
141. Zhang, Z.; Oni, O.; Liu, J., New insights into a classic aptamer: binding sites, cooperativity and more sensitive adenosine detection. *Nucleic Acids Res* **2017**, *45* (13), 7593-7601.
142. Zhang, J.-T.; Wang, L.; Lamont, D. N.; Velankar, S. S.; Asher, S. A., Fabrication of Large-Area Two-Dimensional Colloidal Crystals. *Angew. Chem. Int. Ed.* **2012**, *51*, 6117-6120.
143. Smith, N.; Coukouma, A.; Dubnik, S.; Asher, S., Debye ring diffraction elucidation of 2D photonic crystal self-assembly and ordering at the air-water interface. *Physical Chemistry Chemical Physics* **2017**, *19* (47), 31813-31822.
144. Prevo, B. G.; Velez, O. D., Controlled, Rapid Deposition of Structured Coatings from Micro- and Nanoparticle Suspensions. *Langmuir* **2004**, *20*, 2099-2107.
145. Rehman, F. N.; Audeh, M.; Abrams, E. S.; Hammond, P. W.; Kenney, M.; Boles, T. C., Immobilization of acrylamide-modified oligonucleotides by co-polymerization. *Nucleic Acids Res* **1999**, *27* (2), 649-655.
146. Shibayama, M.; Tanaka, T., Volume Phase Transition and Related Phenomena of Polymer Gels. *Advances in Polymer Science* **1993**, *109*, 1-62.
147. Owczarzy, R.; You, Y.; Moreira, B. G.; Manthey, J. A.; Huang, L.; Behlke, M. A.; Walder, J. A., Effects of sodium ions on DNA duplex oligomers: improved predictions of melting temperatures. *Biochemistry* **2004**, *43* (12), 3537-3554.
148. Owczarzy, R.; Moreira, B. G.; You, Y.; Behlke, M. A.; Walder, J. A., Predicting stability of DNA duplexes in solutions containing magnesium and monovalent cations. *Biochemistry* **2008**, *47* (19), 5336-5353.

149. Zhao, W.; Chiuman, W.; Lam, J. C. F.; McManus, S. A.; Chen, W.; Cui, Y.; Pelton, R.; Brook, M. A.; Li, Y., DNA Aptamer Folding on Gold Nanoparticles: From Colloid Chemistry to Biosensors. *J. Am. Chem. Soc.* **2008**, *130* (11), 3610-3618.
150. Xia, T.; Yuan, J.; Fang, X., Conformational Dynamics of an ATP-Binding DNA Aptamer: A Single-Molecule Study. *J. Phys. Chem. B* **2013**, *117* (48), 14994-15003.
151. Singer, V. L.; Jones, L. J.; Yue, S. T.; Haugland, R. P., Characterization of PicoGreen reagent and development of a fluorescence-based solution assay for double-stranded DNA quantitation. *Analytical biochemistry* **1997**, *249* (2), 228-238.
152. Dragan, A.; Casas-Finet, J.; Bishop, E.; Strouse, R.; Schenerman, M.; Geddes, C., Characterization of PicoGreen interaction with dsDNA and the origin of its fluorescence enhancement upon binding. *Biophysical journal* **2010**, *99* (9), 3010-3019.
153. Munzar, J. D.; Ng, A.; Juncker, D., Duplexed aptamers: history, design, theory, and application to biosensing. *Chemical Society Reviews* **2019**, *48* (5), 1390-1419.
154. Bi, Y.; Du, X.; He, P.; Wang, C.; Liu, C.; Guo, W., Smart bilayer polyacrylamide/DNA hybrid hydrogel film actuators exhibiting programmable responsive and reversible macroscopic shape deformations. *Small* **2020**, *16* (42), 1906998.
155. Gawel, K.; Stokke, B. T., Logic swelling response of DNA-polymer hybrid hydrogel. *Soft Matter* **2011**, *7* (10), 4615-4618.
156. Xue, F.; Meng, Z.; Wang, F.; Wang, Q.; Xue, M.; Xu, Z., A 2-D photonic crystal hydrogel for selective sensing of glucose. *Journal of Materials Chemistry A* **2014**, *2* (25), 9559-9565.
157. Yin, T.; Zhong, D.; Liu, J.; Liu, X.; Yu, H.; Qu, S., Stretch tuning of the Debye ring for 2D photonic crystals on a dielectric elastomer membrane. *Soft Matter* **2018**, *14* (7), 1120-1129.
158. Han, S.; Jin, Y.; Su, L.; Chu, H.; Zhang, W., A two-dimensional molecularly imprinted photonic crystal sensor for highly efficient tetracycline detection. *Analytical Methods* **2020**, *12* (10), 1374-1379.
159. Shen, P.; Li, M.; Li, R.; Han, B.; Ma, H.; Hou, X.; Zhang, Y.; Wang, J.-J., Aptamer-functionalized smart photonic hydrogels: application for the detection of thrombin in human serum. *NPG Asia Materials* **2022**, *14* (1), 1-12.
160. Di Cera, E., Thrombin. *Molecular aspects of medicine* **2008**, *29* (4), 203-254.
161. Mach, A. J.; Adeyiga, O. B.; Di Carlo, D., Microfluidic sample preparation for diagnostic cytopathology. *Lab on a Chip* **2013**, *13* (6), 1011-1026.
162. Antillon, M.; Saad, N. J.; Baker, S.; Pollard, A. J.; Pitzer, V. E., The relationship between blood sample volume and diagnostic sensitivity of blood culture for typhoid and paratyphoid fever: a systematic review and meta-analysis. *The Journal of infectious diseases* **2018**, *218* (suppl\_4), S255-S267.

163. Munzar, J. D.; Ng, A.; Corrado, M.; Juncker, D., Complementary oligonucleotides regulate induced fit ligand binding in duplexed aptamers. *Chemical science* **2017**, *8* (3), 2251-2256.
164. Organization, W. H., *Global status report on noncommunicable diseases 2014*. World Health Organization: 2014.
165. Gowri, A.; Kumar, N. A.; Anand, B. S., Recent advances in nanomaterials based biosensors for point of care (PoC) diagnosis of COVID-19—a minireview. *TrAC Trends in Analytical Chemistry* **2021**, *137*, 116205.
166. Altug, H.; Oh, S.-H.; Maier, S. A.; Homola, J., Advances and applications of nanophotonic biosensors. *Nature nanotechnology* **2022**, *17* (1), 5-16.
167. Chadha, U.; Bhardwaj, P.; Agarwal, R.; Rawat, P.; Agarwal, R.; Gupta, I.; Panjwani, M.; Singh, S.; Ahuja, C.; Selvaraj, S. K., Recent progress and growth in biosensors technology: A critical review. *Journal of Industrial and Engineering Chemistry* **2022**.
168. Peeling, R. W.; Heymann, D. L.; Teo, Y.-Y.; Garcia, P. J., Diagnostics for COVID-19: moving from pandemic response to control. *The Lancet* **2022**, *399* (10326), 757-768.
169. Akgönüllü, S.; Kılıç, S.; Esen, C.; Denizli, A., Molecularly imprinted polymer-based sensors for protein detection. *Polymers* **2023**, *15* (3), 629.
170. Heidt, B.; Siqueira, W. F.; Eersels, K.; Diliën, H.; van Grinsven, B.; Fujiwara, R. T.; Cleij, T. J., Point of care diagnostics in resource-limited settings: A review of the present and future of PoC in its most needed environment. *Biosensors* **2020**, *10* (10), 133.
171. Kang, Y.; Aye, L.; Ngo, T. D.; Zhou, J., Performance evaluation of low-cost air quality sensors: A review. *Science of The Total Environment* **2022**, *818*, 151769.
172. Kimble, K. W.; Walker, J. P.; Finegold, D. N.; Asher, S. A., Progress toward the development of a point-of-care photonic crystal ammonia sensor. *Analytical and bioanalytical chemistry* **2006**, *385*, 678-685.
173. Dincer, C.; Bruch, R.; Costa-Rama, E.; Fernández-Abedul, M. T.; Merkoçi, A.; Manz, A.; Urban, G. A.; Güder, F., Disposable sensors in diagnostics, food, and environmental monitoring. *Advanced Materials* **2019**, *31* (30), 1806739.
174. Das, A. J.; Wahi, A.; Kothari, I.; Raskar, R., Ultra-portable, wireless smartphone spectrometer for rapid, non-destructive testing of fruit ripeness. *Scientific reports* **2016**, *6* (1), 1-8.
175. Kalimuthu, K.; Arivalagan, J.; Mohan, M.; Christyraj, J. R. S. S.; Arockiaraj, J.; Muthusamy, R.; Ju, H.-J., Point of care diagnosis of plant virus: Current trends and prospects. *Molecular and Cellular Probes* **2022**, *61*, 101779.
176. Baldi, P.; La Porta, N., Molecular approaches for low-cost point-of-care pathogen detection in agriculture and forestry. *Frontiers in Plant Science* **2020**, *11*, 570862.

177.Frickmann, H.; Podbielski, A.; Kreikemeyer, B., Resistant gram-negative bacteria and diagnostic point-of-care options for the field setting during military operations. *BioMed Research International* **2018**, *2018*.

178.Sharma, A.; Tok, A. I. Y.; Alagappan, P.; Liedberg, B., Point of care testing of sports biomarkers: Potential applications, recent advances and future outlook. *TrAC Trends in Analytical Chemistry* **2021**, *142*, 116327.

179.Castelli, F. A.; Rosati, G.; Moguet, C.; Fuentes, C.; Marrugo-Ramírez, J.; Lefebvre, T.; Volland, H.; Merkoçi, A.; Simon, S.; Fenaille, F., Metabolomics for personalized medicine: the input of analytical chemistry from biomarker discovery to point-of-care tests. *Analytical and Bioanalytical Chemistry* **2022**, *414* (2), 759-789.

180.García, P. S.; Ciavatta, V. T.; Fidler, J. A.; Woodbury, A.; Levy, J. H.; Tyor, W. R., Concentration-dependent dual role of thrombin in protection of cultured rat cortical neurons. *Neurochemical research* **2015**, *40*, 2220-2229.

181.Wang, X.; Wang, X., Aptamer-functionalized hydrogel diffraction gratings for the human thrombin detection. *Chemical Communications* **2013**, *49* (53), 5957-5959.

182.Nagatoishi, S.; Isono, N.; Tsumoto, K.; Sugimoto, N., Loop residues of thrombin-binding DNA aptamer impact G-quadruplex stability and thrombin binding. *Biochimie* **2011**, *93* (8), 1231-1238.

183.Tasset, D. M.; Kubik, M. F.; Steiner, W., Oligonucleotide inhibitors of human thrombin that bind distinct epitopes11Edited by R. Huber. *Journal of Molecular Biology* **1997**, *272* (5), 688-698.

184.Smith, N. L.; Coukouma, A. E.; Jakubek, R. S.; Asher, S. A., Mechanisms by Which Organic Solvent Exchange Transforms Responsive Pure Protein Hydrogels into Responsive Organogels. *Biomacromolecules* **2019**, *21* (2), 839-853.

185.Coukouma, A. E.; Smith, N. L.; Asher, S. A., Removable interpenetrating network enables highly-responsive 2-D photonic crystal hydrogel sensors. *Analyst* **2015**, *140* (19), 6517-6521.

186.Pierce™ Rapid Gold BCA Protein Assay Kit.  
<https://www.thermofisher.com/order/catalog/product/A53225>.